Ann Med Res

Annals of Medical Research

The Official Journal of Inonu University Faculty of Medicine

Ann Med Res | Volume: 32 | Issue: 12 | December 2025

Original Articles

Image

Ann Med Res

Annals of Medical Research

The Official Journal of Inonu University Faculty of Medicine

Editorial Board | Volume: 32 | Issue: 12 | December 2025

Ann Med Res

Annals of Medical Research

The Official Journal of Inonu University Faculty of Medicine

Editorial Advisory Board | Volume: 32 | Issue: 12 | December 2025

Ann Med Res

Annals of Medical Research

The Official Journal of Inonu University Faculty of Medicine

Table of Contents | Volume: 32 | Issue: 12 | December 2025

Original Articles

Image

Ann Med Res

Current issue list available at Ann Med Res

Annals of Medical Research

journal page: annalsmedres.org

Examination of thoracic deformities in patients with different clinical types of cerebral palsy

Selma Solgun Dag [a], Davut Ozbag [b], Egemen Kizilay [c], Sevda Canbay Durmaz [d,*]

[a] Siirt University, Faculty of Medicine, Department of Anatomy, Malatya, Türkiye
[b] Adıyaman University, Faculty of Medicine, Department of Anatomy, Adıyaman, Türkiye
[c] Malatya Training and Research Hospital, Department of Physical Therapy and Rehabilitation, Malatya, Türkiye
[d] Mardin Artuklu University, Faculty of Medicine, Department of Anatomy, Mardin, Türkiye
*Corresponding author: sevdacnby@hotmail.com (Sevda Canbay Durmaz)

MAIN POINTS

- Thoracic deformities in cerebral palsy are very important because they are life-threatening.
- In thoracic deformities, PE deformity was the most common in the anterior chest wall, while scoliosis was seen in spinal deformities.
- In CP, chest deformity evaluation should be done at an early age. Measurements should be evaluated by comparing over the years.

Cite this article as: Solgun Dag S, Ozbag D, Kizilay E, Canbay Durmaz S. Examination of thoracic deformities in patients with different clinical types of cerebral palsy. *Ann Med Res*. 2025;32(12):521--527. doi: 10.5455/annalsmedres.2025.06.148.

ABSTRACT

Aim: Cerebral Palsy is a clinical condition that causes permanent but non-progressive damage to the developing brain and can affect multiple systems. This study aimed to evaluate functional levels by assessing thoracic deformities across different clinical types of cerebral palsy (CP) and by gender, while also comparing anthropometric measurements between individuals with CP and a healthy control group.

Materials and Methods: Between the ages of 6 and 12 years, a total of 154 patients diagnosed with cerebral palsy (91 males, 63 females) and 40 healthy individuals (20 males, 20 females) were included in the study. Demographic characteristics, clinical type of CP, secondary findings, thoracic deformity, anthropometric measurements, and functionality levels were obtained from the patients. A tape measure and caliper were used for anthropometric measurements.

Results: The results indicated that the spastic type was the most prevalent clinical presentation of CP, with intellectual disability being the most common secondary problem. Among thoracic deformities, pectus excavatum was the most frequent anterior chest wall deformity, observed in 9.52% of females and 16.48% of males. Scoliosis was the most common spinal deformity, affecting 26.98% of females and 21.98% of males. Functionally, most patients were classified at GMFCS level II and Ambulation Group 1, although thoracic deformities were more prevalent in Group 2 patients. Furthermore, anthropometric measurements of patients with CP were significantly lower than those of healthy individuals, with statistically significant differences observed between Group 1, Group 2, and the healthy control group ($p<0.05$).

Conclusion: Cerebral palsy has a substantial impact on anthropometric measurements, musculoskeletal integrity, and the functional performance of the patients. Consequently, regular monitoring of the thoracic area is essential. The inclusion of thoracic evaluations in routine follow-up and treatment plans will likely have a positive impact on the disease's progression.

Keywords: Anthropometry, Functionality, Cerebral palsy, Thoracic deformity

Received: Jun 16, 2025 **Accepted:** Aug 28, 2025 **Available Online:** Dec 25, 2025

INTRODUCTION

Cerebral Palsy (CP) is a group of permanent disorders associated with non-progressive issues in the developing fetal or infant brain, leading to activity limitations that persist throughout life in movement and posture development [1]. Children with CP are generally classified into pyramidal (spastic) and extrapyramidal (non-spastic) types, based on the location and nature of neurological damage. Spastic CP results from corticospinal tract injury and is characterized by increased muscle tone and stiffness, while extrapyramidal CP involves damage to the basal ganglia or cerebellum, causing movement disorders. The non-spastic subgroup includes dyskinetic, ataxic, and hypotonic types. This classification supports individualized assessment and guides functional and therapeutic planning. Spasticity is very common in CP, accounting for 70-80% of cases [2].

The etiology is unknown in 30-40% of CP cases. It has been observed that the most significant cause of CP is prenatal

pathologies in 70-80% of cases. Among these, prematurity is the most common [3]. Motor disorders are often accompanied by secondary problems in CP. A heterogeneous picture emerges, as it may include neurological, psychological, behavioral, social, nutritional, and other issues [4].

The healthy growth and development of the spine happen alongside well-coordinated systems. If the spine experiences uneven muscle strength during growth, deformity can occur [5]. In neuromuscular diseases, abnormal loads result from muscle imbalance in the spine. This imbalance causes asymmetric growth of the vertebral bodies in individuals with immature skeletal systems. Spinal deformity occurs more frequently in CP patients than in the general population. The rate varies depending on the severity of the neurological condition. The incidence of spinal deformity in all CP patients is 25% [6].

Anterior chest wall deformities result from the abnormal development or deformation of the thoracic skeleton. In most cases, these deformities do not cause significant or life-threatening functional impairment of intrathoracic organs [7].

The primary objective of this study is to evaluate thoracic deformities and functional levels in children diagnosed with various clinical types of cerebral palsy—a condition known to affect multiple physiological systems—while examining variations based on gender. A secondary objective is to compare anthropometric measurements between the cerebral palsy group and a healthy control cohort to identify significant disparities.

MATERIALS AND METHODS

Study design and ethical approval

This study was conducted in accordance with the principles of the Declaration of Helsinki. Ethical approval was obtained from the Inonu University Health Sciences Non-Interventional Clinical Research Ethics Committee (decision no. 2021/1001). The study is based on a doctoral thesis completed at Inönü University. After providing comprehensive information about the study's objectives and procedures, written informed consent was obtained from the parents or legal guardians of all participants.

Participants and recruitment

This study included 154 children (91 male, 63 female) aged 6-12 years with a diagnosis of cerebral palsy (CP) and 40 age-matched healthy controls (20 male, 20 female). Participants with CP were recruited from five different rehabilitation centers in Malatya using a purposive sampling method. This non-probability technique allowed for the targeted enrollment of individuals who met the specific inclusion criteria for the study.

Individuals were excluded from the study if they had received botulinum toxin injections within the last six months, had a co-existing lung disease, a history of thoracic surgery, or short-extremity stature.

(a) Round Back: Characterized by an exaggerated thoracic kyphosis, leading to a posterior convex curvature of the upper spine and slouched posture.

(b) Pectus Carinatum: Also known as "keel chest," this deformity involves anterior protrusion of the sternum and costal cartilages, resulting in a rigid and elevated chest wall appearance.

Figure 1. Visual representation of two distinct thoracic deformities commonly encountered in children with spastic CP.

Data collection and assessments

For each patient with CP, the following data were collected: demographic information, clinical type of CP, secondary medical findings, and Gross Motor Function Classification System (GMFCS) level.

- Thoracic Deformity Assessment: The presence of tho-

https://doi.org/10.5455/annalsmedres.2025.06.148

racic deformities (Figure 1a, 1b) was determined by a physical therapy doctor through a comprehensive clinical protocol that combined visual inspection with radiological imaging to ensure diagnostic accuracy.

- Gross Motor Function Classification System (GMFCS): The GMFCS scale for the 6-12 age range was used to classify the functional mobility of the patients. The scale consists of five levels, with Level I representing the highest level of function and Level V representing the most limited. For analytical purposes, patients were divided into two groups based on their ambulation capacity: Group 1 (GMFCS levels I-III), consisting of patients who can walk, and Group 2 (GMFCS levels IV-V), consisting of patients who cannot walk [8].
- Anthropometric Measurements: To enhance reliability and minimize observational bias, all anthropometric measurements were conducted by two independent observers using a standard 1.5-meter tape measure and a Harpenden caliper.

Anthropometric measurement procedures

- Chest Circumference: Measured with a tape measure passing horizontally at the level of the xiphoid process and below the axilla during normal, quiet breathing [9].
- Abdominal Circumference: Measured at the level of the umbilicus with the participant in a supine position.
- Shoulder Circumference: Measured around the shoulder at the most prominent point of the deltoid muscle, passing under the acromion [10].
- Thorax Width: Measured from the anterior aspect at the level of the angulus costae of the 6th rib using a digital caliper.
- Shoulder Width: Measured from the posterior aspect, with the caliper ends placed on the most prominent parts of the deltoid muscles while the arms were relaxed at the sides [11].
- Biacromial Width: Measured from the posterior aspect, with the caliper ends placed on the most lateral points of the acromion processes [10].

Statistical analysis

All statistical analyses were performed using IBM SPSS Statistics (version 26.0).

Quantitative data were summarized as mean ± standard deviation for normally distributed variables and as median (minimum–maximum) for non-normally distributed data. Qualitative variables were expressed as frequencies and percentages. The Shapiro-Wilk and Kolmogorov-Smirnov tests were used to assess the normality of data distribution. For comparing two groups, the Independent Samples t-test was used for normally distributed variables, while the Mann-Whitney U test was used for non-parametric data. For categorical variables, the Pearson Chi-square test was used; if expected cell counts were low, Fisher's exact test was applied.

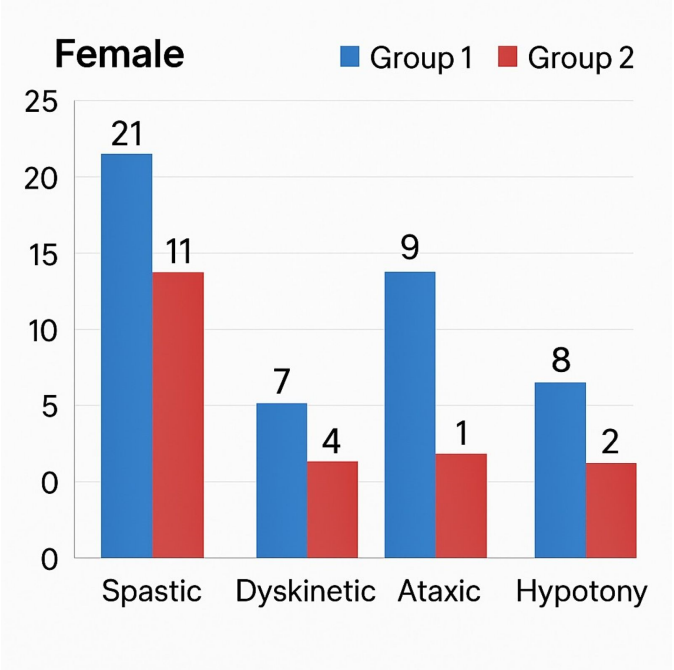

(a) Female.

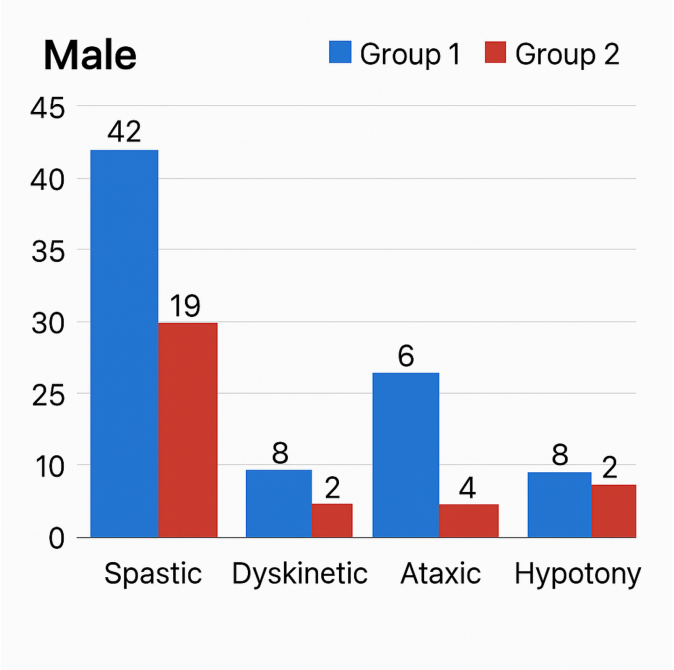

(b) Male.

Figure 2. GMFCS Group 1 and Group 2 distributions of the patient group by gender. (Group 1 includes children with higher functional mobility (Levels I and II), while Group 2 represents those with greater motor limitations (Levels III to V). Notable differences in subgroup prevalence may reflect gender-based variation in clinical presentation and severity).

https://doi.org/10.5455/annalsmedres.2025.06.148

Table 1. Distribution of thoracic deformities in the patient group by gender.

Thoracic Deformity	Female n(%)				Male n(%)				p-value
	Spastic	Dyskinetic	Ataxic	Hypotonic	Spastic	Dyskinetic	Ataxic	Hypotonic	
Kyphosis	1 (3.13)	0 (0.00)	0 (0.00)	0 (0.00)	5 (8.20)	2 (20.00)	0 (0.00)	0 (0.00)	0.048
Scoliosis	10 (31.25)	3 (27.27)	2 (20.00)	2 (20.00)	12 (19.67)	2 (20.00)	2 (20.00)	4 (40.00)	0.037
Hyperlordosis	3 (9.38)	0 (0.00)	0 (0.00)	0 (0.00)	6 (9.84)	0 (0.00)	0 (0.00)	0 (0.00)	0.092
Round Back	2 (6.25)	0 (0.00)	0 (0.00)	1 (10.00)	4 (6.56)	0 (0.00)	2 (20.00)	2 (20.00)	0.066
Flat Back	2 (6.25)	0 (0.00)	0 (0.00)	1 (10.00)	3 (4.92)	2 (20.00)	0 (0.00)	1 (10.00)	0.085
Pectus Excavatum	3 (9.38)	1 (9.09)	0 (0.00)	2 (20.00)	11 (18.03)	0 (0.00)	1 (10.00)	3 (30.00)	**0.022***
Pectus Carinatum	2 (6.25)	0 (0.00)	0 (0.00)	1 (10.00)	6 (9.84)	1 (10.00)	2 (20.00)	1 (10.00)	0.059

*Calculated using Pearson Chi-square or Fisher's exact test depending on expected cell counts. Values in bold indicate statistically significant group differences (p = 0.022).

Table 2. Distribution of Gross Motor Function Classification System (GMFCS) levels by gender in the patient group.

GMFCS	Female n(%)				Male n(%)				p-value
	Spastic	Dyskinetic	Ataxic	Hypotonic	Spastic	Dyskinetic	Ataxic	Hypotonic	
Level I	4 (12.50)	0 (0.00)	0 (0.00)	3 (30.00)	18 (29.51)	0 (0.00)	0 (0.00)	0 (0.00)	**0.021***
Level II	11 (34.38)	2 (18.18)	3 (30.00)	3 (30.00)	18 (29.51)	3 (30.00)	2 (20.00)	1 (10.00)	0.133
Level III	6 (18.75)	5 (45.45)	6 (60.00)	2 (20.00)	6 (9.84)	5 (50.00)	4 (40.00)	1 (10.00)	**0.038***
Level IV	3 (9.38)	2 (18.18)	1 (10.00)	0 (0.00)	4 (6.56)	1 (10.00)	3 (30.00)	1 (10.00)	0.092
Level V	8 (25.00)	2 (18.18)	0 (0.00)	2 (20.00)	15 (24.59)	1 (10.00)	1 (10.00)	7 (70.00)	**0.011***

* Derived using Pearson Chi-square or Fisher's exact test depending on cell frequencies. Bold values indicate statistically significant differences (p<0.05) across gender and clinical types.

Table 3. Thoracic deformity distribution of patients in Group 1 and Group 2 by gender.

Thoracic Deformity	Female n(%)		Male n(%)		p-value
	Group 1	Group 2	Group 1	Group 2	
Kyphosis	0 (0.00)	1 (5.56)	4 (6.90)	3 (9.09)	0.291
Scoliosis	9 (20.00)	8 (44.44)	5 (8.62)	15 (45.45)	**0.014***
Hyperlordosis	2 (4.44)	1 (5.56)	6 (10.34)	0 (0.00)	**0.036***
Round Back	2 (4.44)	1 (5.56)	0 (0.00)	8 (24.24)	**0.019***
Flat Back	2 (4.44)	1 (5.56)	4 (6.90)	2 (6.06)	0.837
Pectus Excavatum	1 (2.22)	5 (27.78)	6 (10.34)	9 (27.27)	**0.022***
Pectus Carinatum	1 (2.22)	2 (11.11)	3 (5.17)	7 (21.21)	**0.038***

*Indicates the statistical significance of deformity distribution between Group 1 and Group 2 (by gender), calculated using Pearson Chi-square or Fisher's exact tests. Bold values denote statistical significance (p<0.05).

Table 4. Anthropometric measurements and significance values of female Group 1 and Group 2 patients and the healthy group.

Anthropometric Measurements	Axillar Circumference	Xiphoid Circumference	Subcostal Circumference	Abdominal Circumference	Shoulder Circumference	Thorax Width	Shoulder Width	Biacromial Circumference
Group 1	63[ab*] (52-95)**	63[ab] (54-86)	57[ab] (45-86)	57[ab] (42-95)	24[b] (15-33)	16[ab] (11-24)	25[ab] (18-37)	19[ab] (14-30)
Group 2	58.50[b] (48-71)	58[b] (48-72)	52[b] (43-63)	49.50[b] (42-63)	21[b] (7-28)	14[b] (11-19)	22[b] (18-28)	17[b] (12-24)
Healthy	69.50 (58-96)	67.50 (58-89)	62.50 (52-86)	66 (53-90)	26.50 (21-42)	18 (14-27)	27.50 (22-40)	23 (18-29)
p***	**<0.001**	**<0.001**	**<0.001**	**<0.001**	**0.00334**	**<0.001**	**<0.001**	**<0.001**

*[a]: Different according to the dyskinetic group, [b]: Different according to the ataxic group, [c]: Different according to the hypotony group, [d]: Different according to the healthy group. **: Variables, 'median (min.-max.)' ***:Kruskal Wallis test.

The Kruskal-Wallis test was used for comparisons across more than two independent groups. A p-value of less than 0.05 was considered statistically significant. An a priori power analysis indicated that a minimum of 64 participants per group was required to achieve 80% power with a medium effect size (Cohen's d = 0.5) at a significance level of $\alpha = 0.05$. The sample size was increased to ensure adequate statistical power for subgroup analyses. Prior to analysis, all data were pre-processed to identify and handle outliers, missing values, and inconsistencies

https://doi.org/10.5455/annalsmedres.2025.06.148

Table 5. Anthropometric measurements and significance values of male Group 1 and Group 2 patients and the healthy group.

Anthropometric Measurements	Axillar Circumference	Xiphoid Circumference	Subcostal Circumference	Abdominal Circumference	Shoulder Circumference	Thorax Width	Shoulder Width	Biacromial Circumference
Group 1	64.50[b*] (53-91)**	63.50[b] (53-88)	57[b] (42-85)	56.50[ab] (46-90)	23[b] (16-35)	16[b] (11-24)	24[b] (19-35)	18.50[b] (13-27)
Group 2	61[b] (49-78)	62[b] (47-78)	56[b] (42-75)	52[b] (39-73)	21[b] (12-34)	15[b] (10-25)	24[b] (17-35)	18[b] (14-31)
Healthy	72.50 (59-90)	69.50 (61-89)	65.50 (53-84)	66.50 (51-87)	25.50 (21-33)	18.50 (16-28)	29 (24-36)	23 (18-27)
p***	**<0.001**	**<0.001**	**<0.001**	**<0.001**	**0.00379**	**<0.001**	**<0.001**	**<0.001**

*[a]: Different according to the dyskinetic group, [b]: Different according to the ataxic group, [c]: Different according to the hypotony group, [d]: Different according to the healthy group. **: Variables, 'median (min.-max.)' ***:Kruskal Wallis test.

RESULTS

A total of 154 CP patients (41% female, 59% male) and 40 healthy individuals (50% female, 50% male) were included in the present study. The CP patients comprised the "patient group," while healthy individuals formed the "control group." According to GMFCS classifications, Levels I–III (Group 1) included ambulatory patients, and Levels IV–V (Group 2) comprised non-ambulatory individuals.

Height and weight were significantly lower in the patient group compared to the control group. Although BMI values were also lower in the patient group, the difference did not reach statistical significance.

Distribution of CP clinical subtypes among females included spastic (n = 32), dyskinetic (n = 11), ataxic (n = 10), and hypotonic (n = 10) presentations. Among males, subtypes were spastic (n = 61), dyskinetic (n = 10), ataxic (n = 10), and hypotonic (n = 10). Secondary conditions frequently observed in CP patients included intellectual disability, speech impairment, behavioral problems, swallowing and drooling difficulties, epilepsy, and visual impairments.

Thoracic deformity distribution by gender is shown in Table 1, while GMFCS levels are provided in Table 2. The distribution of Group 1 and Group 2 patients by gender is visualized in Figure 2, and Table 3 details thoracic deformity distributions across these functional groups. Anthropometric measurements and their statistical comparisons by gender are presented in Tables 4 and 5.

DISCUSSION

This study provided a comprehensive evaluation of thoracic deformities, functional capacity, and anthropometric characteristics in children with various clinical subtypes of cerebral palsy (CP), with a specific focus on gender differences. Unlike previous research that has concentrated primarily on extremity deformities, our study emphasized structural deviations in the spinal and anterior chest wall—areas often overlooked in routine clinical evaluations. Our findings confirm that children with CP exhibit significantly altered anthropometric profiles and a high prevalence of thoracic deformities, the severity of which correlates with functional impairment.

In our cohort, height and weight were significantly lower in individuals with CP compared to healthy controls, a finding consistent with the work of Uygur et al. [12]. However, while we observed lower (BMI) values in the patient group, the difference did not achieve statistical significance. The prevalence of secondary conditions in our sample—such as intellectual disability, speech difficulties, and epilepsy—aligns with trends reported by Durmaz et al., reinforcing the multi-systemic nature of CP. These comorbidities likely compound musculoskeletal dysfunction, limiting growth and contributing to the development of thoracic deformities [13-15].

The rate of thoracic and spinal deformities in our study was notable. We identified pectus excavatum (PE) in 9.52% of females and 16.48% of males, and scoliosis was the most common spinal deformity. This contrasts with earlier studies, such as by Ersöz et al. [16], who found no anterior chest wall deformities, and Öneş et al. [17], who reported a lower overall rate of spinal deformities. We attribute the development of these deformities to a combination of factors inherent to CP, including biomechanical imbalances, asymmetrical muscle tone, impaired proprioception, and postural instability against gravity.

Functionally, our patient cohort demonstrated a higher level of motor ability compared to those in previous Turkish studies. While Karabay et al. [9] and Atay et al. [18] reported a majority of patients in GMFCS Levels III–V, our study found that most participants (71.43% of females and 63.74% of males) were classified in Group 1 (GMFCS Levels I–II). This encouraging trend may reflect advancements in early diagnosis and rehabilitation services. As expected and consistent with the literature [8], our results confirmed a strong relationship between functional level and deformity prevalence; both anterior chest wall and spinal deformities were significantly more common in non-ambulatory Group 2 patients (GMFCS IV-V). As patients' motor independence decreased, the rates of deformity increased.

Our anthropometric findings largely support previous research showing reduced growth parameters in children with CP [10,14]. We observed significantly lower chest (axillary, xiphoid, subcostal), abdominal, and shoulder circumferences,

https://doi.org/10.5455/annalsmedres.2025.06.148

as well as reduced thorax, shoulder, and biacromial widths. These results expand on the findings of Uygur et al. [12], as we also identified significant reductions in xiphoid and subcostal circumferences, which they did not. This discrepancy may be due to our inclusion of more severely affected spastic and dyskinetic subtypes. Furthermore, contrary to the findings of Kosif et al. [19], who reported no significant differences in girls, our study found lower anthropometric values in both males and females. An exception was observed in females with ataxic CP, whose measurements were closer to controls. This can likely be explained by their high functional status, as 90% of them were in GMFCS Level I. This highlights the critical role that motor function plays in musculoskeletal development.

Limitations

This study has certain limitations that should be acknowledged. The sample size, while substantial, may limit the generalizability of our findings to the broader CP population. Additionally, some observed thoracic deformities were complex and could not be classified into standard categories, which may have influenced our reported prevalence rates. Future longitudinal studies are warranted to track the progression of these deformities over time and to assess their impact on respiratory function and quality of life.

CONCLUSION

Cerebral palsy significantly impacts musculoskeletal integrity, anthropometric development, and functional capacity. Our findings underscore the high prevalence of thoracic deformities in this population and their strong correlation with motor impairment. Therefore, routine thoracic evaluation should be integrated into standard physiotherapy assessments for children with CP. Regular monitoring can aid in the early detection of deformities, allowing for timely interventions that may positively influence the disease trajectory and improve long-term outcomes.

This study was previously presented as a oral presentation at 4rd International 33rd National Turkish Biophysics Congress (31 August-1-3 September Adıyaman).

Ethics Committee Approval: The study was conducted afterobtaining the necessary permissions Inonu University Health Sciences Non-Interventional Clinical Research Ethics Committee with the decision number 2021/1001.

Informed Consent: After a detailed explanation of the study, written informed consent was obtained from the participants and their families. Additionally, written informed consent for imaging was obtained from the patient's legal guardian.

Peer-review: Externally peer-reviewed.

Conflict of Interest: There is no conflict of interest between the authors.

Author Contributions: Conception: S.S.D, E.K, S.C.D; Design: S.S.D; E.K; Supervision: S.S.D, D.Ö, E.K, S.C.D; Fundings: S.S.D; Materials: S.S.D,S.C.D; Data Collection and/or Processing: S.S.D, E.K; Analysisand/or Interpretation: D.Ö,S.C.D; Literature Review: S.C.D; Writing: S.S.D; Critical Review: D.Ö, E.K,S.C.D.

Financial Disclosure: This study did not receive any financial support.

REFERENCES

1. Kim F, Maitre N; Cerebral Palsy Foundation. A Call for Early Detection of Cerebral Palsy. *Neoreviews.* 2024;25(1):e1-e11. doi: 10.1542/neo.25-1-e1.
2. Modlesky CM, Matias AB. Muscle in children with cerebral palsy: current evidence, knowledge gaps, and emerging research opportunities : Focus on Cerebral Palsy. *Pediatr Res.* 2024. doi: 10.1038/s41390-024-03422-x.
3. Dar H, Stewart K, McIntyre S, Paget S. Multiple motor disorders in cerebral palsy. *Dev Med Child Neurol.* 2024;66(3):317-325. doi: 10.1111/dmcn.15730.
4. Olmos-Gómez R, Calvo-Muñoz I, Gómez-Conesa A. Treatment with robot-assisted gait trainer Walkbot along with physiotherapy vs. isolated physiotherapy in children and adolescents with cerebral palsy. Experimental study. *BMC Neurol.* 2024;24(1):245. doi: 10.1186/s12883-024-03750-9.
5. Khalifeh K, Brown NJ, Pennington Z, Pham MH. Spinal Robotics in Adult Spinal Deformity Surgery: A Systematic Review. *Neurospine.* 2024;21(1):20-29. doi: 10.14245/ns.2347138.569.
6. Yoshida K, Kajiura I, Suzuki T, Kawabata H. Natural history of scoliosis in cerebral palsy and risk factors for progression of scoliosis. *J Orthop Sci.* 2018;23(4):649-652. doi: 10.1016/j.jos.2018.03.009.
7. Şirazi S, Heydar AM, Bezer M, Yüksel M. Correlation of anterior chest wall anomalies and spinal deformities: a comprehensive descriptive study. *Spine Deform.* 2024;12(6):1615-1622. doi: 10.1007/s43390-024-00918-8.
8. Sloane BM, Kenyon LK, Logan SW, Feldner HA. Caregiver perspectives on powered mobility devices and participation for children with cerebral palsy in Gross Motor Function Classification System level V. *Dev Med Child Neurol.* 2024;66(3):333-343. doi: 10.1111/dmcn.15718.
9. Atay Y. Serebral Paralizi'li Çocukların Farklı Klinik Tiplerinde Antropometrik Özelliklerin Değerlendirilmesi. Sağlık Bilimleri Enstitüsü, Protez Ortez Biyomekani Programı. Yüksek Lisans tezi, *Ankara: Hacettepe Üniversitesi.* 2006.
10. Otman AS, Demirel H, Sade A. Tedavi Hareketlerinde Temel Değerlendirme Prensipleri, 3. Baskı. Ankara. *Hacettepe Üniversitesi Fizik Tedavi ve Rehabilitasyon Yüksekokulu Yayınları.* 2003:11-53.
11. Díaz-Martínez AS, Vaquero-Cristóbal R, Albaladejo-Saura M, Esparza-Ros F. Effect of pre-season and in-season training on anthropometric variables, somatotype, body composition and body proportion in elite basketball players. *Sci Rep.* 2024;14(1):7537. doi: 10.1038/s41598-024-58222-4.
12. Uygur R, Özen OA, Baş O, Uygur E, Songur A. Hemiplejik serebral palsili çocuklarda gövde antropometrik ölçümlerinin değerlendirilmesi. *Int J Basic Clin Med.* 2015;1(1): 7-14.
13. Dormans J, Susman M, Özaras N, Yalçın S. Serebral Palsi Tedavi ve Rehabilitasyon, 1. Baskı. *Mas Matbaacılık.* İstanbul. 2000.
14. Durmaz SC, Karabulut AK, Güngör S, Fazlıoğulları Z, Uysal İİ, Doğan NÜ. Clinical evaluation of cerebral MRI findings in children with cerebralpalsy. *Ann Clin Anal Med.* 2022;13(10):1117-21. doi: 10.4328/acam.21228.
15. Taylor JB, Ingram DG, Kupfer O, Amin R. Neuromuscular Disorders in Pediatric Respiratory Disease. *Clin Chest Med.* 2024;45(3):729-747. doi: 10.1016/j.ccm.2024.02.021.

https://doi.org/10.5455/annalsmedres.2025.06.148

16. Ersöz M, Selçuk B, Gündüz R, Kurtaran A, Akyüz M. Decreased chest mobility in children with spastic cerebral palsy. *Turk J Pediatr*. 2006;48(4): 344-50. PMID: 17290570.
17. Öneş K, Çelik B, Çağlar N, Gültekin Ö, Yılmaz E, Çetinkaya B. Serebralpalsi polikliniğine müracaat eden hastaların demografik ve klinik özellikleri. *Türk Fiz Tip Rehab Derg*. 2008;54(1): 13-6.
18. Karabay İ, Şenlikci HB, Nazlıkul FGU, Tiftik TT, Ersöz M, Akkuş S. Serebralpalsili hastalarda fonksiyonel durum, serebralpalsi tipi ve antropometrik parametrelerin ilişkisi. *Turkish J Pediatr Dis*. 2020; 14(5): 417-21. doi: 10.12956/tchd.674754.
19. Kosif R, Eldeş N, Kutsal E, Aydemir C. On yaşındaki serebralpalsili çocuklarda farklı antropometrik ölçümlerle büyümenin değerlendirilmesi. *Yeni Tip Dergisi*. 2007; 24:35-8.

https://doi.org/10.5455/annalsmedres.2025.06.148

Ann Med Res

Current issue list available at Ann Med Res

Annals of Medical Research

journal page: annalsmedres.org

Metabolic imaging of head and neck lesions: Differentiating dental and maxillofacial conditions using positron emission tomography/computed tomography

Melisa Ocbe [a,*], Mahmut Sabri Medisoglu [b]

[a]Kocaeli Health and Technology University, Faculty of Dentistry, Department of Oral and Maxillofacial Radiology, Kocaeli, Türkiye
[b]Kocaeli Health and Technology University, Faculty of Dentistry, Department of Anatomy, Kocaeli, Türkiye
*Corresponding author: melisa.ocbe@kocaelisaglik.edu.tr (Melisa Ocbe)

MAIN POINTS

- Malignant dentomaxillofacial lesions demonstrated significantly higher FDG uptake (mean SUVmax =12.5) than all non-malignant conditions.
- Among benign pathologies, maxillary sinus diseases and periodontal infections showed moderate FDG uptake, which may mimic malignancy.
- TMJ disorders and dental artifacts exhibited minimal metabolic activity, aiding in their differentiation from true lesions.
- This study highlights the value of SUVmax comparisons to avoid misinterpretation of FDG-PET/CT in the head and neck region.
- The integration of CT/MRI with PET/CT improves diagnostic accuracy in differentiating benign and malignant dentomaxillofacial conditions.

Cite this article as: Ocbe M, Medisoglu MS. Metabolic imaging of head and neck lesions: Differentiating dental and maxillofacial conditions using positron emission tomography/computed tomography. *Ann Med Res*. 2025;32(12):528–534. doi: 10.5455/annalsmedres.2025.06.162.

ABSTRACT

Aim: Fluorine-18-labeled fluoro-2-deoxy-D-glucose positron emission tomography/computed tomography (FDG-PET/CT) is an essential oncologic imaging modality, but its uptake patterns may also be seen in benign inflammatory or structural oral conditions, leading to diagnostic confusion. This study aims to compare metabolic activity with maximum standardized uptake value (SUVmax) among common dento-maxillofacial conditions---dental artifacts, periodontal infections, maxillary sinus pathologies, and temporomandibular joint (TMJ) disorders---against confirmed malignant lesions, to guide differential diagnosis and improve clinical interpretation.

Materials and Methods: A total of 100 FDG-PET/CT scans were retrospectively analyzed. Inclusion criteria comprised pre-treatment scans with available CT or magnetic resonance imaging (MRI) acquired within four weeks. Patients were categorized into five groups: Dental Artifacts (n=19), Periodontal Infections (n=23), Maxillary Sinus Pathologies (n=21), TMJ Pathologies (n=19), and Malignant Dento-maxillofacial Lesions (n=18; control group). All scans were reviewed by an oral and maxillofacial radiologist and a radiologist. SUVmax were calculated using a 42% threshold. Statistical analyses were conducted using Kruskal-Wallis and Mann-Whitney U tests with Bonferroni correction.

Results: Significant differences in SUVmax were observed across all groups (χ^2 = 77.4, p<0.000001). The malignant lesion group demonstrated the highest metabolic activity (mean SUVmax = 12.5 ± 3.0), significantly greater than all other groups (p<0.000001). Among non-malignant conditions, maxillary sinus pathologies showed the highest SUVmax (4.2 ± 1.0), followed by periodontal infections (3.5 ± 0.8). TMJ pathologies and dental artifacts exhibited the lowest FDG uptake (2.0 ± 0.6 and 2.5 ± 0.7, respectively), suggesting minimal metabolic activity.

Conclusion: This study confirms that malignant dento-maxillofacial lesions exhibit significantly higher FDG uptake compared to inflammatory and mechanical conditions. Understanding these uptake patterns is crucial to avoiding false-positive interpretations, especially in oncologic patients. Multimodal imaging and interdisciplinary evaluation are recommended for accurate differentiation of dental and maxillofacial pathologies in FDG-PET/CT interpretation.

Keywords: FDG-PET/CT, SUVmax, Dento-maxillofacial lesions, Oral cancer, Metabolic imaging

Received: Jun 25, 2025 **Accepted:** Sep 08, 2025 **Available Online:** Dec 25, 2025

INTRODUCTION

Fluorine-18-labeled fluoro-2-deoxy-D-glucose-positron emission tomography/computed tomography (FDG-PET/CT) is important in the detection, treatment and follow-up for malignant diseases. This imaging technique provides molecular-level information, allowing early detection of disease activity. It is recognized as a reliable and precise tool for diagnosing and quantifying disease burden, especially in clinical settings. Recent advancements have broadened its clinical use in infectious and inflammatory conditions. The distribution of FDG in these diseases is based on the same mechanisms as in malignancies, characterized by increased cellular metabolism [1,2].

All cells use glucose for energy, but most prefer the more efficient aerobic oxidative phosphorylation. Cancer cells, however, favor the less efficient glycolytic pathway even when oxygen is present. They meet their high glucose demand by increasing the active glucose transporter (GLUT), leading to higher FDG uptake. Once inside the cell, glucose is phosphorylated for further processing, while excess is expelled after dephosphorylation [2,3]. FDG, gets trapped inside cancer cells because it can't be processed further and isn't expelled, resulting in high intracellular concentration. This was initially thought to be specific to cancer cells, but it was discovered that immune cells also use this mechanism, causing false positives in FDG-PET/CT scans [1,4,5].

This manuscript has two primary aims. The first aim is to guide medical radiologists in accurately distinguish dental lesions from potential metastases. By presenting detailed case-based illustrations, the manuscript seeks to prevent misdiagnosis, particularly in complex head and neck regions where PET/CT imaging can present challenges. The second aim is to serve as an educational resource for oral radiologists. It provides insights into the interpretation of PET/CT images specifically in dento-maxillofacial conditions, helping them understand the unique imaging characteristics and potential diagnostic pitfalls associated with these lesions. This study highlights the importance of a multidisciplinary approach in ensuring accurate diagnosis of head and neck lesions.

MATERIALS AND METHODS

This study was conducted in accordance with ethical guidelines and received approval from the Kocaeli Health and Technology University, Non-invasive Clinical Research Ethics Committee (Project No: 2024-101) at 10.10.2024. The study protocol was reviewed and approved by the Institutional Review Board (IRB), ensuring compliance with ethical standards. All procedures performed were in accordance with the ethical standards of the institutional research committee and with the 1964 Helsinki Declaration and its later amendments. All patient data were anonymized to maintain confidentiality.

Patient selection

This research was designed as a retrospective observational cross-sectional study. The study analyzed existing FDG-PET/CT, CT, and MRI images to compare metabolic activity (SUVmax values) in dentomaxillofacial conditions. The study was conducted and reported in accordance with the STROBE (Strengthening the Reporting of Observational Studies in Epidemiology) guidelines to ensure transparent and standardized reporting of observational research [6]. A total of 463 images obtained from Kocaeli City Hospital, Department of Radiology were evaluated. The aim was to investigate dentomaxillofacial lesions, including bone defects, maxillary sinus diseases and inflammatory conditions, using FDG-PET/CT imaging which were not only specifically acquired for head and neck pathology but were evaluated for detection of hypermetabolism in the area. Between January 2022 and March 2024, a total of 2,843 FDG-PET/CT scans of the head and neck region were reviewed. Each case was screened systematically according to predefined inclusion and exclusion criteria. Inclusion criteria were; availability of pre-treatment FDG-PET/CT imaging of the head and neck region, accompanying diagnostic CT or MRI of the same region performed within four weeks of the PET/CT scan, histopathological confirmation of diagnosis for all malignant lesions, images of high diagnostic quality without severe artifacts and patients who provided informed consent for the scientific use of their imaging data. Exclusion criteria were; prior surgery, chemotherapy, or radiotherapy before the imaging date, missing or incomplete correlation studies (CT or MRI not performed within four weeks), motion-degraded or low-resolution scans unsuitable for accurate SUV measurement, lack of consent for scientific use of data. Following these criteria, 100 patients were included in the study. Patients were categorized into five diagnostic groups based on radiological and clinical interpretation: Dental artifacts (n=19), Common dental and periodontal infections (n=23), Maxillary sinus pathologies (n=21), Temporomandibular joint (TMJ) pathologies (n=19), Malignant dentomaxillofacial lesions (n=18, control group). This study included all eligible cases identified from the institutional imaging archive. A non-probability purposive sampling strategy was applied.

All imaging data were fully anonymized before analysis, with identifying patient information removed from Digital Imaging and Communications in Medicine (DICOM) headers. The images were reviewed blinded to patient names, demographic details, and clinical history beyond basic inclusion criteria. Group categorization was based on imaging findings.

Imaging protocols

Fasting patients with serum blood glucose levels below 12 mmol/L were administered a standardized dose of 18F-FDG in accordance with the protocol of Kocaeli City Hospital. Following injection, patients rested supine for one hour in a warm environment. FDG-PET/CT, CT, and MRI images were evaluated in an optimal environment. Scans were conducted using integrated PET/CT systems. FDG-PET/CT scans were analyzed on a GE Healthcare Workstation, enabling the viewing of CT, MRI, and PET/CT images in overlay mode across three planes simultaneously. PET/CT scans were evaluated for maximum standardized uptake values (SUVmax) to measure metabolic activity. Abnormally increased FDG uptake in the dentomaxillofacial region was identified and recorded. The SUVmax within regions of interest was assessed using a volume-of-interest tool with a 42% SUVmax threshold, with manual adjustments for individual lesions when necessary. The Revolution™ EVO/Optima™ CT660 CT Scanner (GE Healthcare Japan Corporation, Tokyo, Japan) was used for CT scans, and the SIGNA™ Pioneer (GE Medical Systems, Waukesha, USA) was used for

https://doi.org/10.5455/annalsmedres.2025.06.162

MR imaging.

The primary outcome of this study was the SUVmax of fluorine-18-labeled FDG within each identified dento-maxillofacial lesion. Secondary outcomes included qualitative imaging characteristics (lesion location, structural involvement, presence of dental artifacts) and descriptive analysis of patient demographics (age, sex, and diagnostic category). Maxillary sinus pathologies in this study included mucosal thickening, retention cysts, and inflammatory polyps, while TMJ pathologies included degenerative and structural changes such as condylar flattening, osteophyte formation, and joint space narrowing. Cases classified as benign showed no radiological evidence of aggressive behavior, bone destruction, or suspicious enhancement and were confirmed by clinical records when accessible. Inclusion of malignant or suspicious lesions in this study required histopathological confirmation.

Statistical analysis

Statistical analyses were performed using IBM SPSS Statistics for Windows, Version 23.0 (IBM Corp., Armonk, NY, USA). Prior to hypothesis testing, the normality of SUVmax distributions was assessed using the Shapiro–Wilk test, and homogeneity of variances was evaluated with Levene's test. As SUVmax values were not normally distributed, non-parametric tests were applied. The Kruskal–Wallis H test was used to compare SUVmax values among the five diagnostic groups. For pairwise group comparisons, Mann–Whitney U tests were conducted with Bonferroni correction to control for multiple comparisons. Quantitative variables are reported as mean ± standard deviation (SD) and range (min–max); categorical variables are presented as counts and percentages. Quantitative variables (e.g., SUVmax values, age) were summarized using mean ± standard deviation (SD), minimum and maximum values, and medians with interquartile ranges (IQRs) when appropriate. Qualitative variables (e.g., gender, diagnostic group) were summarized as counts and percentages. Receiver Operating Characteristic (ROC) curve analysis was performed to assess the diagnostic performance of SUVmax in differentiating malignant lesions from benign conditions. The optimal cut-off value was determined using the Youden index, and the area under the curve (AUC), sensitivity, and specificity were calculated. Statistical significance was defined as $p<0.05$, and exact p-values are reported in all tables.

RESULTS

Demographic analysis

A total of 100 patients were included in the study. The mean age of participants varied across groups, with the Malignant Lesions group presenting the highest average age at 59.3 years (SD: 7.09; range: 47–74 years). This was followed by the Maxillary Sinus Pathologies group, which had a mean age of 57.8 years (SD: 9.56; range: 34–72 years). Participants in the Periodontal Infections group had a mean age of 51.95 years (SD: 10.65; range: 32–68 years), while the Temporomandibular Joint (TMJ) Pathologies and Dental Artifacts groups had slightly younger averages of 50.95 years (SD: 12.66; range: 28–77 years) and 49.7 years (SD: 9.70; range: 32–67 years), respectively (Table 1).

Regarding gender distribution, the Dental Artifacts group included 11 females and 8 males, showing a slight female predominance. The Periodontal Infections group consisted of 9 females and 11 males, while the Maxillary Sinus Pathologies group had a nearly balanced distribution of 9 females and 12 males. The TMJ Pathologies group also showed a similar distribution with 10 females and 9 males. In contrast, the Malignant Lesions group had a marked male predominance with 13 males and 5 females (Table 1).

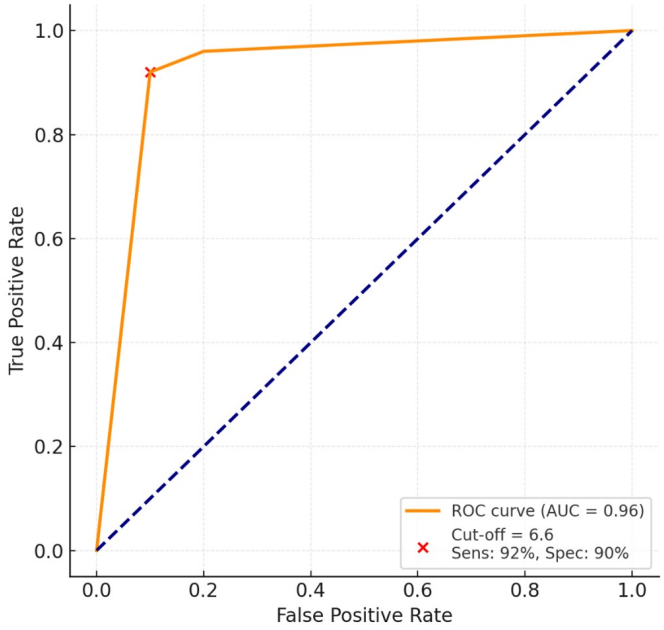

Figure 1. Receiver Operating Characteristic (ROC) curve of SUVmax in differentiating malignant lesions from benign dento-maxillofacial pathologies.

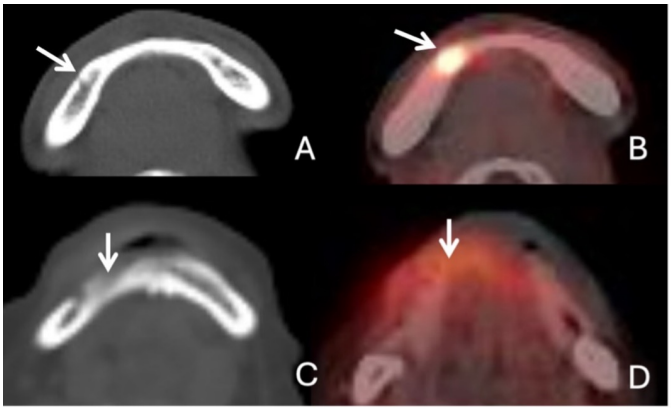

Figure 2. Axial CT section of an apical osteitis lesion in the anterior mandible (A) was revealed high FDG uptake (B). Note that bone socket after the extraction of right mandibular canine (C) also revealed high FDG uptake (D).

https://doi.org/10.5455/annalsmedres.2025.06.162

Table 1. Demographic features of the groups.

Group	Mean Age	SD (Age)	Age Range	Female (n)	Male (n)
Dental Artifacts	49.7	9.70	32 -- 67	11	8
Periodontal Infections	51.95	10.65	32 -- 68	9	11
Maxillary Sinus Pathologies	57.8	9.56	34 -- 72	9	12
Temporomandibular Joint Pathologies	50.95	12.66	28 -- 77	10	9
Malignant Lesions (Control)	59.3	7.09	47 -- 74	5	13

Table 2. Distribution of SUVmax values according to diagnostic group.

Diagnostic Group	Mean ± SD	Minimum	Maximum
Dental Artifacts	2.5 ± 0.7	1.4	3.9
Periodontal Infections	3.5 ± 0.8	2.1	5.2
Maxillary Sinus Pathologies	4.2 ± 1.0	2.7	6.1
Temporomandibular Joint Pathologies	2.0 ± 0.6	1.0	3.1
Malignant Lesions (Control)	12.5 ± 3.0	7.9	18.1

Table 3. Pairwise comparisons of SUVmax amongst the diagnostic groups and malignant lesions.

Comparison Group	Test Used	Adjusted p-value (Bonferroni)
Dental Artifacts vs. Malignant Lesions	Mann-Whitney U	p = 0.00000128
Periodontal Infections vs. Malignant Lesions	Mann-Whitney U	p = 0.00000285
Maxillary Sinus Pathologies vs. Malignant Lesions	Mann-Whitney U	p = 0.00000323
TMJ Pathologies vs. Malignant Lesions	Mann-Whitney U	p = 0.00000156

Table 4. Normal FDG uptake in oral and maxillofacial PET/CT imaging: Regions and Reasons.

Region	FDG Uptake Characteristics
Waldeyer's ring	Presence of lymphatic tissue
Nasopharyngeal tonsils	Lymphatic tissue activity
Major salivary glands	Accumulation and secretion with saliva, potential asymmetrical uptake due to pooling, which can mimic malignancy
Muscle (scalene, sternocleidomastoid, pterygoid, etc.)	Increased metabolic activity, often associated with muscle use or tension
Brown fat	Function of producing thermal energy, requiring CT correlation

Table 2 presents the descriptive statistics for standardized uptake values (SUVmax) across the five diagnostic groups. The Malignant Lesions group demonstrated the highest metabolic activity, with a mean SUVmax of 12.5 ± 3.0 (range: 7.9–18.1), which was significantly greater than all other groups ($p<0.001$ for all comparisons). This finding aligns with the high glycolytic activity commonly observed in malignant tumors. Among the non-malignant conditions, the Maxillary Sinus Pathologies group exhibited the highest mean SUVmax, measured at 4.2 ± 1.0 (range: 2.7–6.1). Although elevated, these values were still markedly lower than those observed in malignant lesions, indicating limited but notable metabolic activity—likely due to inflammatory or reactive changes. The Periodontal Infections group followed, with a mean SUVmax of 3.5 ± 0.8 (range: 2.1–5.2), consistent with the metabolic demand associated with acute or active dental infections. Dental Artifacts and Temporomandibular Joint (TMJ) Pathologies groups exhibited the lowest SUVmax values, with means of 2.5 ± 0.7 and 2.0 ± 0.6, respectively. These low values suggest minimal FDG uptake, consistent with the non-inflammatory, mechanical, or artifact-related nature of these findings. The TMJ group in particular showed the lowest overall metabolic activity (range: 1.0–3.1), reinforcing that structural joint changes are not typically associated with hypermetabolism (Table 2).

All diagnostic groups demonstrated significantly lower SUVmax values compared to the malignant lesion group ($p<0.001$ in all cases) (Supplementary Table). Among the non-malignant conditions, maxillary sinus pathologies exhibited the highest mean SUVmax, yet remained significantly lower than malignant lesions. TMJ pathologies and dental artifacts showed the lowest SUVmax values, indicating minimal metabolic activity in these structural or mechanical conditions (Table 3). ROC analysis showed that SUVmax had excellent discriminative ability for differentiating malignant lesions from benign conditions (AUC = 0.96, 95% CI: 0.91–0.99, $p<0.001$). A cut-off value of 6.6 provided a sensitivity of 92% and specificity of 90% (Figure 1).

https://doi.org/10.5455/annalsmedres.2025.06.162

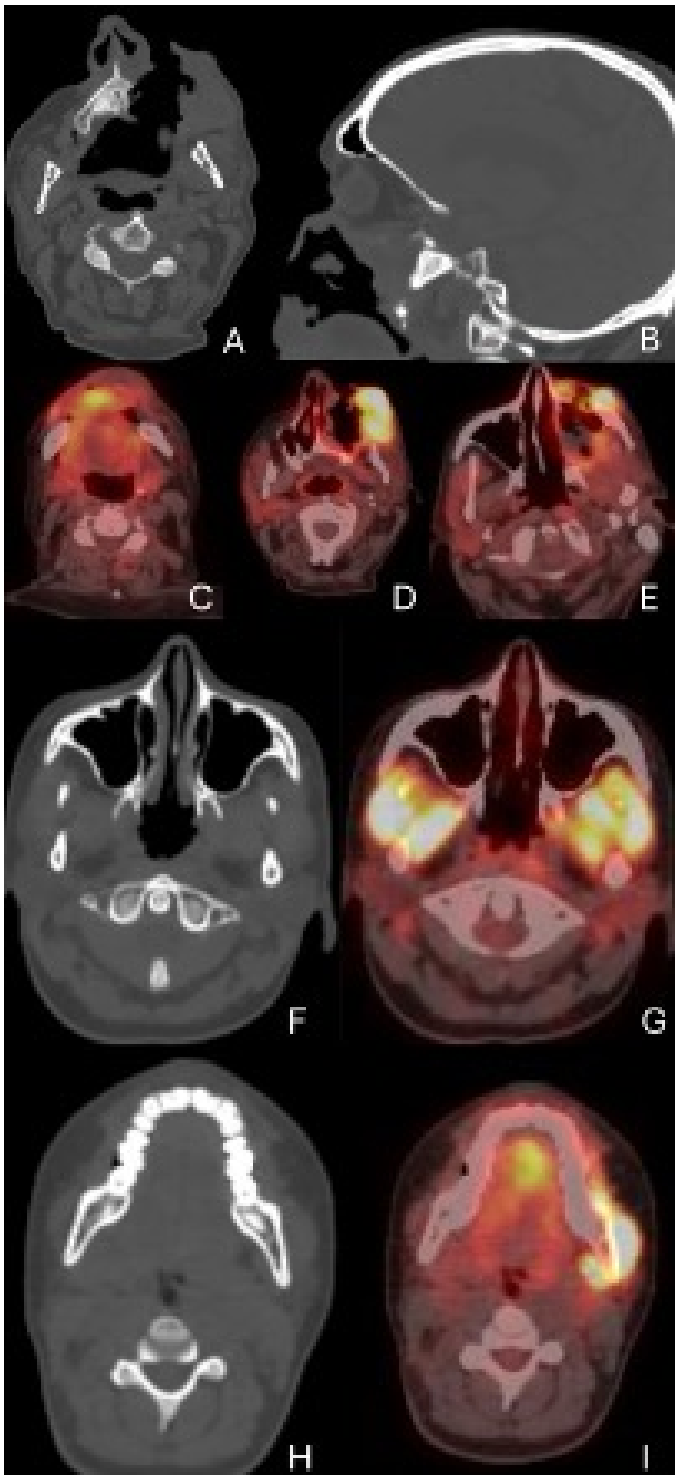

Figure 3. A 66-year-old male with sinonasal carcinoma invading the maxilla and maxillary sinus region (A, B), demonstrating high metabolic activity on FDG-PET/CT imaging (C, D, E). A 19-year-old female presenting with increased metabolic activity observed in the masseter and medial pterygoid muscles bilaterally, attributed to temporomandibular overuse, as depicted on PET/CT imaging. The patient had no previous TMJ pathology diagnosis (F, G, H, I).

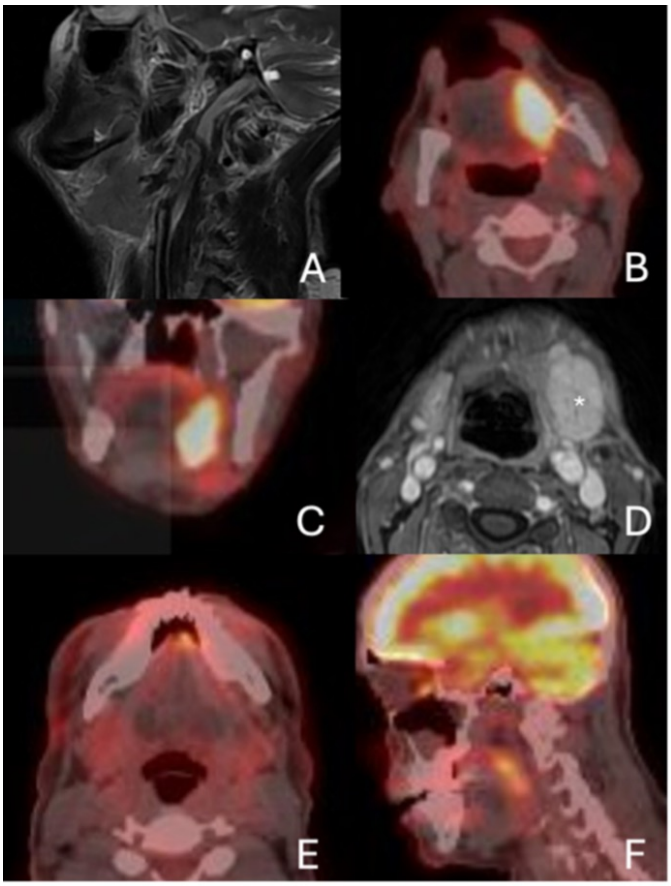

Figure 4. A 70-year-old male diagnosed with squamous cell carcinoma (SCC) of the tongue, characterized by a contrast-enhancing lesion measuring 20x14x35 mm in the left posterior region (A). PET/CT imaging showed a maximum standardized uptake value (SUVmax) of 20.75 within the lesion (B, C). Additionally, enlargement of the left submandibular gland was noted (D). A 53-year-old male diagnosed with SCC of the anterior tongue as the primary lesion. PET/CT imaging revealed mild FDG uptake in 11 mm lymph nodes in the left submandibular and upper jugular regions, indicative of metastasis (E, F).

DISCUSSION

This study evaluated the role of FDG-PET/CT imaging and SUVmax measurements in differentiating malignant from benign oral and maxillofacial pathologies, using histopathological confirmation for all malignant lesions and imaging-based criteria for benign diagnoses. The results demonstrated that SUVmax were significantly higher in malignant lesions than in all benign groups, supporting previous reports [8-14]. Representative images for each group are presented in Figures 2-5. Figures illustrate the wide spectrum of SUVmax observed in both malignant and benign dento-maxillofacial conditions.

Malignant lesions consistently demonstrated high FDG uptake (Figure 4), and this showed their high metabolic activity, while benign findings—including inflammatory maxillary sinus disease, periodontal infections, and degenerative temporomandibular joint changes—showed variable but occasionally lower SUVmax. Benign lesions with inflammatory or reparative activity can mimic malignancy on PET/CT. Misinterpretation of these findings may lead to unnecessary biopsies, treatment delays, or unwarranted anxiety. This study also highlights that low SUVmax do not always rule out malignancy. Some malignant tumors, especially low-grade, early-stage, or histologically less metabolically active cancers can demonstrate SUVmax overlapping with benign conditions

https://doi.org/10.5455/annalsmedres.2025.06.162

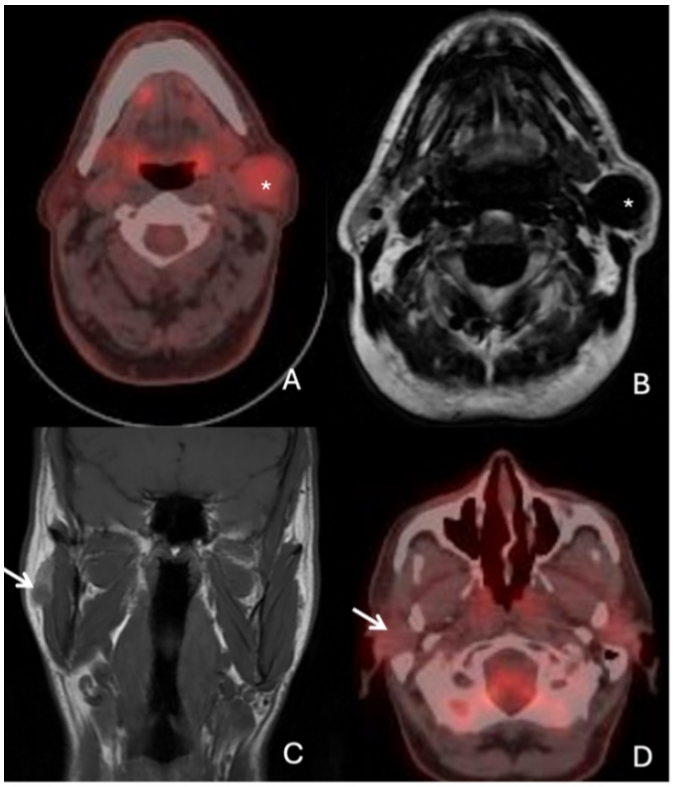

Figure 5. A 60-year-old female diagnosed with adenocystic carcinoma of the left parotid gland. Imaging revealed a solid lesion measuring 27x25x40 mm in the posterior inferior part of the gland (A), characterized by hypointense lesion on axial LAVA Flex MR image (B). A 45-year-old male initially diagnosed with a pleomorphic adenoma of the right parotid gland based on imaging findings showing dimensions of 12.5 x 13.5 x 13 mm with mild hypointense lesion on coronal Fast Spin Echo T1-weighted images (C). PET/CT imaging, however, revealed no malignant activity within the lesion (D).

(Figure 5). Such findings present a critical limitation of relying only on SUVmax thresholds for diagnosis. Careful interpretation of imaging context, lesion morphology, and histopathological confirmation remains essential to avoid misdiagnosis or delayed treatment.

FDG-PET/CT is a powerful diagnostic tool but must be interpreted with caution in the head and neck due to physiological uptake. As summarized in Table 4, normal uptake in Waldeyer's ring, salivary glands, muscles, and brown fat may mimic malignancy [1,3,5,7]. Co-registration with CT enables precise localization of FDG activity, helping distinguish normal physiology from pathology (Table 4).

Our findings demonstrate that malignant lesions displayed higher SUVmax than benign conditions ($p<0.01$). Prior studies reporting SUVmax thresholds of 6.0–12.0 for head and neck squamous cell carcinoma and other malignancies [8-13]. The ROC analysis of this present study revealed a cut-off of 6.6, which is a correlated finding with Schwaninger et al. [8]. Schwaninger et al. [8] reported FDG accumulation in acute periapical inflammation, though they found no correlation with periapical index scores. Ito et al. [9] demonstrated the value of PET/CT in assessing periodontal disease and predicting complications such as osteonecrosis. Yamashiro et al. [10] similarly noted that FDG uptake was present in acute infections but absent in chronic apical infections, supporting PET/CT as a screening tool for high-risk infections. Our results are consistent with these findings, as no FDG uptake was observed in chronic periodontal disease cases in this study. Chronic maxillary sinusitis typically demonstrates minimal or absent hypermetabolic activity on PET/CT, whereas sinonasal carcinoma shows markedly increased FDG uptake (Figure 3). These imaging patterns correlate with CT findings; sinonasal carcinoma often exhibits ill-defined, irregular borders and invasive features, helping radiologists differentiate malignant tumors from inflammatory or benign sinonasal conditions [12,13].

Identifying infection foci before cancer therapy is critical, especially in patients scheduled for head and neck radiotherapy or chemotherapy. Chronic lesions may appear inactive on PET/CT but can exacerbate during treatment, leading to osteonecrosis or delayed healing [9,13,14]. Schuurhuis et al. [15] emphasized that severe periodontal disease increases the risk of post-radiotherapy complications. Early detection of hypermetabolic lesions on PET/CT can guide referral to oral care specialists [10,15,16].

This study identified dental prosthetic artifacts affecting FDG-PET/CT quality, emphasizing the need to remove dentures before scanning. PET/CT also revealed the heterogeneity of FDG uptake in malignancies; SUVmax variability across tumor types and stages reflects the biological diversity of cancers [17,18]. Prior studies indicate SUVmax can predict disease progression and survival [17,19], which is valuable as a biomarker.

Limitations

This study is limited by its retrospective design, single-center scope, and small sample size. Intraoral examinations, which are critical for comprehensive cancer treatment planning, were not available. Additionally, SUVmax variability can be influenced by patient preparation, imaging protocols, and FDG uptake timing; standardizing these parameters could improve reproducibility. Larger, prospective studies are needed to validate these findings and further characterize FDG uptake in diverse dentomaxillofacial pathologies.

CONCLUSION

The objectives of this study were to evaluate the distribution and metabolic activity of dento-maxillofacial lesions and potential inflammatory pathologies on FDG-PET/CT scans, and to compare these findings on CT and MR images. This study indicated that a significant proportion of radiologically detected periapical lesions, areas of marginal periodontal bone loss, and other possible inflammatory jaw pathologies did not exhibit increased metabolic activity or signs of acute inflammation on FDG-PET/CT, regardless of their radiological extent or location. However, the study did identify various cases

https://doi.org/10.5455/annalsmedres.2025.06.162

that could be valuable for future research and radiologic assessments. These findings show the necessity for further studies to evaluate a broader range of images, potentially improving our understanding of the metabolic activity in various dento-maxillofacial pathologies.

Data Availability: The data supporting the findings of this study are available from the corresponding author upon reasonable request.

Ethics Committee Approval: This study was approved by Kocaeli Health and Technology University Non-Invasive Clinical Research Ethics Committee with project no: 2024-101 at 10.01.2024.

Informed Consent: In this study, only patients with present informed consent were included.

Peer-review: Externally peer-reviewed.

Conflict of Interest: The authors declare that there are no conflicts of interest regarding this study.

Author Contributions: Concept: MSM, MÖ; Methodology: MÖ, MSM; Data Collection: MÖ; Data Analysis: MÖ; Writing: MSM; Review & Editing: MÖ, MSM.

Financial Disclosure: The authors declare that this research received no specific grant from any funding agency in the public, commercial, or not-for-profit sectors and that they have no financial interests related to the study.

REFERENCES

1. Kung BT, Seraj SM, Zadeh MZ, et al. An update on the role of 18F-FDG-PET/CT in major infectious and inflammatory diseases. *Am J Nucl Med Mol Imaging.* 2019;9(6): 255-73. PMID: 31976156.
2. Machiels JP, René Leemans C, Golusinski W, et al. Squamous cell carcinoma of the oral cavity, larynx, oropharynx and hypopharynx: EHNS-ESMO-ESTRO Clinical Practice Guidelines for diagnosis, treatment and follow-up. *Ann Oncol.* 2020;31(11): 1462-75. doi: 10.1016/j.annonc.2020.07.011.
3. Childs L, Thompson A, Jones H, Hameeduddin A, Ghufoor K, Adams A. Atypical 18F-FDG PET-CT uptake in the head and neck; a case-based pictorial review. *Clin Imaging.* 2018;49:136-43. doi: 10.1016/j.clinimag.2018.01.006.
4. Pfister DG, Spencer S, Adelstein D, et al. Head and Neck Cancers, Version 2.2020, NCCN Clinical Practice Guidelines in Oncology. *J Natl Compr Canc Netw.* 2020;18(7): 873-98. doi: 10.6004/jnccn.2020.0031.
5. Purohit BS, Ailianou A, Dulguerov N, Becker CD, Ratib O, Becker M. FDG-PET/CT pitfalls in oncological head and neck imaging. *Insights Imaging.* 2014;5(5): 585-602. doi: 10.1007/s13244-014-0349-x.
6. Von Elm E, Altman DG, Egger M, Pocock SJ, Gøtzsche PC, Vandenbroucke JP; STROBE Initiative. The Strengthening the Reporting of Observational Studies in Epidemiology (STROBE) statement: guidelines for reporting observational studies. *Lancet.* 2007;370(9596):1453–7. doi: 10.1016/S0140-6736(07)61602-X.
7. Park JY, Lee YH. The Role of 18F-FDG PET/CT for Evaluation of Cervical Metastatic Lymph Nodes in a Patient with Metallic Artifacts from Dental Prosthesis: A case report. *Nucl Med Mol Imaging.* 2020;54(5): 252-5. doi: 10.1007/s13139-020-00658-3.
8. Schwaninger DR, Hüllner M, Bichsel D, et al. FDG-PET/CT for oral focus assessment in head and neck cancer patients. *Clin Oral Investig.* 2022;26(6): 4407-18. doi: 10.1007/s00784-022-04403-2.
9. Ito K, Takumi K, Meibom SK, Qureshi MM, Fujima N, Andreu-Arasa VC, Truong MT, Salama AR, Kaneda T, Sakai O. Risk assessment of osteoradionecrosis associated with periodontitis using 18F-FDG PET/CT. *Eur J Radiol.* 2020;132:109259. doi: 10.1016/j.ejrad.2020.109259.
10. Yamashiro K, Nakano M, Sawaki K, Okazaki F, Hirata Y, Takashiba S. The potential of positron emission tomography/computerized tomography (PET/CT) scanning as a detector of high-risk patients with oral infection during preoperative staging. *Oral Surg Oral Med Oral Pathol Oral Radiol.* 2016;122(2):242-9. doi: 10.1016/j.oooo.2016.04.006.
11. Shimamoto H, Tatsumi M, Kakimoto N, Hamada S, Shimosegawa E, Murakami S, Furukawa S, Hatazawa J. (18)F-FDG accumulation in the oral cavity is associated with periodontal disease and apical periodontitis: an initial demonstration on PET/CT. *Ann Nucl Med.* 2008;22(7):587-93. doi:10.1007/s12149-008-0153-0.
12. Umeda N, Hayama M, Nakamura A, Maeda Y, Inohara H. An Unusual Case of Maxillary Sinus Cholesterol Granuloma Showing FDG Uptake on PET/CT. *Clin Nucl Med.* 2021;46(2):e131-e132. doi: 10.1097/RLU.0000000000003327.
13. Meerwein CM, Nakadate M, Stolzmann P, et al. Contrast-enhanced 18F-FDG-PET/CT for Differentiating Tumour and Radionecrosis in Head and Neck Cancer: Our experience in 37 Patients. *Clin Otolaryngol.* 2018;43(6):1594-99. doi: 10.1111/coa.13185.
14. Meerwein CM, Queiroz M, Kollias S, Hüllner M, Veit-Haibach P, Huber GF. Post-treatment surveillance of head and neck cancer: pitfalls in the interpretation of FDG PET-CT/MRI. *Swiss Med Wkly.* 2015;145:14116. doi: 10.4414/smw.2015.14116.
15. Schuurhuis JM, Stokman MA, Witjes MJH, et al. Patients with advanced periodontal disease before intensity-modulated radiation therapy are prone to develop bone healing problems: a 2-year prospective follow-up study. *Support Care Cancer.* 2018;26(4):1133-42. doi: 10.1007/s00520-017-3934-y.
16. Joshi VK. Dental treatment planning and management for the mouth cancer patient. *Oral Oncol.* 2010;46(6):475-9. doi: 10.1016/j.oraloncology.2010.03.010.
17. Kwak YK, Park HH, Choi KH, et al. SUVmax Predicts Disease Progression after Stereotactic Ablative Radiotherapy in Stage I Non-small Cell Lung Cancer. *Cancer Res Treat.* 2020;52(1):85-97. doi: 10.4143/crt.2019.007.
18. Riva G, Imparato S, Savietto G, et al. Potential role of functional imaging in predicting outcome for patients treated with carbon ion therapy: a review. *Br J Radiol.* 2021;94(1128):20210524. doi: 10.1259/bjr.20210524.
19. Inubushi M, Saga T, Koizumi M, et al. Predictive value of 3'-deoxy-3'-[18F]fluorothymidine positron emission tomography/computed tomography for outcome of carbon ion radiotherapy in patients with head and neck mucosal malignant melanoma. *Ann Nucl Med.* 2013;27(1):1-10. doi: 10.1007/s12149-012-0652-x.

https://doi.org/10.5455/annalsmedres.2025.06.162

Ann Med Res

Current issue list available at Ann Med Res

Annals of Medical Research

journal page: annalsmedres.org

Association of hOGG1 and APE1 gene polymorphisms with disease severity in ulcerative colitis: A case-control study

Elif Altunel Kilinc [a,*], Yuksel Seckin [b], Gonca Gulbay [c], Elif Yesilada [c], Yasir Furkan Cagin [b], Ibrahim Orman [b]

[a]Mersin City Training and Research Hospital, Department of Rheumatology, Mersin, Türkiye
[b]Inonu University, Faculty of Medicine, Department of Gastroenterology, Malatya, Türkiye
[c]Inonu University, Faculty of Medicine, Department of Medical Biology and Genetics, Malatya, Türkiye
*Corresponding author: elifaltunel@hotmail.com (Elif Altunel Kilinc)

MAIN POINTS

- The hOGG1 Ser326Cys polymorphism was significantly associated with severe ulcerative colitis activity, suggesting its potential role in disease progression.
- The APE1 Asp148Glu polymorphism showed no significant association with disease presence or severity.
- Impaired base excision repair (BER) capacity may contribute to increased oxidative DNA damage and inflammation in UC.
- The hOGG1 Ser326Cys variant could serve as a genetic biomarker for disease severity and guide personalized management in UC patients.

Cite this article as: Altunel Kilinc E, Seckin Y, Gulbay G, Yesilada E, Cagin YF, Orman I. Association of hOGG1 and APE1 gene polymorphisms with disease severity in ulcerative colitis: A case-control study. *Ann Med Res*. 2025;32(12):535–540. doi: 10.5455/annalsmedres.2025.07.186.

ABSTRACT

Aim: Ulcerative colitis (UC) is a chronic inflammatory disease of the colon characterized by excessive oxidative stress and impaired DNA repair mechanisms. This study aimed to investigate the relationship between two key base excision repair gene polymorphisms---APE1 (Asp148Glu) and hOGG1 (Ser326Cys)---and clinical features of UC, particularly disease activity.

Materials and Methods: Ninety-nine UC patients, 50 colorectal cancer (CRC) patients, and 50 age- and gender-matched healthy controls were enrolled. Peripheral blood samples were collected for DNA extraction, and genotyping was performed using real-time PCR and melting curve analysis. Clinical data, including disease duration, location, and activity based on the Truelove-Witts index, were analyzed about genetic variants.

Results: No significant differences were found in the genotype or allele frequencies of APE1 and hOGG1 between UC, CRC, and control groups. However, the hOGG1 Ser326Cys polymorphism was significantly more frequent in UC patients with severe disease activity ($p = 0.034$), suggesting a possible role in disease progression.

Conclusion: The hOGG1 Ser326Cys polymorphism may be associated with increased disease severity in UC and could serve as a potential prognostic biomarker. Further studies are needed to validate this finding in larger cohorts.

Keywords: Ulcerative colitis, DNA repair, Genetic polymorphism, Reactive oxygen species

Received: Jul 17, 2025 **Accepted:** Sep 09, 2025 **Available Online:** Dec 25, 2025

INTRODUCTION

Ulcerative colitis (UC) is a chronic inflammatory disorder characterized by recurring inflammation of the colonic mucosa, often extending from the rectum to the cecum [1]. One of the key pathogenic mechanisms in UC is oxidative stress, which arises from an imbalance between prooxidant and antioxidant systems. This imbalance promotes the excessive production of reactive oxygen species (ROS) that interact with cellular components, leading to damage to DNA, proteins, and lipids [2,3].

In addition to oxidative stress and impaired DNA repair, ulcerative colitis is increasingly recognized as an autoimmune disorder driven by complex immune dysregulation. Imbalances in innate and adaptive immunity, particularly alterations in T helper subsets, regulatory T-cell dysfunction, and plasmablast-skewed humoral responses, play central roles in sustaining chronic mucosal inflammation [4,5]. Furthermore, environmental and dietary factors are now considered important modulators of oxidative stress and disease course, with evidence linking processed food intake, microbiota composition, and eating behaviors to UC pathogenesis [6-8]. Integrating genetic, immunological, and environmental perspectives therefore provides a more comprehensive framework for understanding UC pathophysiology.

DNA damage caused by ROS includes single-base modifications, strand breaks, and intra/inter-strand cross-links [3].

Under physiological conditions, such damage is counteracted by complex DNA repair systems, among which base excision repair (BER) plays a central role in repairing oxidative lesions [9–11]. Key enzymes in this pathway include apurinic/apyrimidinic endonuclease 1 (APE1) and human 8-oxoguanine DNA glycosylase (hOGG1), which recognize and excise oxidized bases to maintain genomic stability [12,13].

Genetic polymorphisms in BER enzymes may impair their activity and contribute to reduced DNA repair capacity. In particular, the APE1 Asp148Glu and hOGG1 Ser326Cys polymorphisms have been associated with altered enzymatic function [13,14]. These polymorphisms can potentially exacerbate oxidative stress by reducing DNA repair efficiency, thereby contributing to persistent inflammation and increasing susceptibility to neoplastic transformation [15,16].

Although much of the literature has focused on the role of these variants in colorectal cancer (CRC), their impact on the severity and clinical course of UC remains less clear. Given the shared pathophysiological mechanisms of oxidative stress and inflammation in UC and CRC, investigating these polymorphisms in UC may offer insights into disease progression and outcomes.

This study aims to investigate the prevalence of APE1 (Asp148Glu) and hOGG1 (Ser326Cys) polymorphisms in UC patients and to assess their associations with clinical characteristics, including disease duration, location, and activity. By comparing UC patients with CRC patients and healthy controls, this study seeks to clarify whether these DNA repair variants play a role in the clinical phenotype of UC and may serve as potential biomarkers for disease severity or prognosis.

MATERIALS AND METHODS

Study design and participants

This cross-sectional study included three groups: 99 patients diagnosed with UC, 50 patients with histopathologically confirmed CRC, and 50 age- and gender-matched healthy controls. Ethical approval was obtained from the İnönü University Ethics Committee (Approval Number: 2017/58). Written informed consent was obtained from all participants in accordance with the Declaration of Helsinki.

The required sample size was estimated using G*Power software for a chi-square test comparing genotype distributions across three independent groups (UC, CRC, and healthy controls). Assuming a medium effect size (w = 0.3), a significance level of $\alpha = 0.05$, and a power of 0.80, the minimum recommended sample size was 108 participants (approximately 36 per group). Our study included 99 UC patients, 50 CRC patients, and 50 healthy controls, exceeding the minimum requirement for adequate statistical power.

Clinical evaluation and classification

Demographic data, including age, gender, disease duration, and disease location, were collected from hospital electronic medical records. For UC patients, disease activity was assessed using the Truelove-Witts index at the time of admission [17]. Based on clinical and laboratory parameters, disease activity was categorized as:

- *Mild disease:* ≤4 stools/day, erythrocyte sedimentation rate <30 mm/h, absence of fever and tachycardia, mild anemia.
- *Severe disease:* >6 bloody stools/day, fever >37.5°C, hemoglobin <75% of normal, tachycardia >100 bpm.
- *Moderate disease:* Findings between mild and severe presentations.

UC patients were further classified by disease extent:

- *Proctitis:* Limited to the rectum
- *Left-sided colitis:* Involving colon up to the splenic flexure
- *Extensive colitis (pancolitis):* Extending beyond the splenic flexure

CRC patients were grouped based on tumor location: rectum, left colon, or right colon.

Sample collection and DNA extraction

Peripheral blood samples (2 mL) were collected in EDTA tubes from all participants. Genomic DNA was extracted using the PureLink Genomic DNA Mini Kit (Invitrogen, Thermo Fisher Scientific) following the manufacturer's instructions.

Genotyping and polymorphism analysis

Genotyping of APE1 (Asp148Glu) and hOGG1 (Ser326Cys) polymorphisms was performed using real-time PCR and melting curve analysis on the LightCycler 2.0 system (Roche). The assays measured fluorescence during amplification, and melting curves were used to distinguish between genotypes.

- *APE1 (Asp148Glu):* A T-to-G substitution at nucleotide 2197 causes an Asp→Glu change at codon 148. Genotypes (Asp/Asp [AA], Asp/Glu [AG], Glu/Glu [GG]) were identified using LightSNiP assays (TIB-MolBiol, Berlin, Germany).
- *hOGG1 (Ser326Cys):* A C-to-G substitution at nucleotide 1245 results in a Ser→Cys change at codon 326. Genotypes (Ser/Ser [SS], Ser/Cys [SC], Cys/Cys [CC]) were determined using the same platform.

https://doi.org/10.5455/annalsmedres.2025.07.186

Statistical analysis

Statistical analyses were performed using IBM SPSS Statistics version 22.0 (Armonk, NY: IBM Corp.). The Kolmogorov–Smirnov test was applied to assess the normality of continuous variables. Since the distribution of age was not normal, results were summarized as median (minimum–maximum), and comparisons among the three groups (UC, CRC, and controls) were conducted using the Kruskal–Wallis test. As no significant difference was detected, post-hoc pairwise analyses were not performed. Categorical variables were expressed as counts and percentages, and comparisons were performed using the Pearson Chi-Square or Fisher's exact test as appropriate. A p-value <0.05 was considered statistically significant.

RESULTS

Demographic and clinical characteristics

A total of 99 UC patients (42.4% female; median age: 46 [min:36 max:58] years), 50 CRC patients (42% female; median age: 48 [min:41 max:55] years), and 50 healthy controls (42% female; median age: 44 [min:40 max:56] years) were included. There were no statistically significant differences among the three groups in terms of age (p = 0.778) or gender distribution (p = 0.998).

Table 1. Demographic and clinical characteristics of ulcerative colitis patients.

UC patients, n	99
Age (years), median (min-max)	46 (36-58)
Female, n(%)	42 (42.4)
Disease duration, month	81.32
Location, n(%)	
• Proctitis	21 (21.2)
• Left colon	56 (56.4)
• Extensive	22 (22.2)
Truelove-Witts disease activity index, n(%)	
• Mild	71 (71.7)
• Moderate	20 (20.2)
• Severe	8 (8.1)

UC: Ulcerative colitis, SD: Standard deviation.

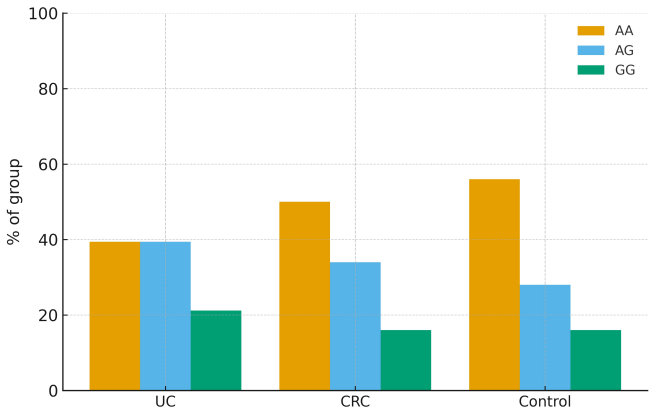

Figure 1. APE1 genotype distribution among study groups.

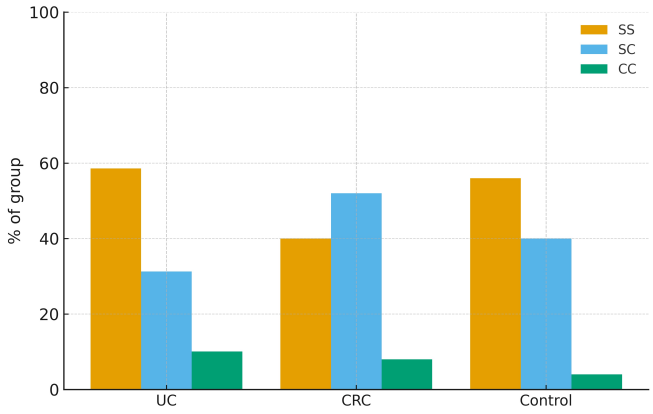

Figure 2. hOGG1 genotype distribution among study groups.

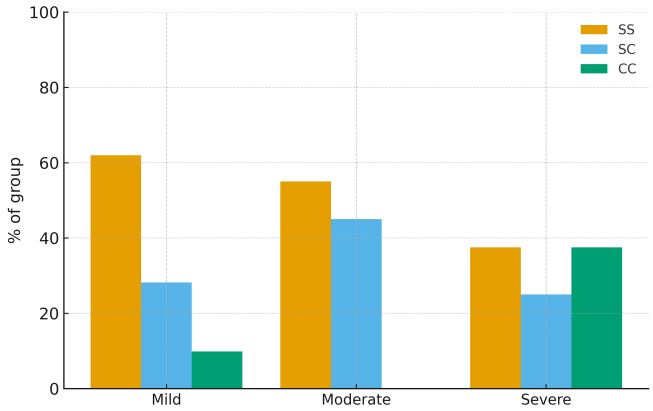

Figure 3. hOGG1 genotype distribution according to disease severity in ulcerative colitis.

The mean disease duration was 81.3 months in UC patients. UC localization was: proctitis (22%), left-sided colitis (56%), and pancolitis (22%). According to the Truelove-Witts index, disease activity was mild in 71.7%, moderate in 20.2%, and severe in 8.1% of UC patients (Table 1).

CRC group characteristics were as follows; of the 50 patients, 42% were female, and the mean age was 48 ± 2 years. The average disease duration was 62.5 months. Tumor localization showed that 58% of CRC patients had rectal involvement, 30% had tumors located in the left colon, and 12% had right-sided colon involvement.

Genotype and allele distribution of APE1 and hOGG1

In the APE1 polymorphism analysis, the distribution of genotypes across UC, CRC, and control groups was as follows; in the UC group, 39.4% had the AA genotype, 39.4% had AG, and 21.2% had GG. Among CRC patients, 50% had AA, 34% AG, and 16% GG. In the control group, the frequencies were 56% (AA), 28% (AG), and 16% (GG). No statistically significant differences were observed among the three groups regarding genotype distribution (p = 0.384) or allele frequencies (p = 0.135) (Figure 1).

Regarding the hOGG1 polymorphism; in the UC group,

https://doi.org/10.5455/annalsmedres.2025.07.186

Table 2. Genotypic distribution of disease severity and APE1 and hOGG1 in UC.

Disease Severity	APE1						P-value	hOGG1						P-value
	AA		AG		GG			SS		SC		CC		
	n	%	n	%	n	%		n	%	n	%	n	%	
Mild	27	38	29	40	15	21.1		44	61.9	20	28.3	7	9.8	
Moderate	8	40	7	35	5	25	0.940	11	55	9	45	0	0	0.034*
Severe	4	50	3	37.5	1	12.5		3	37.5	2	25	3	37.5	

APE1: The apurinic/apyrimidinic endonuclease 1, A: Aspartic acid, C: Cysteine, G: Glutamic acid hOGG1: The human 8- oksoguanin DNA glycosylase, S: Serin, , *p<0.05.

58.6% had the SS genotype, 31.3% SC, and 10.1% CC. Among CRC patients, 40% had SS, 52% SC, and 8% CC. In controls, 56% were SS, 40% SC, and 4% CC. Again, there were no significant differences among the groups in genotype distribution (p = 0.110) or allele frequencies (p = 0.219) (Figure 2).

Association between polymorphisms and disease location

The distribution of APE1 and hOGG1 genotypes according to disease or tumor location was analyzed in both UC and CRC groups. Among UC patients, those with proctitis exhibited APE1 genotypes as follows: AA 47.6%, AG 38.1%, and GG 14.3%; hOGG1 genotypes were SS 52%, SC 28.6%, and CC 19%. In patients with left-sided colitis, APE1 genotypes were AA 37.5%, AG 42.9%, and GG 19.6%; hOGG1 genotypes were SS 62.5%, SC 33.9%, and CC 3.6%. In those with pancolitis, the APE1 distribution was AA 36.4%, AG 31.8%, and GG 31.8%; hOGG1 distribution was SS 54.5%, SC 27.3%, and CC 18.2%. Statistical analysis showed no significant association between genotype and disease location in UC patients for either APE1 (p = 0.724) or hOGG1 (p = 0.170).

Similarly, in the CRC group, among patients with rectal tumors, APE1 genotypes were distributed as AA 48.3%, AG 37.9%, and GG 13.8%; hOGG1 genotypes were SS 34.5%, SC 55.2%, and CC 10.3%. For left colon tumors, APE1 distribution was AA 46.7%, AG 33.3%, and GG 20%; hOGG1 distribution was SS 53.5%, SC 40%, and CC 6.7%. In patients with right colon tumors, APE1 genotypes were AA 66.7%, AG 16.7%, and GG 16.7%; hOGG1 genotypes were SS 33.3%, SC 66.7%, and CC 0%. No significant differences were observed in the distribution of genotypes by tumor location in CRC patients for either APE1 (p = 0.905) or hOGG1 (p = 0.690).

Association between gene polymorphisms and disease activity in UC

No significant association was found between APE1 genotypes and disease activity in UC patients (p = 0.940). In contrast, hOGG1 genotypes were significantly associated with disease activity (p = 0.034). The Cys/Cys genotype was more frequently observed in patients with severe UC, suggesting a potential role in disease severity (Table 2) (Figure 3). Although the overall association between hOGG1 genotype and UC disease severity was statistically significant, post-hoc pairwise Fisher's exact tests with Bonferroni adjustment did not reveal significant differences between specific severity categories. The strongest trend was observed between the moderate and severe groups (p=0.051, adjusted), where the Cys/Cys genotype was more frequent in severe UC.

Allele frequencies by disease severity

Although the frequency of the C allele of hOGG1 appeared higher in patients with severe disease (50%) compared to those with mild (23.9%) or moderate (22.5%) disease, this trend did not reach statistical significance (p = 0.680).

DISCUSSION

In this case-control study, we evaluated the association between two critical base excision repair (BER) gene polymorphisms—APE1 (Asp148Glu) and hOGG1 (Ser326Cys)—and clinical characteristics of ulcerative colitis (UC), particularly disease activity. Although no significant differences were observed in the overall distribution of these polymorphisms between UC, colorectal cancer (CRC), and healthy control groups, our results revealed a statistically significant association between the hOGG1 Cys/Cys genotype and severe UC activity. These findings highlight the possible role of impaired DNA repair mechanisms in modulating disease severity in UC.

The hOGG1 enzyme plays a pivotal role in excising 8-oxoguanine, one of the most mutagenic oxidative DNA lesions generated by reactive oxygen species (ROS) during chronic inflammation. The Ser326Cys polymorphism, which causes a serine-to-cysteine substitution at codon 326, has been shown to reduce hOGG1 enzymatic efficiency, impairing the repair of oxidative DNA damage [11,13]. This reduction in DNA repair capacity can lead to the accumulation of oxidative lesions in epithelial cells, which in turn sustains inflammation, disrupts mucosal integrity, and may drive more severe clinical manifestations in UC. Our finding that the Cys/Cys genotype is significantly more frequent among patients with severe UC activity supports this proposed mechanism.

This result aligns with prior research showing increased expression of OGG1 in inflamed and dysplastic colonic mucosa of UC patients and in tissues undergoing malignant transformation [18,19]. The accumulation of unrepaired oxidative

https://doi.org/10.5455/annalsmedres.2025.07.186

DNA damage in individuals with the Cys/Cys genotype may contribute to enhanced activation of DNA damage response pathways such as p53, NF-κB, and STAT3, thereby amplifying the inflammatory process and mucosal injury. Moreover, oxidative stress in UC has been implicated in epithelial apoptosis, barrier dysfunction, and dysbiosis—all of which are hallmarks of severe disease. These mechanistic links between impaired DNA repair and inflammation offer a plausible biological explanation for our observed genotype-phenotype association.

In contrast, the APE1 (Asp148Glu) polymorphism did not demonstrate a significant association with UC severity or with the presence of disease in our cohort. While APE1 is a crucial enzyme in the BER pathway responsible for cleaving the DNA backbone at abasic sites, the functional consequences of the Asp148Glu variant are more nuanced and may be tissue- or context-specific. Some studies have reported increased risk of UC with this variant, particularly in cohorts with high inflammatory activity [20]. However, our cohort included a relatively low proportion of patients with severe disease, which may have limited the statistical power to detect subtle associations.

Additionally, APE1 has dual roles—not only in DNA repair but also in redox regulation of transcription factors involved in inflammation. These regulatory functions may be differentially expressed in colonic tissue compared to peripheral blood, which we used for genotyping. Studies using colonic biopsies have demonstrated increased APE1 expression in inflamed mucosa, suggesting that tissue-level post-translational modifications or epigenetic changes may influence the functional impact of this polymorphism [21]. Therefore, the lack of association in our study may reflect the importance of local tissue environment and dynamic gene expression over static germline variants.

Although our study design included a CRC group due to the shared pathogenic features with UC, particularly oxidative stress and chronic inflammation, neither polymorphism was significantly enriched in CRC patients compared to controls. This may be due to the relatively small sample size or to the multifactorial nature of CRC, where cumulative somatic mutations, microsatellite instability, and environmental exposures play a dominant role beyond single-gene polymorphisms. Nevertheless, the overlap between pathways implicated in UC and CRC—especially those involving ROS and DNA repair—warrants further longitudinal studies to explore whether hOGG1 variants in UC patients could predict neoplastic transformation risk over time.

The identification of the hOGG1 Ser326Cys variant as a potential marker of severe UC activity has clinical implications. First, it supports the hypothesis that genetic susceptibility related to oxidative DNA damage modulates disease progression. Second, it highlights the need for genotype-guided risk stratification in UC management. Patients with the Cys/Cys genotype may benefit from closer endoscopic surveillance and more aggressive anti-inflammatory or antioxidant therapies. Third, this variant may represent a candidate biomarker for identifying individuals at increased risk of complications such as treatment resistance or CRC development.

Identification of UC patients carrying the hOGG1 Ser326Cys variant, particularly the Cys/Cys genotype, may provide valuable information for individualized disease management. Since these patients appear to be more prone to severe disease activity, clinicians could consider closer clinical and endoscopic monitoring, earlier escalation of medical therapy, and stricter surveillance for complications such as treatment resistance or colorectal neoplasia. Integrating genetic risk markers like hOGG1 into follow-up strategies may therefore improve prognostic stratification and guide more personalized approaches to long-term UC care.

Limitations

Our study has several limitations. The relatively small number of patients with severe UC limits the generalizability of our findings. The cross-sectional design precludes causal inference, and functional assays of hOGG1 or APE1 activity were not performed. Furthermore, environmental factors such as smoking, diet, or microbiome composition—which can modulate oxidative stress—were not controlled for. Future studies should include mucosal tissue analysis, longitudinal follow-up, and integration of transcriptomic or epigenetic data to clarify the functional consequences of these polymorphisms. In addition, environmental and dietary factors, which are known to influence oxidative stress and inflammatory responses, were not assessed in our study. As such, we cannot exclude the possibility that these unmeasured variables may have contributed to the observed genotype–phenotype correlations.

CONCLUSION

In summary, our study suggests that the hOGG1 Ser326Cys polymorphism is associated with increased disease severity in ulcerative colitis, potentially due to impaired DNA repair and enhanced oxidative stress. While the APE1 Asp148Glu variant did not show a similar association, its context-dependent role warrants further investigation. These findings underscore the relevance of BER gene variants in UC pathogenesis and may inform future biomarker development for prognostic and therapeutic purposes.

Ethics Committee Approval: Ethical approval was obtained from the İnönü University Ethics Committee (Approval Number: 2017/58).

Informed Consent: Written informed consent was obtained from all participants included in the study.

Peer-review: Externally peer-reviewed.

Conflict of Interest: The authors declare that they have no conflict of interest.

https://doi.org/10.5455/annalsmedres.2025.07.186

Author Contributions: Conceptualization: E.A.K, Y.S. Methodology: E.A.K., Y.S., E.Y, G.G. Formal analysis and investigation: E.A.K., Y.S, G.G. Writing - original draft preparation: E.A.K., Y.F.Ç., İ.O. Writing - review and editing: E.A.K., Y.F.Ç., İ.O., G.G. Funding acquisition: E.A.K., Y.F.Ç., İ.O, Y.S, E.Y. Resources: E.A.K., Y.F.Ç., İ.O. Supervision: E.A.K., Y.F.Ç., İ.O, Y.S, E.Y., G.G.

Financial Disclosure: Our study was supported by the İnönü University Scientific Research Projects Unit (Project code: TTU-2017-708).

REFERENCES

1. Meier J, Sturm A. Current treatment of ulcerative colitis. *World J Gastroenterol.* 2011;17(27):3204-3212. PMID: 21912469.
2. DE Angelis PM, Dorg L, Pham S, Andersen SN. DNA Repair Protein Expression and Oxidative/Nitrosative Stress in Ulcerative Colitis and Sporadic Colorectal Cancer. *Anticancer Res.* 2021;41(7):3261-3270. doi: 10.21873/anticanres.15112.
3. Melis JP, van Steeg H, Luijten M. Oxidative DNA damage and nucleotide excision repair. *Antioxid Redox Signal.* 2013;18(18):2409-19. doi: 10.1089/ars.2012.5036.
4. Kobayashi T, Siegmund B, Le Berre C, Wei SC, Ferrante M, Shen B, et al. Ulcerative colitis. *Nat Rev Dis Primers.* 2020;6(1):74. doi: 10.1038/s41572-020-0205-x.
5. Tang X, Zhao Y, Chen Y, Yang Y. Immune dysregulation in ulcerative colitis: current perspectives and future directions. *Front Cell Dev Biol.* 2025;13:1610435. doi: 10.3389/fcell.2025.1610435.
6. Liang Y, Li Y, Lee C, Yu Z, Chen C, Liang C. Ulcerative colitis: molecular insights and intervention therapy. *Mol Biomed.* 2024;5(1):42. doi: 10.1186/s43556-024-00207-w.
7. Qin L, Sun R, Zhao Y, Li J, Wang H. Dietary content and eating behavior in ulcerative colitis: insights into pathogenesis and management. *Nutr J.* 2025;24(1):12. doi: 10.1186/s12937-025-01075-y.
8. Calvez V, Li X, Zeng H, Gomez-Nguyen A, Patel D, Zhou Y, et al. Novel insights into inflammatory bowel disease pathogenesis from multi-omics approaches. *Biomedicines*. 2025;13(2):305. doi: 10.3390/biomedicines13020305.
9. Ford JM, Kastan MB. DNA damage response pathways and cancer. Abeloff's Clinical Oncology. 2020;154-164.e154.
10. de Boer J, Hoeijmakers JHJ. Nucleotide excision repair and human disease. *Carcinogenesis.* 2000;21(3):453-460. doi: 10.1093/carcin/21.3.453.
11. Sancar A, Lindsey-Boltz LA, Unsal-Kaçmaz K, Linn S. Molecular mechanisms of mammalian DNA repair and the DNA damage checkpoints. *Annu Rev Biochem.* 2004;73:39-85. doi: 10.1146/annurev.biochem.73.011303.073723
12. Robertson AB, Klungland A, Rognes T, Leiros I. DNA repair in mammalian cells: Base excision repair: the long and short of it. *Cell Mol Life Sci.* 2009;66(6):981-93. doi: 10.1007/s00018-009-8736-z.
13. Gu D, Wang M, Wang S, Zhang Z, Chen J. The DNA repair gene APE1 T1349G polymorphism and risk of gastric cancer in a Chinese population. *PLoS One.* 2011;6(12):e28971. doi: 10.1371/journal.pone.0028971.
14. Park HW, Kim IJ, Kang HC, et al. The hOGG1 Ser326Cys polymorphism is not associated with colorectal cancer risk. *J Epidemiol.* 2007;17(5):156-60. doi: 10.2188/jea.17.156.
15. Goode EL, Ulrich CM, Potter JD. Polymorphisms in DNA repair genes and associations with cancer risk. *Cancer Epidemiol Biomarkers Prev.* 2002;11(12):1513-1530. PMID: 12496039.
16. Bütüner Bilge D, Kantarcı G. Mutasyon, dna hasari, onarim mekanizmalari ve kanserle ilişkisi. *Ankara Ecz. Fak. Derg.* 2006;35(2):149-170.
17. Truelove SC, Witts LJ. Cortisone in ulcerative colitis; final report on a therapeutic trial. *Br Med J.* 1955;2(4947):1041-1048. doi: 10.1136/bmj.2.4947.1041.
18. Vodicka P, Stetina R, Polakova V, et al. Association of DNA repair polymorphisms with DNA repair functional outcomes in healthy human subjects. *Carcinogenesis.* 2007;28(3):657-64. doi: 10.1093/carcin/bgl187.
19. Kumagae Y, Hirahashi M, Takizawa K, et al. Overexpression of MTH1 and OGG1 proteins in ulcerative colitis-associated carcinogenesis. *Oncol Lett.* 2018;16(2):1765-1776. doi: 10.3892/ol.2018.8812.
20. Bardia A, Tiwari SK, Gunisetty S, Anjum F, Nallari P, Habeeb MA, et al. Functional polymorphisms in XRCC-1 and APE-1 contribute to increased apoptosis and risk of ulcerative colitis. *Inflamm Res.* 2012;61(4):359-65. doi: 10.1007/s00011-011-0418-2.
21. Hofseth LJ, Khan MA, Ambrose M, et al. The adaptive imbalance in base excision-repair enzymes generates microsatellite instability in chronic inflammation. *J Clin Invest.* 2003;112(12):1887-94. doi: 10.1172/JCI19757.

https://doi.org/10.5455/annalsmedres.2025.07.186

Ann Med Res

Current issue list available at Ann Med Res

Annals of Medical Research

journal page: annalsmedres.org

In silico characterization of missense mutations in PI3K/AKT/mTOR signaling genes in breast cancer and their role in therapeutic resistance

Betul Akcesme [a,*], Haris Lokvančić [b], Nadia Islam [b]

[a] University of Health Sciences, Hamidiye Faculty of Medicine, Department of Medical Biology , Istanbul, Türkiye
[b] International University of Sarajevo, Faculty of Engineering and Natural Sciences, Department of Genetics and Bioengineering, Sarajevo, Bosnia and Herzegovina
*Corresponding author: betul.akcesme@sbu.edu.tr (Betul Akcesme)

MAIN POINTS

- Comprehensive in silico analysis identified recurrent missense mutations in PI3K/AKT/mTOR pathway genes in breast cancer that are predicted to disrupt protein function.
- The PTEN (D92H, D92N, R130G, R130Q, C136R, and C136Y), AKT1 (L52R), and AKT2 (R170W) variants demonstrated strong deleterious effects across multiple computational prediction tools.
- Structural modeling and interaction analysis revealed that these mutations caused significant alterations in protein stability and non-covalent interactions.
- These findings highlight potential biomarkers for therapeutic resistance and provide candidate targets for future breast cancer precision medicine strategies.

Cite this article as: Akcesme B, Lokvančić H, Islam N. In silico characterization of missense mutations in PI3K/AKT/mTOR signaling genes in breast cancer and their role in therapeutic resistance. *Ann Med Res*. 2025;32(12):541--551. doi: 10.5455/annalsmedres.2025.07.185.

ABSTRACT

Aim: This study aimed to investigate the most frequent missense mutations in key genes of the PI3K/AKT/mTOR signaling pathway to evaluate their potential role in the progression of breast cancer and the development of therapy resistance using computational analyses.

Materials and Methods: Nine genes involved in the PI3K/AKT/mTOR pathway were systematically analyzed by screening mutation databases and applying a range of computational prediction tools to assess the possible deleterious effects of missense variants on protein function and pathway regulation.

Results: Several mutations with predicted deleterious effects were identified, including *PTEN* (D92H, D92N, R130G, R130Q, C136R, and C136Y), *AKT1* (L52R), and *AKT2* (R170W). These variants were predicted to contribute to aberrant PI3K/AKT/mTOR pathway activation, enhanced cancer cell survival, and therapeutic resistance in breast cancer.

Conclusion: The findings provided insights into the mutational landscape of breast cancer, proposing potential biomarkers for risk stratification and novel therapeutic targets. Further experimental validation and functional studies are recommended to clarify the clinical significance of these mutations and to guide the development of personalized interventions for breast cancer.

Keywords: Breast cancer, PI3K/AKT/mTOR pathway, Missense mutations, Computational analysis, Therapy resistance

Received: Jul 10, 2025 **Accepted:** Sep 22, 2025 **Available Online:** Dec 25, 2025

INTRODUCTION

Breast cancer (BC) is one of the leading causes of death among females worldwide and although less common, can also affect men. Currently, chemotherapy, endocrine therapy, and targeted therapy have a high success rate in both disease treatment and disease prevention [1]. The PI3K/AKT/mTOR pathway is linked to disease progression and is also responsible for the development of drug resistance [2]. Currently, only a limited number of therapies are available for the treatment of various subtypes of breast cancer. Endocrine therapy (ET) is used to treat HR+ disease, HER2+ disease is treated with HER2-targeted therapy, and chemotherapy and immunotherapy are used to treat patients with BRCA mutations with triple-negative breast cancer (TNBC). Drug resistance eventually leads to tumor relapse in BC, as well as overexpression of the BC resistance protein (BCRP) and a variety of other events [1,3].

The PI3K/AKT/mTOR pathway plays a critical role in various cellular processes, including cell growth and metabolism [4]. Activation of this pathway typically occurs in response to external stimuli, such as growth factors, leading to the activation of phosphoinositide 3-kinase (PI3K). Subsequent PI3K

activation promotes the recruitment of AKT to the plasma membrane, where AKT is then phosphorylated and activated by phosphoinositide-dependent kinase 1 (PDK1) and the mammalian target of rapamycin complex 2 (mTORC2) [5]. Once activated, AKT promotes the activation of the mechanistic target of rapamycin (mTOR), enabling the regulation of downstream signaling events associated with cellular growth and metabolic control [1,3].

PI3KCA leads to PI3K activation and is one of the most frequently mutated genes in BC. The main role of *PTEN* is to dephosphorylate PIP3 molecules, and AKT cannot be phosphorylated by mTORC2 [6]. *AKT1, AKT2*, and *AKT3* are AKT and are major downstream targets of PI3K. IRS1 activates the PI3K/Akt/mTOR pathway, and its variants are the most studied because they are expressed in different tissues [7]. GSK3B, together with *AKT1, AKT2*, and *AKT3*, activates AKT [8]. TSC1 and TSC2 impact the phosphorylation of mTOR and its downstream effector molecules [9].

Dysregulation of the PI3K/AKT/mTOR pathway is seen in various cancer types [10] and this pathway should serve as a target for therapeutic treatment due to its specific role. Studies conducted on several chemotherapeutic drugs, such as doxorubicin, docetaxel, fluorouracil tamoxifen, and paclitaxel, have shown that chemoresistance can develop, and the main cause is mutations in the PI3K/AKT/mTOR pathway [1,11,12].

This study focused on the PI3K/AKT/mTOR pathway and the genes most frequently mutated in patients with BC. The investigation examines the involvement of the PI3K/AKT/mTOR signaling pathway in drug resistance, with particular attention to specific genes within this pathway. In addition, missense variants in these genes were analyzed to better understand their potential contributions to drug resistance processes. By comprehensively examining the PI3K/AKT/mTOR pathway, its associated genes, and the effects of missense variants, the project aims to provide insights into the molecular mechanisms underlying BC treatment resistance.

MATERIALS AND METHODS

This retrospective, in silico study focused on nine key genes of the PI3K/AKT/mTOR pathway (*PIK3CA, PIK3CB, PIK3CD, PIK3R1, AKT1, AKT2, AKT3, PTEN*, and *MTOR*). We collected somatic missense variants reported in breast cancer from mutation databases (cBioPortal). The most frequent variants were prioritized based on recurrence in breast cancer cohorts and functional impact was assessed using multiple computational prediction tools (PredictSNP, SNPs&GO). Variants predicted as deleterious were further mapped to protein domains (DynaMut and DUET) to predict their impact on protein stability, flexibility, and pathway context. The primary endpoint of the study was the identification of the most frequent missense mutations in the nine PI3K/AKT/mTOR pathway genes, while the secondary endpoint was the predicted functional effect of these variants on protein function and pathway regulation using computational tools.

Retrieval of the target genes

Genes for this study were selected based on their well-established involvement in the PI3K/AKT/mTOR signaling pathway, which plays a pivotal role in BC progression and is recognized as a significant contributor to therapeutic resistance. A recent literature review identified nine pertinent genes for analysis: *PIK3CA, PTEN, AKT1, AKT2, AKT3, IRS1, GSK3B, TSC1,* and *TSC2*. By concentrating on these key regulators within the pathway, this study aims to examine their potential contribution to BC treatment resistance.

The cBioPortal for Cancer Genomics (https://www.cbioportal.org/) was used to identify the most frequent genetic alterations in genes involved in the PI3K/AKT/mTOR pathway among patients with BC. This database provides access to large-scale cancer genomics datasets across various cancer types, including tools for visualization, mutation analysis, and data retrieval. For this study, the "Breast Cancer (METABRIC, Nature 2012 & Nat Commun 2016)" dataset, which includes data from 2,509 patients with BC, was selected as one of the largest datasets in the breast cancer portal.

Identification of mutations in selected genes

Mutations in the selected genes associated with the PI3K/AKT/mTOR pathway were analyzed using the cBioPortal database. These genes were chosen based on their recognized roles within this signaling pathway and their documented associations with BC treatment resistance. Only missense mutations were considered for subsequent analysis. Following stratification by mutation type, the most frequently occurring missense mutations within the BC cohort were identified and prioritized for downstream analysis.

Sequence-based methods for predicting gene pathogenicity

The functional impact of the most frequent missense mutations was evaluated using two sequence-based computational tools: PredictSNP (https://loschmidt.chemi.muni.cz/predictsnp/) and SNPs&GO (https://snps-and-go.biocomp.unibo.it/snps-and-go/). To predict whether a given mutation is likely to be disease-causing or benign and to estimate the potential effect of the mutation on protein function, PredictSNP aggregates results from six individual methods: MAPP, PhD-SNP, PolyPhen-1, PolyPhen-2, SIFT, and SNAP. Alongside the classification, PredictSNP provides a prediction score expressed as a percentage, indicating the prediction's expected accuracy. Higher percentages correspond to greater classification reliability; for example, a score of 85% indicates that the prediction is expected to be correct in 85% of cases based on the integrated tools' benchmarking.

https://doi.org/10.5455/annalsmedres.2025.07.185

Variants predicted as deleterious with high percentage scores were prioritized for downstream analyses. SNPs&GO is another predictive platform that classifies single-point protein mutations as either neutral or associated with protein functional changes. For each variant, SNPs&GO provides a probability score and a Reliability Index (RI) value, which reflects the prediction's confidence level. Higher RI values indicate greater reliability of the classification (Usually RI $\geq$ 7 were considered reliable disease-associated predictions).

FASTA sequences for *PTEN* (P60484), *AKT1* (P31749), and *AKT2* (P31751) were retrieved from the UniProt database (https://www.uniprot.org/).

Structure-based methods for protein stability prediction

DynaMut (https://biosig.lab.uq.edu.au/dynamut/), a structure-based computational tool that applies normal mode analysis to predict changes in protein stability resulting from point mutations, was used to evaluate the impact of the selected mutations on protein stability. The predicted $\Delta\Delta G$ values describe the impact of mutations on protein stability: negative values ($\Delta\Delta G < 0$) indicate destabilization, whereas positive values ($\Delta\Delta G > 0$) suggest stabilization of the protein structure. DynaMut provides vibrational entropy ($\Delta\Delta S$) values to estimate the effect of mutations on molecular flexibility. A positive $\Delta\Delta S$ indicates increased flexibility, whereas a negative $\Delta\Delta S$ reflects reduced flexibility and a more rigid structure. Together, these predictions allow the assessment of both the thermodynamic stability and dynamic behavior of the protein upon mutation. The Protein Data Bank in Europe Knowledge Base (PDBe-KB, https://www.ebi.ac.uk/pdbe/pdbe-kb/) was used to obtain accurate protein structures for analysis, prioritizing those with the lowest resolution values and the largest covered sequences. Moreover, PDBe-KB provided information about the ligand binding sites relevant to each structure. The effect of single-point mutations on protein stability was assessed using the DUET web server (https://biosig.lab.uq.edu.au/duet/), an integrated computational approach that combines the results of two independent methods: mCSM and SDM. DUET utilizes a machine-learning framework to improve the accuracy of stability predictions by incorporating both environment-specific substitution matrices and graph-based signatures of protein structure. The output is presented as a change in the Gibbs free energy ($\Delta\Delta G$, kcal/mol), where negative values indicate destabilizing mutations and positive values indicate stabilizing effects on the protein structure. The corresponding protein files were downloaded from the Protein Data Bank in Europe (https://www.ebi.ac.uk/pdbe/) for use in the DynaMut and DUET analyses.

Visualization of interactions in wild type (WT) and mutant structures

BIOVIA Discovery Studio 2021 was employed to facilitate the detailed examination of the selected proteins in both wild-type and mutant configurations. This platform offers robust capabilities for molecular visualization and interaction analysis, enabling comprehensive protein structure and surrounding exploration [13]. The immediate molecular environment of specific residues, both in their native and mutated forms, was visualized using Discovery Studio to investigate potential changes in noncovalent interactions, such as hydrogen bonding, hydrophobic and electrostatic interactions.

RESULTS

According to the literature, *PIK3CA, PTEN, AKT1, AKT2, AKT3, IRS1, GSK3B, TSC1,* and *TSC2* are recognized components of the PI3K/AKT/mTOR signaling pathway. These genes were further investigated to identify relevant mutations using cBioPortal and the "Breast Cancer (METABRIC, Nature 2012 & Nat Commun 2016)" dataset. *PTEN*, *AKT1*,

Table 1. List of the selected genes with the mutation percentages from 2509 BC samples.

No	Gene	Mutation (%)	Domain
1.	*PIK3CA*	40.1%	PI3Ka
2.	*PTEN*	3.9%	DSPc
3.	*AKT1*	4.1%	PH
4.	*AKT2*	0.5%	Pkinase
5.	*AKT3*	/	/
6.	*IRS1*	/	/
7.	*GSK3B*	/	/
8.	*TSC1*	/	/
9.	*TSC2*	/	/

Table 2. List of the selected genes with the corresponding mutations identified in this study.

Gene	Mutation
PIK3CA	H1047R H1047L H1047Y H1047Q E545K E545A E545G E545D E545Q E542K E542A E542V
PTEN	D92A D92E D92G D92H D92N R130Q R130G C136R C136Y
AKT1	E17K L52R Q79K
AKT2	R170W

https://doi.org/10.5455/annalsmedres.2025.07.185

Table 3. Sequence-based prediction results from Predict SNP and consensus tools.

Gene	Mutation	PredictSNP	MAPP	PhD-SNP	PolyPhen-1	PolypPhen-2	SIFT	SNAP
PIK3CA	H1047R	60% (+)	43% (-)	77% (-)	67% (+)	71% (+)	45% (-)	58% (+)
	H1047L	63% (+)	74% (+)	73% (-)	59% (-)	72% (+)	90% (+)	71% (+)
	H1047Y	75% (+)	63% (+)	77% (-)	67% (+)	76% (+)	77% (+)	77% (+)
	H1047Q	74% (+)	73% (+)	51% (+)	67% (+)	71% (+)	46% (-)	58% (+)
	E545K	60% (+)	74% (+)	68% (-)	67% (+)	Unknown	79% (-)	50% (+)
	E545A	63% (+)	71% (+)	58% (+)	67% (+)	54% (-)	79% (-)	50% (+)
	E545G	51% (-)	72% (+)	82% (-)	67% (+)	54% (-)	79% (-)	50% (+)
	E545D	68% (+)	74% (+)	72% (+)	67% (+)	54% (-)	43% (-)	67% (+)
	E545Q	63% (+)	80% (+)	58% (+)	67% (+)	54% (-)	79% (-)	55% (+)
	E542K	65% (+)	76% (+)	51% (+)	67% (+)	43% (-)	46% (-)	58% (+)
	E542A	75% (+)	70% (+)	68% (+)	67% (+)	Unknown	46% (-)	50% (+)
	E542V	61% (-)	72% (+)	68% (-)	67% (+)	68% (-)	79% (-)	56% (-)
PTEN	D92A	76% (-)	78% (-)	88% (-)	67% (+)	68% (-)	79% (-)	85% (-)
	D92E	65% (-)	77% (-)	68% (-)	67% (+)	Unknown	79% (-)	72% (-)
	D92G	76% (-)	76% (-)	88% (-)	67% (+)	68% (-)	79% (-)	81% (-)
	D92H	87% (-)	77% (-)	88% (-)	74% (-)	81% (-)	79% (-)	87% (-)
	D92N	87% (-)	57% (-)	86% (-)	59% (-)	81% (-)	79% (-)	81% (-)
	R130Q	87% (-)	77% (-)	88% (-)	59% (-)	68% (-)	79% (-)	81% (-)
	R130G	87% (-)	84% (-)	86% (-)	74% (-)	43% (-)	79% (-)	85% (-)
	C136R	87% (-)	86% (-)	88% (-)	59% (-)	43% (-)	79% (-)	85% (-)
	C136Y	87% (-)	62% (-)	88% (-)	74% (-)	43% (-)	53% (-)	72% (-)
AKT1	E17K	76% (-)	65% (+)	73% (-)	74% (-)	81% (-)	79% (-)	56% (-)
	L52R	87% (-)	88% (-)	86% (-)	74% (-)	68% (-)	79% (-)	72% (-)
	Q79K	55% (-)	73% (+)	61% (-)	67% (+)	68% (-)	46% (-)	62% (-)
AKT2	R170W	87% (-)	56% (-)	88% (-)	74% (-)	68% (-)	79% (-)	62% (-)

% expected accuracy; (+) neutral; (-) deleterious.

Table 4. Sequence-based prediction results based on the SNP&GO computational tool.

Gene	Mutation	SNPs&GO	
		Effect	RI
PIK3CA	H1047R	Neutral	5
	H1047L	Neutral	6
	H1047Y	Neutral	6
	H1047Q	Neutral	4
	E545K	Neutral	2
	E545A	Neutral	5
	E545G	Disease Related Polymorphism	0
	E545D	Neutral	4
	E545Q	Neutral	5
	E542K	Neutral	3
	E542A	Neutral	5
	E542V	Neutral	3
PTEN	D92A	Disease Related Polymorphism	10
	D92E	Disease Related Polymorphism	10
	D92G	Disease Related Polymorphism	10
	D92H	Disease Related Polymorphism	10
	D92N	Disease Related Polymorphism	10
	R130Q	Disease Related Polymorphism	10
	R130G	Disease Related Polymorphism	10
	C136R	Disease Related Polymorphism	10
	C136Y	Disease Related Polymorphism	10
AKT1	E17K	Disease Related Polymorphism	10
	L52R	Disease Related Polymorphism	10
	Q79K	Disease Related Polymorphism	10
AKT2	R170W	Disease Related Polymorphism	4

RI reliability index.

https://doi.org/10.5455/annalsmedres.2025.07.185

Table 5. Stability results of mutation effects from DynaMut and DUET.

Genes	Substitution	ΔΔG DynaMut (kcal/mol)	ΔΔG ENCoM (kcal/mol)	ΔΔG mCSM (kcal/mol)	ΔΔG SDM (kcal/mol)	ΔΔG DUET (kcal/mol)	ΔΔSVib mCSM (kcal.mol^{-1} K^{-1})
PTEN	D92H	-0.284(-)	-0.119(-)	-0.228(-)	0.740(+)	-0.050(-)	0.149(++)
PTEN	D92N	-0.424(-)	-0.144(-)	-0.351(-)	-0.130(-)	-0.266(-)	0.180(++)
PTEN	R130Q	-0.541(-)	-0.208(-)	-1.302(-)	-1.660(-)	-1.487(-)	0.260(++)
PTEN	R130G	-1.481(-)	-1.090(-)	-1.720(-)	-1.700(-)	-2.008(-)	1.362(++)
PTEN	C136R	-1.146(-)	0.109(-)	-1.378(-)	-1.460(-)	-1.204(-)	-0.137(--)
PTEN	C136Y	-0.754(-)	0.761(+)	-0.989(-)	-1.670(-)	-1.230(-)	-0.952(--)
AKT1	L52R	1.821(+)	2.189(+)	-1.236(-)	-1.860(-)	-1.211(-)	-2.736(--)
AKT2	R170W	0.051(+)	0.073(-)	-0.505(-)	0.320(+)	-0.438(-)	-0.091(--)

ΔΔG change in the Gibbs free energy; ΔΔSVib change in vibrational entropy energy between wild-type and mutant; (+) stabilizing; (-) destabilizing; (++) increased molecule flexibility; (–) decreased molecule flexibility.

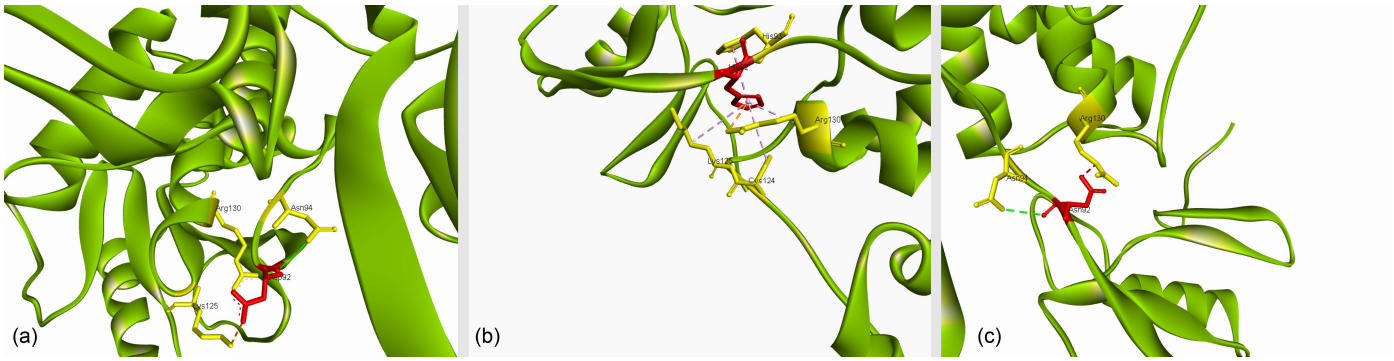

Figure 1. Structural visualization of PTEN at residue 92. (a) Wild-type Asp92 and its interactions. (b) D92H and (c) D92N mutants, illustrating the differences in local residue interactions resulting from these point mutations. The target amino acids are highlighted in red, and the interacting residues are shown in yellow.

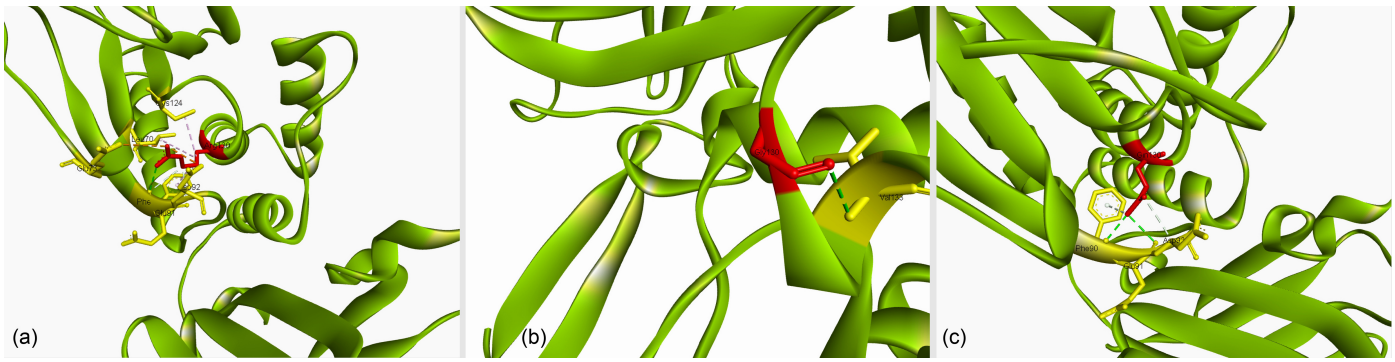

Figure 2. Structural visualization of PTEN at residue 130. (a) Interaction network of wild-type Arg130. (b) and (c) R130Q and R130G mutants, respectively, demonstrating the alteration of molecular interactions following mutation. The target amino acids are highlighted in red, and the interacting residues are shown in yellow.

and *AKT2* were selected as the primary target genes for detailed analysis. The selected target genes are presented in Table 1.

The subsequent step involved identifying the most frequent missense mutations in the four selected genes (*PIK3CA, PTEN, AKT1*, and *AKT2*) by analyzing the cBioPortal database. For *PIK3CA*, H1047R/L/Y/Q mutations were observed in 471 patients, E545K/A/G/D/Q in 191 patients, and E542K/A/V in 101 patients. In *PTEN*, D92A/E/G/H/N mutations were present in 5 patients, R130Q/G in 3 patients, and C136R/Y in 2 patients. For *AKT1*, the E17K, L52R, and Q79K mutations were identified in 79, 5, and 2 patients, respectively, whereas the *AKT2* R170W mutation was detected in 1 patient. Table 2 lists the selected genes with the corresponding mutations identified in this study.

Sequence-based prediction using the PredictSNP computational tool, in conjunction with consensus-based methods, indicated that only *PTEN* (D92H, D92N, R130Q, R130G, C136R, and C136Y), *AKT1* (L52R), and *AKT2* (R170W) mutations are likely to be deleterious (Table 3). The SNPs&GO computational method classified 14 mutations as disease-related polymorphisms (Table 4).

Based on comprehensive sequence-based predictions (Tables

https://doi.org/10.5455/annalsmedres.2025.07.185

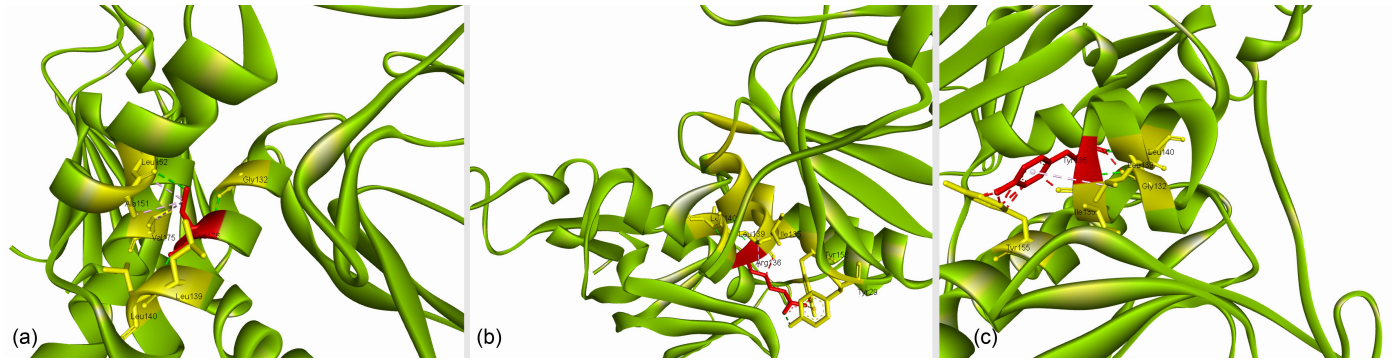

Figure 3. Structural visualization of PTEN at residue 136. (a) Wild-type Cys136 and its associated interactions. (b) and (c) Effects of C136R and C136Y mutations on the interaction profile of this site. The target amino acids are highlighted in red, and the interacting residues are shown in yellow.

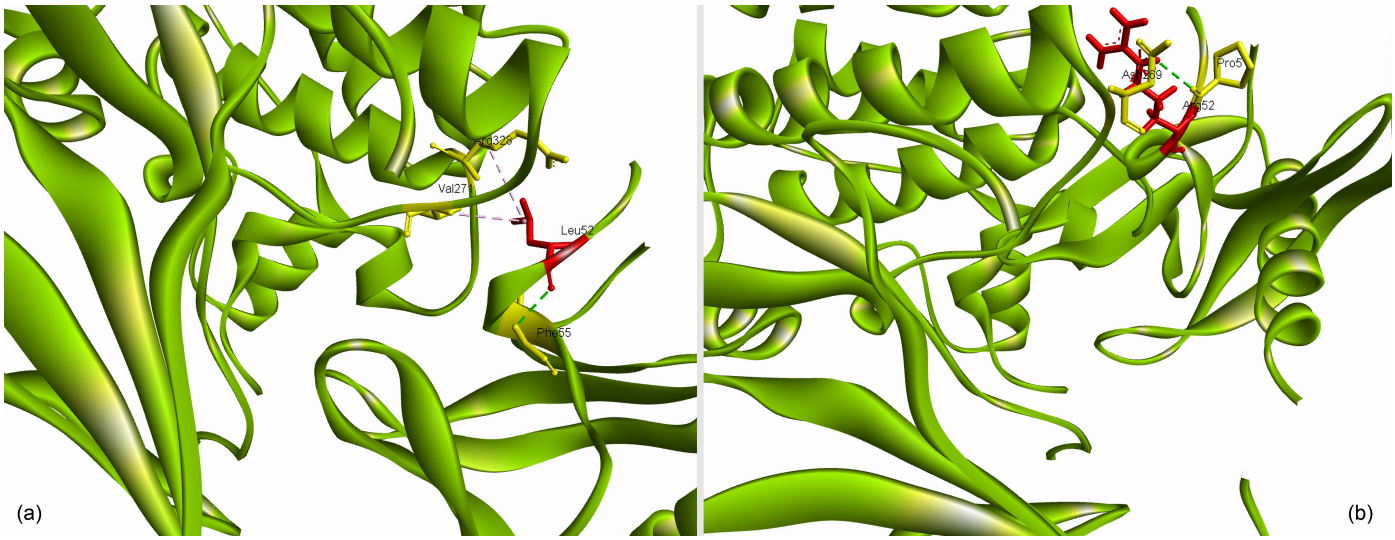

Figure 4. Structural visualization of AKT1 at residue 52. (a) Wild-type Leu52 interactions. (b) L52R mutant and resultant changes in local residue interactions. The target amino acids are highlighted in red, and the interacting residues are shown in yellow.

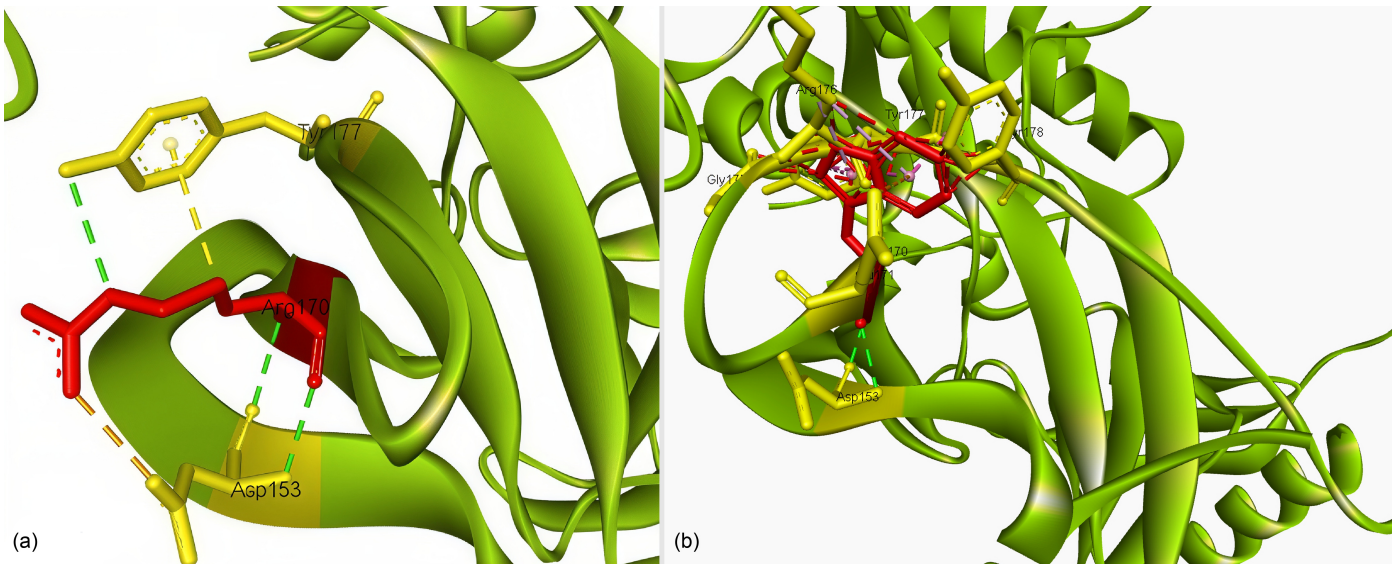

Figure 5. Structural visualization of AKT2 at residue 170. (a) Interactions of wild-type Arg170. (b) R170W mutant, highlighting differences in the interaction landscape. The target amino acids are highlighted in red, and the interacting residues are shown in yellow.

3 and 4), only the *PTEN* mutations D92H, D92N, R130Q, R130G, C136R, and C136Y; the *AKT1* mutation L52R; and the *AKT2* mutation R170W were consistently classified as deleterious by all computational tools employed (PredictSNP,

https://doi.org/10.5455/annalsmedres.2025.07.185

MAPP, PhD-SNP, PolyPhen-1, PolyPhen-2, SIFT, SNAP, and SNP&GO). The unanimous "deleterious" and "disease-related polymorphism" scores across these algorithms indicate that these variants are highly likely to impact protein function, thereby warranting their selection for further structural analysis. Table 5 summarizes the deleterious missense variants prioritized for structural analysis, along with consensus prediction, stability outputs, and representative interaction changes.

Representative high-resolution protein structures were obtained from the PDBe-KB and PDBe databases, with *PTEN, AKT1*, and *AKT2* modeled using 1D5R (chain A), 7NH5 (chain A), and 8Q61 (chain A), respectively. Structural impact assessments (Table 5) revealed that most of the evaluated mutations destabilized the protein structure or significantly altered molecular flexibility.

Differences in the interactions between wild-type and mutant structures were identified for *PTEN*, *AKT1*, and *AKT2* (Figures 1–5). The target amino acids are depicted in red and interacting residues are highlighted in yellow in each case.

Asp92 forms three key interactions in the *PTEN* wild-type structure: a conventional hydrogen bond with Asn94, a salt bridge with Lys125, and an attractive charge interaction with Arg130 (Figure 1a). The D92H mutation results in a pi–pi stacked interaction with His93, accompanied by three pi–alkyl interactions with Lys125, Cys124, and Arg130 (Figure 1b). The D92N mutant retained a conventional hydrogen bond with Asn94 and gained an unfavorable bump interaction with Arg130 (Figure 1c).

Wild-type Arg130 in *PTEN* participates in two attractive charge interactions with Glu73 and Asp92, two alkyl interactions with Cys124 and Leu70, a pi–alkyl interaction with Phe90, and a carbon hydrogen bond with Glu91 (Figure 2a). The R130Q mutant exhibited a pi donor hydrogen bond with Phe90, a carbon hydrogen bond with Asp92, and a conventional hydrogen bond with Glu91 (Figure 2b). The R130G mutation results in a single conventional hydrogen bond interaction with Val133 (Figure 2c).

Wild-type Cys136 in *PTEN* forms four conventional hydrogen bond interactions with Ala151, Gly132, Leu139, and Leu140 and two alkyl interactions with Val175 and Leu152 (Figure 3a). The C136R mutation results in conventional hydrogen bonds with Tyr29 and Leu140, two unfavorable bump interactions with Tyr155 and Ile135, and an alkyl interaction with Leu139 (Figure 3b). The C136Y mutant forms a pi–alkyl interaction with Leu139, two unfavorable bump interactions with Tyr155 and Ile135, and two conventional hydrogen bonds with Gly132 and Leu140 (Figure 3c).

In *AKT1*, wild-type Leu52 establishes two alkyl interactions with Arg328 and Val271 and a conventional hydrogen bond with Phe55 (Figure 4a). The L52R mutant forms a conventional hydrogen bond with Pro51 and an unfavorable bump interaction with Asn269 (Figure 4b).

For *AKT2*, wild-type Arg170 displays a salt bridge and two conventional hydrogen bond interactions with Asp153, an additional conventional hydrogen bond with itself, and both a conventional hydrogen bond and pi–alkyl interaction with Tyr177 (Figure 5a). The R170W mutation introduces a conventional hydrogen bond with Asp153, an unfavorable bump interaction with Gly175, a pi–alkyl interaction with Arg176, two amide–pi stacked interactions with Tyr177 and Tyr178, and a pi–anion interaction with Glu171 (Figure 5b).

DISCUSSION

The activation of the PI3K/AKT/mTOR signaling pathway has been widely linked to BC cell growth, survival, and drug resistance, making it a critical focus for cancer research. Dysregulation of this pathway is frequently observed in multiple forms of BC, contributing to tumor development, disease progression, metastasis and resistance to various therapies [14]. The PI3K/AKT/mTOR pathway interacts with numerous other signaling cascades, adding to the BC's molecular complexity and heterogeneity. Targeting specific components (nodes) of this pathway holds promise for the advancement of more personalized and effective treatments for patients with BC [1,3]. Many genes, including but not limited to *PIK3CA, PTEN, AKT1, AKT2, AKT3, IRS1, GSK3B, TSC1*, and *TSC2*, are involved in the PI3K/AKT/mTOR pathway [1,3]. These genes play important regulatory roles at different points within the pathway. *PTEN* functions as a tumor suppressor by dephosphorylating phosphatidylinositol (3,4,5)-trisphosphate (PIP3) in the cell membrane [15], which inhibits AKT activation and downstream signaling. *PTEN* contains domains such as the phosphatase domain that are critical for its tumor-suppressive activity [16]. Loss of *PTEN* function, often due to missense mutations, leads to uncontrolled activation of the PI3K/AKT/mTOR pathway, promoting cell growth and survival and increasing cancer risk, including in BC [3]. *AKT1* and *AKT2* are serine/threonine kinases and major downstream effectors of PI3K signaling [17]. *AKT1* mainly regulates cell proliferation and survival, while *AKT2* plays an essential role in cell metabolism and migration. Both proteins contain a PH domain, a kinase domain, and a regulatory domain, all of which contribute to their activities and regulation [18]. *AKT1* or *AKT2* mutations can disrupt normal signaling, contributing to tumor growth and therapeutic resistance in BC. *PTEN, AKT1*, and *AKT2* were selected for analysis, and their most frequent missense mutations were examined to better understand their potential contributions to BC progression and drug resistance.

In this study, we identified the *PTEN* variants D92H, D92N, R130G, R130Q, C136R, and C136Y as deleterious. Several of these mutations are located within regions critical for protein-ligand interactions, affecting both PIP2 binding and inhibition of downstream pathways. Karn et al., performed molecular docking analyses and found that D92H and R130Q mutations disrupt PTEN's ability to bind PIP2.

https://doi.org/10.5455/annalsmedres.2025.07.185

The loss of PIP2 interaction primarily impairs the dephosphorylation process, directly affecting the phosphatase function of *PTEN* [19]. Matreyek et al., reported that the D92H variant represents a highly abundant yet phosphatase-inactive form of *PTEN*. This mutation can dysregulate AKT signaling even in the presence of wild-type *PTEN*, indicating that D92H can act in a dominant-negative manner. Importantly, these dominant-negative variants were observed in BC according to cancer genomics datasets, highlighting their potential relevance in the pathogenesis of BC [20]. Researchers investigated the clinical overlap between *PTEN* deficiency and activated PI3K delta syndrome 1 (APDS1). Their analysis included a patient with a pathogenic *PTEN* mutation (C136R), one of the deleterious variants identified in this study. The patient exhibited immune dysregulation phenotypes similar to APDS1, including hyper IgM, low IgG, increased transitional B cells, and lymphoproliferation. Functional assays confirmed dysregulation of the PI3K/AKT/mTOR pathway. Importantly, treatment with sirolimus, an mTOR inhibitor, effectively resolved lymphoproliferation and splenic abnormalities. These findings highlight that *PTEN* loss-of-function mutations can phenocopy PI3K pathway activation and indicate that targeted therapies may benefit patients with BC harboring similar *PTEN* mutations [21]. The *PTEN* C136R mutation compromises phosphatase activity, contributing to increased proteasome activity and protein instability [22]. Several studies have classified C136R as a pathogenic alteration, including in patients with BC from diverse populations [23,24]. Gervas et al., specifically identified this mutation in a patient with hereditary BC of mongoloid origin, emphasizing the relevance of *PTEN* analysis in addition to *BRCA1* and *BRCA2* screening. While *BRCA1/2* mutations are well-characterized in hereditary BC, the importance of investigating alternative pathways that contribute to cancer development is becoming increasingly recognized. The PI3K/AKT/mTOR signaling cascade is central to key cellular processes such as growth, survival, and metabolism, and disruptions in this pathway are frequently linked to tumorigenesis and BC progression [1,3,6,7]. Cetintas et al., conducted detailed computational and experimental analyses of several *PTEN* missense mutations. According to multiple computational tools, their investigation demonstrated that certain mutations, including C136Y, displayed strong deleterious effects. Molecular dynamics simulations indicated that the C136Y mutation resulted in significant residual fluctuations in the protein structure and was associated with the least compact conformation among the variants analyzed. These structural alterations were correlated with decreased protein stability and were predicted to impair *PTEN* function. Given the central role of *PTEN* in regulating cell proliferation and survival, such mutations are likely to contribute to protein dysfunction and promote tumorigenic processes. The findings support the disease relevance of C136Y and other *PTEN* alterations in cancer development and provide further evidence for their potential pathogenic impact in BC when present [25].

Beyond regulating cell growth and survival, the PI3K/AKT/mTOR pathway is implicated in the development of chemoresistance, presenting substantial challenges for the treatment of BC. All genes evaluated in this study are connected to the emergence of therapy resistance in different ways. Huang et al., (2021) reported C136Y in patients with BC, often alongside other *PTEN* mutations such as D92G, D92V, K125T, G127V, and G129E, emphasizing the diversity of variants contributing to disease complexity [26]. Additionally, researchers described C136Y among mutations found in patients with BC with disease progression, together with variants such as G127E, R130Q, G36E, and Q97* [24]. These findings support the clinical significance of C136Y and related *PTEN* mutations in BC, particularly in the context of aggressive disease and therapeutic resistance.

Sharma et al., identified several harmful *PTEN* nsSNPs, including R130G and R130Q, which overlapped with mutations classified as deleterious in this study. Their computational analysis showed that these variants disrupt the structural stability of *PTEN*, compromise catalytic sites, and impair the PI3K/AKT pathway regulation. These results further validate the pathogenic potential of R130G and R130Q in BC and underscore the broader impact of *PTEN* missense mutations on tumor suppressor function [27]. The *PTEN* R130Q mutation has also been closely associated with the BC phenotype, and several research groups are investigating PTEN-targeted strategies for treating BC [28]. In their study, Naidu and Suneetha characterized R130Q as a deleterious variant that reduces protein stability. As noted by Kim et al. [29], R130Q, along with R130G, represents one of the most common oncogenic mutations in *PTEN*. Functional studies further indicate that arginine at position 130 is essential for the catalytic activity and overall protein function of *PTEN*, highlighting the pathogenic significance of alterations at this site [30].

The other two proteins in our study: *AKT1* and *AKT2* belong to the AKT family of serine threonine protein kinases, which is known as protein kinase B (PKB). They regulate a variety of biological activities, including cell survival, proliferation, growth, metabolism, and angiogenesis. *AKT1* is involved in cell survival pathways, promoting cell survival, and regulating protein synthesis [31]. Furthermore, *AKT2* shares almost all functional similarities with *AKT2* but plays some distinct roles in specific cellular processes, such as glucose metabolism regulation and insulin signaling. *AKT1* and *AKT2* are involved in tumor initiation, metastasis, and therapeutic resistance in cancer [32].

Several *AKT1* mutations, including D32Y, K39N, P42T, L52R, C77F, and Q79K, have been reported in recent BC studies [33,34]. Among these, the L52R variant is a recurrent, activating mutation that enhances Akt phosphorylation and is classified as oncogenic [34]. This specific mutation

https://doi.org/10.5455/annalsmedres.2025.07.185

has been identified in patients with BC, further implicating *AKT1* in disease progression [35]. Structural and biochemical analyses indicate that such activating mutations can lead to constitutive kinase activity, promoting downstream signaling even in the absence of upstream stimuli. This dysregulation contributes to uncontrolled proliferation and survival, which are central to malignant transformation and therapeutic resistance. Recent functional and clinical investigations have further defined the significance of the *AKT1* L52R mutation. Shrestha Bhattarai et al., demonstrated that L52R is among the activating, non-E17K *AKT1* mutations capable of driving growth factor-independent AKT activation. Their study revealed that such mutations can sensitize tumor cells to ATP-competitive AKT inhibitors, such as capivasertib. In a phase II clinical trial that included patients with various solid tumors harboring AKT1-3 alterations, an individual with an *AKT1* L52R-mutant cancer exhibited a durable partial response to capivasertib, highlighting the therapeutic potential of directly targeting these activating mutations. These findings indicate that allele-specific activation profiles influence pharmacological sensitivities and suggest that tailored AKT inhibitor therapy may benefit BC cases with *AKT1* L52R or similar mutations [36]. Recent in vitro research has demonstrated that *AKT1* L52R mutation contributes to paclitaxel resistance in BC cells. The study found that the L52R variant, along with other PH domain mutations, was associated with increased resistance to paclitaxel in MDA-MB-231 cells compared to wild-type *AKT1*. Although *AKT1* L52R protein levels were lower than those of the wild-type, this mutation still resulted in enhanced AKT pathway activation and cell survival. These findings underscore the functional impact of the L52R variant in chemoresistance promotion and highlight its potential as a biomarker for treatment response in BC [37].

Although the *AKT1* E17K mutation is more frequently reported and widely studied in BC, emerging evidence highlights the clinical relevance of other activating mutations, such as L52R. Both E17K and L52R have been associated with increased resistance to multiple chemotherapeutics, not only in BC but also in other types of cancer, such as colorectal cancer [38]. These mutations often co-occur with additional driver alterations but may also act independently to promote oncogenic signaling and contribute to therapy resistance [39]. Moreover, the feasibility of liquid biopsy for monitoring disease and guiding targeted therapeutic strategies in advanced-stage BC is demonstrated by the blood-based detection of *AKT1* mutations [39]. Taken together, these findings support the use of *AKT1* L52R, alongside E17K, as a potential predictive biomarker for drug resistance and treatment planning in BC, reinforcing the importance of precision medicine approaches for patients with *AKT1* pathway alterations [38].

AKT2, although highly homologous to *AKT1*, is distinguished by its essential role in glucose metabolism and insulin signaling, processes that are often altered during tumorigenesis. Although rare in human cancers, the R170W mutation in *AKT2* affects regulatory mechanisms by potentially disrupting kinase activity and substrate specificity [40]. Notably, our study did not find any existing research directly connecting the *AKT2* R170W variant to BC in the experimental or clinical settings. This highlights a significant gap in the literature and underscores the need for targeted in vivo studies to clarify the functional and clinical relevance of this particular mutation. The *PTEN* and *AKT1* mutations identified in our analysis are well supported by in vivo and clinical evidence, reinforcing their established pathogenic and therapeutic roles in BC. Therefore, our findings provide a rationale for future translational investigations, particularly regarding the potential impact of *AKT2* R170W in BC biology and treatment resistance.

Although the present study focused on BC, the PI3K/AKT/mTOR axis is relevant in other malignancies. This pathway has been identified as a therapeutic target in chordoma [9] and dysregulation has been reported across diverse cancers [10]. Pathogenic *PTEN* missense variants have been functionally characterized in glioblastoma [25], reinforcing the broader importance of PTEN-AKT signaling in oncogenic processes. These pathway-wide observations support the wider interest of the present mutation-focused findings for additional tumor types.

Conclusion

Identifying deleterious genetic mutations in BC using computational methods represents a significant step in understanding the molecular basis of this disease. Researchers have identified specific variants with potential functional impact using computational tools. These findings offer key insights into the genetic landscape of BC, supporting risk stratification and development of targeted therapeutics. The PI3K/AKT/mTOR pathway requires further investigation to clarify its role in the pathogenesis and progression of BC. Progress in this area could improve the clinical outcomes of patients with BC. This study focuses on *PTEN, AKT1*, and *AKT2* and assesses their most frequent mutations and pathogenic effects. Further research is necessary to achieve more clinically relevant results, and integrating bioinformatics and genomics remains vital for uncovering BC genetics and advancing personalized medicine.

Ethics Committee Approval: This study did not involve human participants, animal experiments, or the use of personal identifiable data. Therefore, approval from the ethics committee was not required.

Informed Consent: Not required for this study.

Peer-review: Externally peer-reviewed.

Conflict of Interest: The authors declare that there are no existing or potential conflicts of interest, including financial, consultancy, institutional, or other relationships, that could be

https://doi.org/10.5455/annalsmedres.2025.07.185

perceived as leading to potential bias or a conflict of interest regarding the submitted manuscript.

Author Contributions: Conceptualization: B.A.; Investigation: B.A., H.L., N.I.; Data curation: H.L.; Formal analysis: H.L.; Methodology: B.A., H.L. Software: H. L ; Visualization: H. L and N. I. ; Writing–original draft: B.A., H.L., N.I. ; Writing, review, and editing: B.A., H.L., N.I. . All authors have approved the final version of the manuscript.

Financial Disclosure: The authors declare that no funds, grants, or other support were received during the preparation of this manuscript.

REFERENCES

1. Dong C, Wu J, Chen Y, Nie J, Chen C. Activation of PI3K/AKT/mTOR Pathway Causes Drug Resistance in Breast Cancer. *Front Pharmacol.* 2021;12:628690. doi: 10.3389/fphar.2021.628690.
2. Hou Z, Ma W, Ren D, Shen N, Bi W, et al. Exportin-T Promotes Breast Cancer Progression via PI3K/AKT/mTOR Signaling Pathway. *J Inflamm Res.* 2025;18:6467–6481. doi: 10.2147/JIR.S512905.
3. Li H, Prever L, Hirsch E, Gulluni F. Targeting PI3K/AKT/mTOR Signaling Pathway in Breast Cancer. *Cancers (Basel).* 2021;13(14):3517. doi: 10.3390/cancers13143517.
4. Peng Y, Wang Y, Zhou C, Mei W, Zeng C. PI3K/Akt/mTOR Pathway and Its Role in Cancer Therapeutics: Are We Making Headway? *Front Oncol.* 2022;12:819128. doi: 10.3389/fonc.2022.819128.
5. Khorasani ABS, Hafezi N, Sanaei M-J, Jafari-Raddani F, Pourbagheri-Sigaroodi A, Bashash D. The PI3K/AKT/mTOR signaling pathway in breast cancer: Review of clinical trials and latest advances. *Cell Biochem Funct.* 2024;42(3):e3998. doi: 10.1002/cbf.3998.
6. Miricescu D, Totan A, Stanescu-Spinu I-I, Badoiu SC, Stefani C, Greabu M. PI3K/AKT/mTOR Signaling Pathway in Breast Cancer: From Molecular Landscape to Clinical Aspects. *Int J Mol Sci.* 2020;22(1):173. doi: 10.3390/ijms22010173.
7. Ortega MA, Fraile-Martínez O, Asúnsolo Á, Buján J, García-Honduvilla N, Coca S. Signal Transduction Pathways in Breast Cancer: The Important Role of PI3K/Akt/mTOR. *J Oncol.* 2020;2020:9258396. doi: 10.1155/2020/9258396.
8. Sharma VR, Gupta GK, Sharma AK, Batra N, Sharma DK, Joshi A, et al. PI3K/Akt/mTOR Intracellular Pathway and Breast Cancer: Factors, Mechanism and Regulation. *Curr Pharm Des.* 2017;23(11):1633–8. doi: 10.2174/1381612823666161116125218.
9. Presneau N, Shalaby A, Idowu B, Gikas P, Cannon SR, Gout I, et al. Potential therapeutic targets for chordoma: PI3K/AKT/TSC1/TSC2/mTOR pathway. *Br J Cancer.* 2009;100(9):1406–14. doi: 10.1038/sj.bjc.6605019.
10. Hussain MS, Moglad E, Afzal M, Gupta G, Hassan Almalki W, Kazmi I, et al. Non-coding RNA mediated regulation of PI3K/Akt pathway in hepatocellular carcinoma: Therapeutic perspectives. *Pathol Res Pract.* 2024;258:155303. doi: 10.1016/j.prp.2024.155303.
11. Ghayad SE, Cohen PA. Inhibitors of the PI3K/Akt/mTOR pathway: new hope for breast cancer patients. *Recent Pat Anticancer Drug Discov.* 2010;5(1):29–57. doi: 10.2174/157489210789702208.
12. Scherbakov AM, Basharina AA, Sorokin DV, Mikhaevich EI, Mizaeva IE, Mikhaylova AL, et al. Targeting hormone-resistant breast cancer cells with docetaxel: a look inside the resistance. *Cancer Drug Resist.* 2023;6(1):103–15. doi: 10.20517/cdr.2022.96.
13. Scribd [Internet]. Biovia Discovery Studio Overview Datasheet | PDF | Docking (Molecular) | Proteins [cited 2025 Jun 26]. Available from: https://www.scribd.com/document/798537219/biovia-discovery-studio-overview-datasheet.
14. Wan L, Wang Y, Li J, Wang Y, Zhang H. Inhibition of the AKT/mTOR pathway negatively regulates PTEN expression via miRNAs. *Acta Biochim Biophys Sin (Shanghai).* 2022;54(11):1637–47. doi: 10.3724/abbs.2022159.
15. Vazquez F, and Devreotes P. Regulation of PTEN Function as a PIP3 Gatekeeper Through Membrane Interaction. *Cell Cycle.* 2006;5(14):1523–7. doi: 10.4161/cc.5.14.3005.
16. Jang H, Smith IN, Eng C, Nussinov R. The mechanism of full activation of tumor suppressor PTEN at the phosphoinositide-enriched membrane. *iScience.* 2021;24(5):102438. doi: 10.1016/j.isci.2021.102438.
17. Guerau-de-Arellano M, Piedra-Quintero ZL, Tsichlis PN. Akt isoforms in the immune system. *Front Immunol.* 2022;13:990874. doi: 10.3389/fimmu.2022.990874.
18. Basu A, Lambring CB. Akt Isoforms: A Family Affair in Breast Cancer. *Cancers (Basel).* 2021;13(14):3445. doi: 10.3390/cancers13143445.
19. Karn R, Emerson IA. Molecular dynamic study on PTEN frameshift mutations in breast cancer provide c2 domain as a potential biomarker. *J Biomol Struct Dyn.* 2022;40(7):3132–43. doi: 10.1080/07391102.2020.1845802.
20. Matreyek KA, Stephany JJ, Ahler E, Fowler DM. Integrating thousands of PTEN variant activity and abundance measurements reveals variant subgroups and new dominant negatives in cancers. *Genome Med.* 2021;13(1):165. doi: 10.1186/s13073-021-00984-x.
21. Smith M, Haddad C, Salih A, Vargas-Hernandez A, Carmona MS, Sauceda AR, et al. PTEN Deficiency: a phenocopy phenomenon. *Clin Immunol.* 2023;250:109442. doi: 10.1016/j.clim.2023.109442.
22. He X, Arrotta N, Radhakrishnan D, Wang Y, Romigh T, Eng C. Cowden syndrome-related mutations in PTEN associate with enhanced proteasome activity. *Cancer Res.* 2013;73(10):3029–40. doi: 10.1158/0008-5472.CAN-12-3811.
23. Gervas P, Molokov A, Schegoleva A, Kiselev A, Babyshkina N, Pisareva L, et al. New germline mutations in non-BRCA genes among breast cancer women of Mongoloid origin. *Mol Biol Rep.* 2020;47(7):5315–21. doi: 10.1007/s11033-020-05612-2.
24. Li G, Guo X, Chen M, Tang L, Jiang H, Day JX, et al. Prevalence and spectrum of AKT1, PIK3CA, PTEN and TP53 somatic mutations in Chinese breast cancer patients. *PLoS One.* 2018;13(9):e0203495. doi: 10.1371/journal.pone.0203495.
25. Cetintas VB, Duzgun ,Zekeriya, Akalin ,Taner, Ozgiray ,Erkin, Dogan ,Eda, Yildirim ,Zafer, et al. Molecular dynamic simulation and functional analysis of pathogenic PTEN mutations in glioblastoma. *J Biomol Struct Dyn.* 2023;41(21):11471–83. doi: 10.1080/07391102.2022.2162582.
26. Huang C-C, Tsai Y-F, Liu C-Y, Chao T-C, Lien P-J, Lin Y-S, et al. Comprehensive molecular profiling of Taiwanese breast cancers revealed potential therapeutic targets: prevalence of actionable mutations among 380 targeted sequencing analyses. *BMC Cancer.* 2021;21(1):199. doi: 10.1186/s12885-021-07931-4.
27. Sharma D, Singh H, Arya A, Choudhary H, Guleria P, Saini S, et al. Comprehensive computational analysis of deleterious nsSNPs in PTEN gene for structural and functional insights. *Mol Biol Res Commun.* 2025;14(3):219–39. doi: 10.22099/mbrc.2025.52148.2092.
28. Naidu CK, Suneetha Y. Prediction and Analysis of Breast Cancer Related Deleterious Non-Synonymous Single Nucleotide Polymorphisms in the PTEN Gene. *Asian Pac J Cancer Prev.* 2016;17(4):2199–203. doi: 10.7314/apjcp.2016.17.4.2199.
29. Kim M, Kim J, Seo AN, Jeong JY, Park NJ-Y, Chong GO, et al. Comparison of immunohistochemistry and next-generation sequencing results in oncogenic PTEN missense mutations. *Pathol Res Pract.* 2023;251:154879. doi: 10.1016/j.prp.2023.154879.
30. Smith IN, Briggs JM. Structural mutation analysis of PTEN and its genotype-phenotype correlations in endometriosis and cancer. *Proteins.* 2016;84(11):1625–43. doi: 10.1002/prot.25105.
31. Wachira J. Morphological Alterations of CAD Cells Overexpressing AKT1. *Microsc Microanal.* 2020;26(Suppl 2):1354–8. doi: 10.1017/s1431927620017821.

32. Chen X, Ariss MM, Ramakrishnan G, Nogueira V, Blaha C, Putzbach W, et al. Cell-Autonomous versus Systemic Akt Isoform Deletions Uncovered New Roles for Akt1 and Akt2 in Breast Cancer. *Mol Cell.* 2020;80(1):87-101.e5. doi: 10.1016/j.molcel.2020.08.017.
33. Mundi PS, Sachdev J, McCourt C, Kalinsky K. AKT in cancer: new molecular insights and advances in drug development. *Br J Clin Pharmacol.* 2016;82(4):943–56. doi: 10.1111/bcp.13021.
34. Yi KH, Axtmayer J, Gustin JP, Rajpurohit A, Lauring J. Functional analysis of non-hotspot AKT1 mutants found in human breast cancers identifies novel driver mutations: implications for personalized medicine. *Oncotarget.* 2013;4(1):29–34. doi: 10.18632/oncotarget.755.
35. Roylance R, Kilburn L, Kernaghan S, Wardley AM, Macpherson I, Baird RD, et al. Abstract P1-19-11: Results from plasmaMATCH trial treatment cohort C: A phase II trial of capivasertib plus fulvestrant in ER positive breast cancer patients with an AKT1 mutation identified via ctDNA screening (CRUK/15/010). *Cancer Res.* 2020;80(4_Supplement):P1-19–11. doi: 10.1158/1538-7445.SABCS19-P1-19-11.
36. Shrestha Bhattarai T, Shamu T, Gorelick AN, Chang MT, Chakravarty D, Gavrila EI, et al. AKT mutant allele-specific activation dictates pharmacologic sensitivities. *Nat Commun.* 2022;13(1):2111. doi: 10.1038/s41467-022-29638-1.
37. Altiparmak-Ulbegi G, Hasbal-Celikok G, Aksoy-Sagirli P. AKT1 and CTNNB1 mutations as drivers of paclitaxel resistance in breast cancer cells. *Oncol Lett.* 2025;30(1):324. doi: 10.3892/ol.2025.15070.
38. Hasbal-Celikok G, Aksoy-Sagirli P, Altiparmak-Ulbegi G, Can A. Identification of AKT1/β-catenin mutations conferring cetuximab and chemotherapeutic drug resistance in colorectal cancer treatment. *Oncol Lett.* 2021;21(3):209. doi: 10.3892/ol.2021.12470.
39. Rudolph M, Anzeneder T, Schulz A, Beckmann G, Byrne AT, Jeffers M, et al. AKT1 (E17K) mutation profiling in breast cancer: prevalence, concurrent oncogenic alterations, and blood-based detection. *BMC Cancer.* 2016;16:622. doi: 10.1186/s12885-016-2626-1.
40. Vivanco I, Chen ZC, Tanos B, Oldrini B, Hsieh W-Y, Yannuzzi N, et al. A kinase-independent function of AKT promotes cancer cell survival. *eLife.* 2014;3:e03751. doi: 10.7554/eLife.03751.

https://doi.org/10.5455/annalsmedres.2025.07.185

Ann Med Res

Current issue list available at Ann Med Res

Annals of Medical Research

journal page: annalsmedres.org

Time-dependent exposure to venetoclax induces ferroptosis in human neuroblastoma cells via upregulated transferrin gene expression and lipid peroxidation

Zubeyir Elmazoglu [a], Erva Ozkan [b,*]

[a] Ankara Medipol University, Faculty of Pharmacy, Department of Pharmacology, Ankara, Türkiye
[b] Ankara Medipol University, Faculty of Pharmacy, Department of Biochemistry, Ankara, Türkiye
*Corresponding author: erva.ozkan@ankaramedipol.edu.tr (Erva Ozkan)

MAIN POINTS

- This study demonstrated for the first time that venetoclax induces ferroptosis in human neuroblastoma cells.
- Venetoclax alters intracellular iron homeostasis by upregulating the expression of transferrin and downregulating the expression of ferroportin1, resulting in enhanced labile iron pool content.
- Venetoclax increases oxidative stress and lipid peroxidation in neuroblastoma cells, which are inhibited by the iron chelator deferoxamine.

Cite this article as: Elmazoglu Z, Ozkan E. Time-dependent exposure to venetoclax induces ferroptosis in human neuroblastoma cells via upregulated transferrin gene expression and lipid peroxidation. *Ann Med Res*. 2025;32(12):552–559. doi: 10.5455/annalsmedres.2025.07.192.

ABSTRACT

Aim: Neuroblastoma is one of the most widely diagnosed extracranial tumors in pediatric patients with poor survival rates. Despite the available treatment options, alternative treatment strategies are required, especially for high-risk patients. Venetoclax (VTX) is a small-molecule inhibitor of the anti-apoptotic protein Bcl-2, originally approved for the treatment of acute myeloid and chronic lymphocytic leukemia. Mounting evidence indicates that VTX may also be a promising agent against other types of cancer. However, data on the alternative mechanisms of VTX toxicity are limited. The present study aimed to unveil the potential of the agent against neuroblastoma. The effect of VTX on iron metabolism and ferroptotic cell death in neuroblastoma cells was investigated for the first time.

Materials and Methods: Cell viability was determined using the MTT assay. Oxidative stress, intracellular iron content, and lysosomal integrity were visualized using confocal microscopy. The MDA assay was performed to detect lipid peroxidation. The expression of TFR, FPN1, and GPX4 was determined by RT-qPCR.

Results: VTX significantly reduced cell viability in a time- and concentration-dependent manner, which was reversed by the addition of ferroptosis inhibitors. Further experiments revealed that VTX induces ROS generation, leads to lysosomal degradation and iron accumulation followed by lipid peroxidation, all of which are ferroptosis markers. RT-qPCR analyses indicated that VTX upregulates TFR gene expression while downregulating GPX4 and FPN1.

Conclusion: The present study demonstrated for the first time that VTX activates ferroptotic pathways in neuroblastoma cells and may be considered as a promising agent for add-on therapies.

Keywords: Ferroptosis, Iron, Neuroblastoma, Oxidative stress, Venetoclax

Received: Jul 14, 2025 **Accepted:** Sep 22, 2025 **Available Online:** Dec 25, 2025

INTRODUCTION

Neuroblastoma is a common pediatric malignant tumor that originates from neuronal progenitor cells [1]. Current treatment options include surgery, chemotherapy, and radiotherapy. However, high-risk patients have a poor prognosis with an overall survival rate of 50%. Therefore, it is crucial to develop novel treatment options with higher efficacy [2].

Venetoclax (VTX) is a small molecule that was first developed as a selective Bcl-2 inhibitor against acute myeloid leukemia (AML). FDA approval for relapsed or refractory chronic lymphocytic leukemia (CLL) was obtained in 2016 [3]. Bcl-2 is often highly expressed in cancer cells, including lung and hematological cancers [4,5]. Similarly, neuroblastoma cells usually manage to escape apoptosis via increased Bcl-2 expression, indicating that these tumors may be more sensitive to Bcl-2 inhibitors [6]. Thus, navitoclax was first developed as a potent Bcl-2 inhibitor. However, it was less selective to Bcl-2 and caused severe thrombocytopenia [7]. Therefore, VTX was developed as a more selective Bcl-2 inhibitor that did not cause thrombocytopenia and was well tolerated by patients. Even though VTX was found to be weak as a single agent, there are reports demonstrating increased sensitiv-

ity to chemotherapy following the addition of VTX in conventional regimens [8,9]. On the other hand, preclinical studies have also shown that the upregulation of Bcl-2 may cause resistance to the agent [10]. Discovering alternative mechanisms of VTX may provide more effective treatment approaches in cancer.

Ferroptosis is a distinct type of regulated cell death mechanism discovered in 2012 by Dixon et al. in 2012 [11]. Unlike apoptosis and autophagy, intracellular iron accumulation, oxidative stress, and iron-dependent lipid peroxidation are considered hallmarks of this unique cell death [12]. The different mechanisms of ferroptosis make it particularly advantageous against cancer cells resistant to other cell death pathways. Numerous studies have reported that ferroptosis activation significantly increases cancer cell susceptibility to chemotherapy [13]. Hence, developing new approaches to treatment has become a trending focus of cancer research. Yu et al. [14] reported that VTX may have the potential to induce ferroptotic pathways in AML [14]. However, its effect on iron metabolism or ferroptotic pathways in neuroblastoma cells has not been investigated.

The present study aimed to shed light on the alternative pathways of VTX. The ferroptotic activity of VTX in human neuroblastoma cells was determined for the first time. The status of iron and lipid-related markers was investigated following VTX treatment, and the observed cytotoxic effect of the agent was compared with that of L929 healthy cells. Due to the multiple advantages such as tolerability, low risk of thrombocytopenia and ability to cross the blood-brain barrier, VTX may be a potential candidate for add-on therapies in neuroblastoma [15].

MATERIALS AND METHODS

Cell culture, Chemicals, and Experimental design

SH-SY5Y neuroblastoma and L929 fibroblast cells were purchased from the American Type Culture Collection (ATCC) (USA). MTT (3-(4,5-dimethylthiazol-2-yl)-2,5-diphenyl tetrazolium bromide) was purchased from Sigma-Aldrich (Germany). Dulbecco's Modified Eagle Medium (DMEM), fetal bovine serum (FBS), trypsin-EDTA, and penicillin-streptomycin were obtained from Capricorn Scientific (Germany). Venetoclax was obtained from BLD Pharm (China). Trolox, mannitol, N-acetylcysteine, ferrostatin-1, and deferoxamine were purchased from Sigma-Aldrich (Germany). PCR primers were obtained from Sentromer DNA Technologies (Turkey).

SH-SY5Y and L929 cells were maintained in high-glucose DMEM supplemented with 10% FBS, 1% penicillin/streptomycin, 1% L-glutamine. Both cell lines were incubated in a humidified atmosphere with 5% CO_2 at 37°C. Venetoclax was dissolved in dimethyl sulfoxide (DMSO) and diluted in DMEM to prepare various concentrations. The final DMSO concentration did not exceed 0.1%. Untreated cells were used as controls. Each experiment was performed in triplicate, and cell viability, oxidative stress, and ferroptotic hallmarks were evaluated.

In vitro cell viability

The effect of VTX on cell viability was evaluated using the MTT assay. Cells were seeded in 96-well plates and incubated overnight. Then, VTX (0.5-50 μM) was administered in the presence or absence of scavengers (trolox, mannitol, and N-acetylcysteine) and ferroptosis inhibitors (ferrostatin-1 and deferoxamine). After 24 h of incubation, the MTT reagent (5 mg/ml) was added to fresh medium for 3 h. The resulting formazan particles were dissolved in SDS-HCl, and the absorbance was measured at 540 nm using a microplate reader (Thermo, Germany).

ROS Generation

The state of intracellular ROS following VTX treatment was determined using a 2',7'-dichlorofluorescein diacetate fluorescent (DCFH-DA) probe. Cells were exposed to VTX in the presence or absence of deferoxamine, mannitol, ferrostatin-1, or N-acetylcysteine. Then, the plate was washed twice with 1X PBS and incubated for 30 min with DCFH-DA (20 μM) and Hoechst 33342 (1 μg/ml) probe prepared in serum-free medium. After a final wash of 3 times with 1X PBS, the acquired green fluorescence was visualized with a confocal microscope at wavelengths of 361⁄497 nm (ex/em) and 488/535 nm (ex/em) (LSM 900, Carl Zeiss, Germany). Each experiment was performed in at least 2 replicates, taking 4 images from each group (10X) [16].

Determination of lipid peroxidation

Lipid peroxidation in VTX-treated neuroblastoma cells was determined by measuring the end-product, malondialdehyde (MDA). Before the experiment, cells were seeded in culture plates and incubated overnight. Following the administration of VTX (25 μM) for 24 h, the cells were harvested and lysed in cell lysis buffer (Cell Signaling, Germany). The lysates were used for the assay according to the TBARS method [17]. The absorbance of the acquired pink color was measured at 532 nm using a microplate reader (MultiskanSky, Thermo, Germany).

Detection of labile iron pool and lipid accumulation

Intracellular iron content and lysosomal integrity were visualized by calcein-acetoxymethyl ester (calcein-AM) and neutral red (NRU) staining [18]. VTX-treated cells were washed twice with 1X PBS and then incubated for 30 min with calcein-AM (10 μM), neutral red (10 μM), and Hoechst 33342 (1 μg/ml) probe in serum-free medium. After the final wash, images of the acquired fluorescence were captured using confocal microscopy at 495⁄515 nm (ex/em), 470/580 nm (ex/em), and 488/535 nm (ex/em) (LSM 900, Carl Zeiss, Germany). Experiments were conducted in at least 2 replicates, taking 4 images from each group (10X).

https://doi.org/10.5455/annalsmedres.2025.07.192

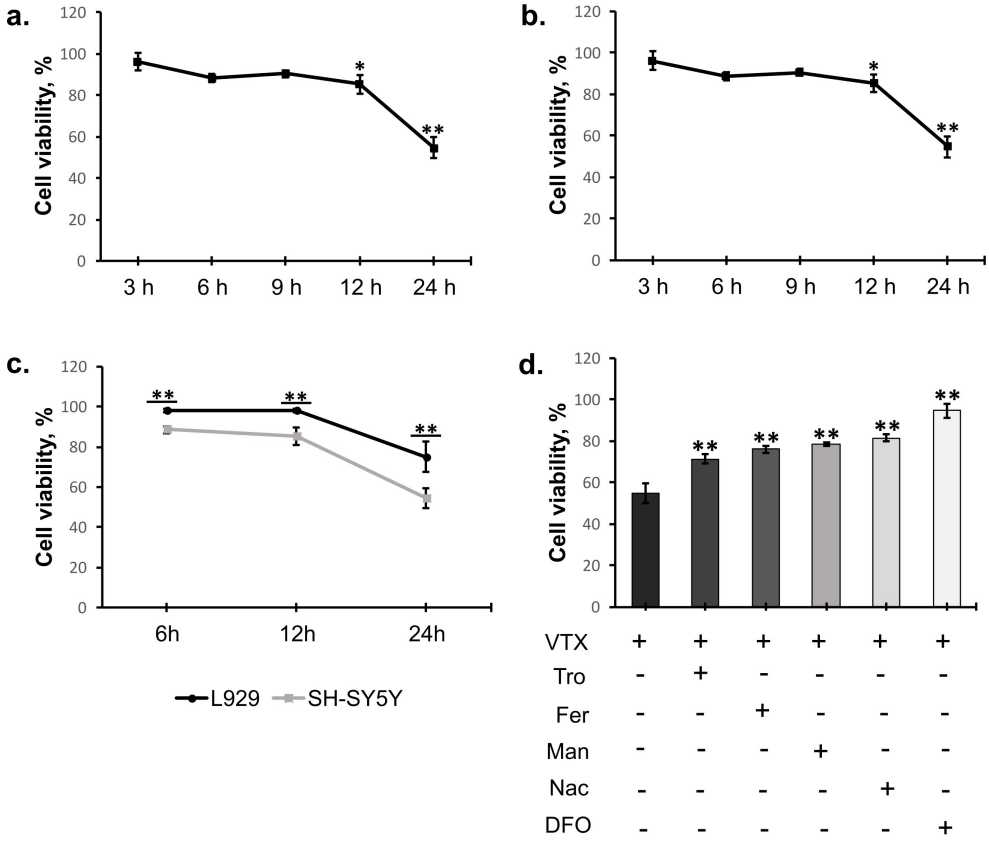

Figure 1. The cytotoxic effect of VTX on human neuroblastoma cells. (a) SH-SY5Y cells were treated with VTX (0.5-50 µM) for 24 h and the cell viability was determined with MTT assay. (b) The time-dependent effect of VTX (25 µM) on neuroblastoma cell viability. (c) The comparison of VTX toxicity between SH-SY5Y neuroblastoma cells and L929 normal cells. (d) Cells were treated with VTX (25 µM) alone and in the presence of scavengers (trolox, mannitol, n-acetylcysteine) and ferroptosis inhibitors (ferrostatin-1, deferoxamine), and the viable cells were detected with MTT assay. Data represent the average of at least 4 replicates, *p<0.01, **p<0.001. VTX: Venetoclax, Tro: Trolox, Fer: Ferrostatin-1, Man: Mannitol, Nac: N-acetylcysteine, DFO: Deferoxamine.

RT-qPCR

RNA was extracted using TRIzol reagent (ABP Biosciences, USA) according to the manufacturer's instructions. cDNA from each sample was synthesized using a High-Capacity cDNA Reverse Transcription Kit (Applied Biosystems, CA, USA). RT-qPCR was performed using SYBR Green (Wizbiosolutions Inc., Korea) according to the manufacturer's protocol. The PCR conditions were as follows: 1 cycle of 95 oC 5 mins, 40 cycles of 95 oC 30 seconds and 65 oC 60 seconds, 1 cycle of 95 oC 5 seconds. Data analysis was performed using ΔΔCt method. Glyceraldehyde 3-phosphate dehydrogenase (GAPDH) was used as the internal control. The primer sequences for each gene are provided in Supplementary Table 1.

Statistical analysis

Data obtained from the experiments were analyzed using SPSS 20.0 (IBM Co, USA, 5725-A54). One-way analysis of variance (ANOVA) was employed for multiple comparisons, followed by Tukey's test. The difference between the two groups was determined using Student's t-test. All data are expressed as mean ± standard deviation (SD) with $p<0.05$ being considered statistically significant.

RESULTS

Venetoclax exhibits a significant cytotoxic effect on neuroblastoma cells in a time- and concentration-dependent manner

SH-SY5Y neuroblastoma cells were treated with 0.5, 1, 5, 10, 25 and 50 µM VTX and the viable cells were determined after 24 h Results showed that VTX was significantly toxic at 25 and 50 µM with 54.70 ± 4.94 and 34.06 ± 8.82 (%) viability ($p=0.000013$ for both values) (Figure 1a). Time-dependent activity of the minimum toxic concentration of the agent (25 µM) revealed that the cytotoxic effect starts at 12 h and increases over 24 h (Figure 1b). Compared with L929 healthy cells, a significant selectivity was observed in all time periods (Figure 1c). To understand whether VTX-induced cell death is related to ferroptosis, several inhibitors were applied along with the agent. The results indicated that the antioxidants trolox (25 µM), mannitol (10 mM), N-acetylcysteine (1 mM), ferroptosis inhibitors ferrostatin-1 (1 µM), and deferoxamine (250 µM) reversed the effect of VTX, with the ferrop-

https://doi.org/10.5455/annalsmedres.2025.07.192

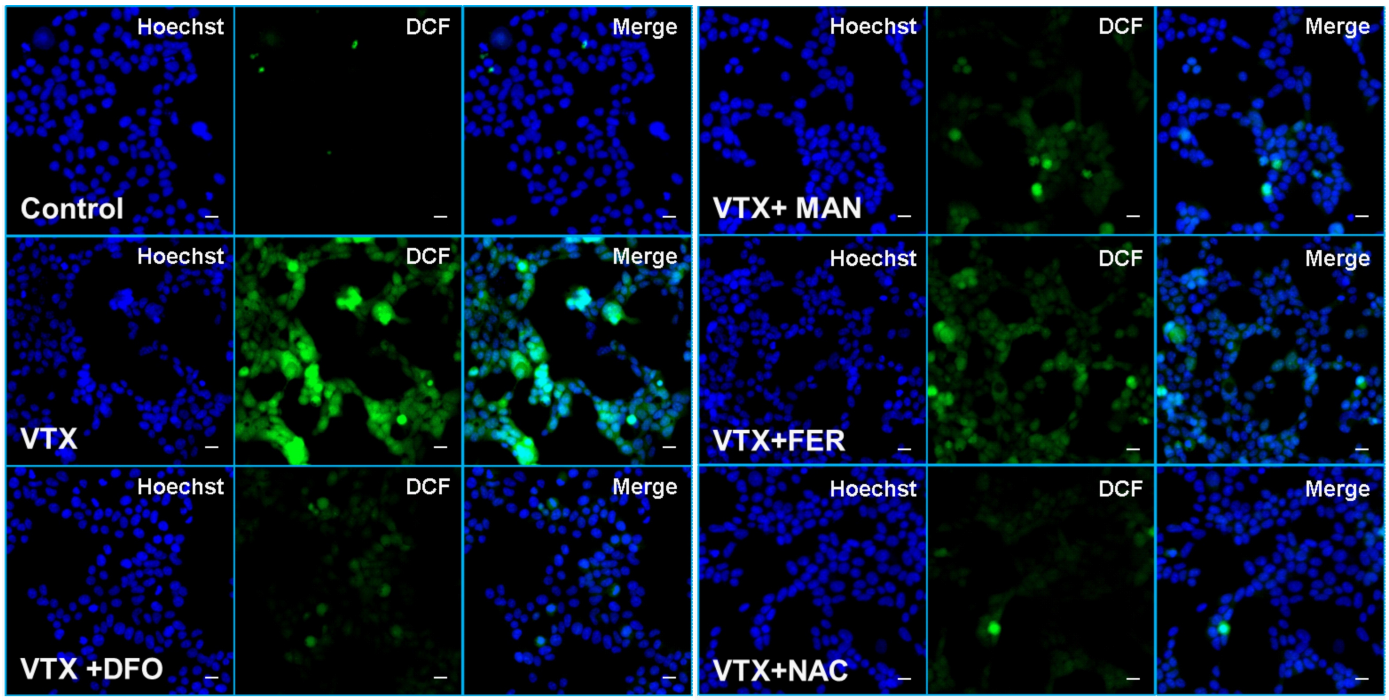

Figure 2. Visualization of ROS generation in SH-SY5Y cells treated with VTX (25 μM) alone or in combination with inhibitors for 12 h Cells were stained with DCF, and fluorescence emission was detected using confocal microscopy. VTX: Venetoclax, DFO: Deferoxamine, MAN: Mannitol, FER: Ferrostatin-1, NAC: N-acetylcysteine.

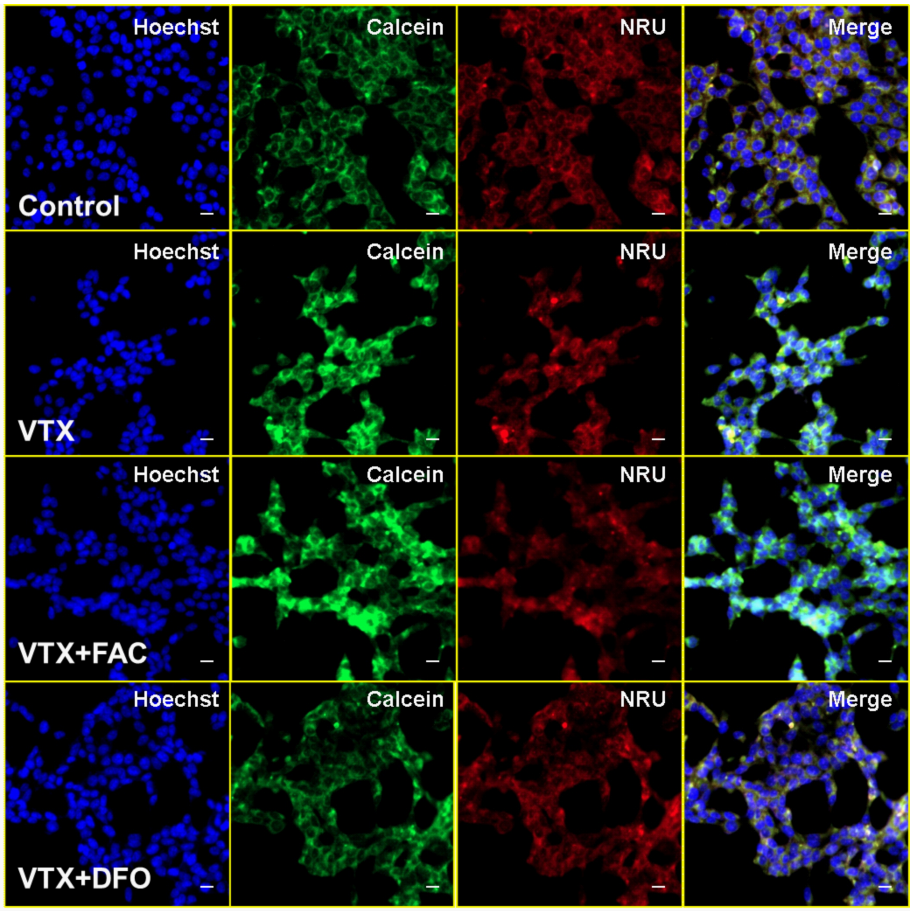

Figure 3. Imaging the enhanced iron and lysosomal degradation in SH-SY5Y neuroblastoma cells treated with VTX (25 μM) in the presence of ferric ammonium citrate (FAC) or iron chelator deferoxamine (DFO) for 12 h. Iron was detected with calcein staining, and lysosomal degradation was visualized with neutral red staining using confocal microscopy.

https://doi.org/10.5455/annalsmedres.2025.07.192

tosis inhibitor deferoxamine achieving the best reversal (p = 0.000024) (Figure 1d).

ROS generation, iron and lysosomal degradation increased following venetoclax treatment

The state of oxidative stress in VTX-treated cells was visualized using confocal microscopy. The cells were treated with VTX (25 μM) for 12 h and stained with DCF. The acquired images indicated an apparent increase in ROS generation in the VTX-treated group compared with the untreated control, which was clearly inhibited by the addition of ferroptosis inhibitors and scavengers (Figure 2). Next, the iron content and lysosomal integrity of the cells were detected with Hoechst/calcein/neutral red triple staining, where calcein showed a labile iron pool and neutral red showed lysosomal integrity, simultaneously. The results indicated that both iron and lysosomal degradation increased following VTX treatment compared to the untreated control group. Similar results were observed with the addition of FAC, which was suppressed by deferoxamine (Figure 3).

Venetoclax induces iron-dependent lipid peroxidation

To investigate the lipid peroxidation status in cells treated with VTX, the end-product MDA levels were measured in different time periods using the TBARS method. Following 12 and 24 h of incubation with VTX (25 μM), MDA levels were significantly higher than those in the control group, by 134.02 ± 2.00 and 204.83 ± 7.84 (%), respectively (p = 0.006264) (Figure 4a). Further experiments revealed that scavengers and ferroptosis inhibitors suppressed the increased lipid peroxidation, with the highest suppressive effect observed by deferoxamine (p = 0.005496) (Figure 4b).

TFR, FPN1, and GPX4 gene expressions were significantly altered in Venetoclax-treated neuroblastoma cells

Cells were administered with VTX for 12 h, and the mRNA expression of iron-related genes, TFR and FPN1, and the cellular antioxidant enzyme GPX4 were analyzed by RT-qPCR. The results revealed a significant upregulation of TFR, which was detected as approximately 2-fold, whereas FPN1 was downregulated by 5-fold and GPX4 was downregulated by 1.5-fold ($p<0.05$).

DISCUSSION

Neuroblastoma is an extracranial pediatric malignant tumor observed in approximately 1 in 10 children. Due to the low survival rates in high-risk patients, extensive research has been conducted on alternative therapeutics [19]. Venetoclax is primarily used against hematological cancers and has recently drawn attention for its potential in different types of cancers. Several studies have reported that it exhibits antitumoral behavior in glioma and lung and breast cancers [20–22]. Furthermore, a case study reported that VTX may contribute to neuroblastoma treatment when combined with conventional chemotherapeutics [8]. However, VTX is mostly known for its Bcl-2 inhibitory effect, and data on its alternative mechanisms of action are very limited. Deciphering these pathways induced by VTX, beyond Bcl-2 inhibition, may provide a more effective and rational combinatorial therapy regimen.

The ferroptotic activity of VTX was investigated in neuroblastoma cells. First, the concentration-dependent effect of the agent was determined and 25 μM was selected for further experiments because it yielded an approximate IC_{50} value (Figure 1a). Time-dependent cell viability analysis demonstrated that 25 μM of VTX causes a significant death starting from 12 h, which gradually increases over 24 h (Figure 1b). Furthermore, it was observed that some antioxidants reversed the cytotoxic effect of VTX, which correlates with the ROS-generating role of the agent [14]. However, the iron chelator and ferroptosis inhibitor deferoxamine exhibited the highest inhibition rate, indicating that iron is a major contributor to VTX-induced cell death (Figure 1d). To confirm this, confocal microscopy was used to visualize the labile iron pool in VTX-treated cells, which reflected an obvious increase in the iron content. Similar results were obtained when the cells were treated with FAC, which is an iron source. To investigate the role of iron in VTX-induced cell death, neuroblastoma cells were exposed to both VTX and FAC, and neutral red staining was performed to highlight the integrity of lysosomes. As shown in Figure 3, both VTX and FAC aggravated lysosomal degradation. The close relationship between lysosomal function and ferroptosis is well established. Because lysosomes contain iron and proteolytic enzymes, the breakdown of lysosomal membranes results in the release of iron, which contributes to the increase in the labile iron pool [23].

Oxidative stress and iron-dependent lipid peroxidation are among the essential hallmarks of ferroptotic cell death, which may be induced by VTX [14,20]. In this study, ROS generation was detected using DCF staining. The acquired images showed that VTX treatment enhances the available ROS in cells. Generally, cancer cells increase their antioxidant defense capacity to overcome cellular damage caused by excess ROS. Glutathione peroxidases (GPx) are major players in this regard because they neutralize free radicals [24]. GPx4 is a critical suppressor of ferroptotic cell death; thus, downregulation of this enzyme is particularly important to enable ROS generation and the subsequent events [25]. RT-qPCR analyses demonstrated that 12 h of VTX treatment significantly suppressed GPx4 gene expression in neuroblastoma cells, which may explain the increase in ROS generation. Excess ROS in the cellular environment damage lipid–based structures, especially polyunsaturated fatty acids (PUFAs) found in cell membranes, leading to lipid peroxidation [26]. To verify this, the end-product of lipid peroxides (MDA) was measured following VTX treatment. The results demonstrated a significant elevation in MDA levels in a time-dependent manner, which correlated with the results of the previous experiments (Figure 4a). To confirm that lipid peroxides were iron-dependent,

https://doi.org/10.5455/annalsmedres.2025.07.192

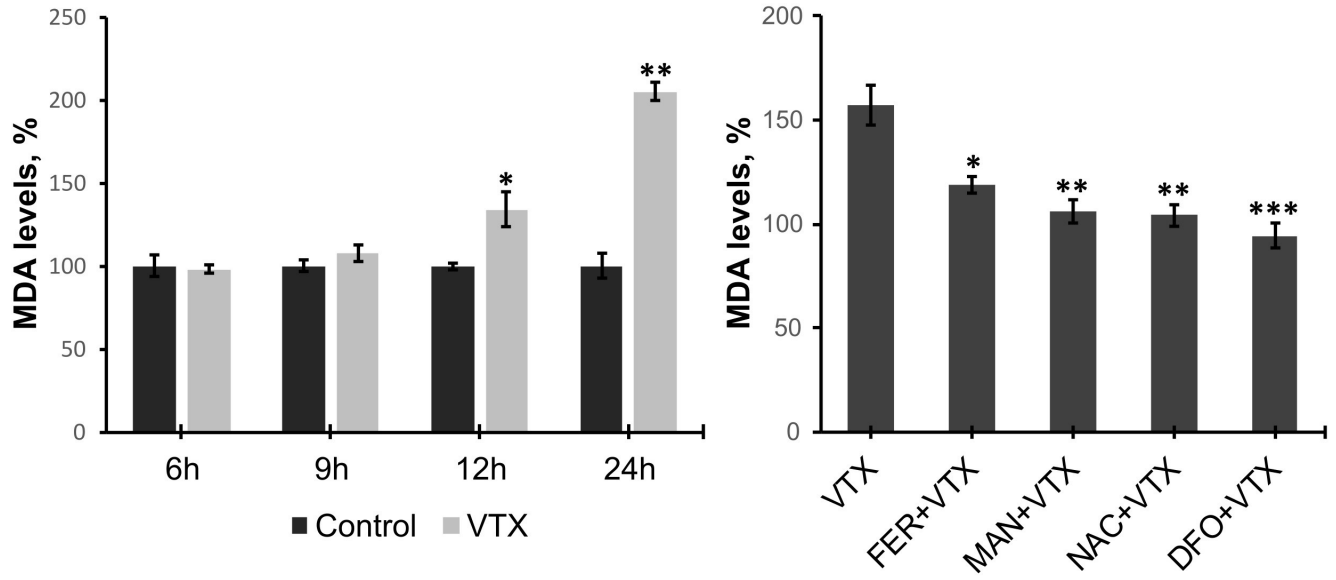

Figure 4. Detection of lipid peroxidation in SH-SY5Y cells. (a) Following VTX (25 μM) treatment, cells were lysed, and the end-product of lipid peroxidation, malondialdehyde (MDA), was measured using the TBARS method. (b) The effect of VTX (25 μM) combined with scavengers and ferroptosis inhibitors on lipid peroxidation. Data represent the average of at least 3 replicates, *p<0.01, **p<0.001, ***p<0.0001. VTX: Venetoclax, FER: Ferrostatin-1, MAN: Mannitol, NAC: N-acetylcysteine, DFO: Deferoxamine.

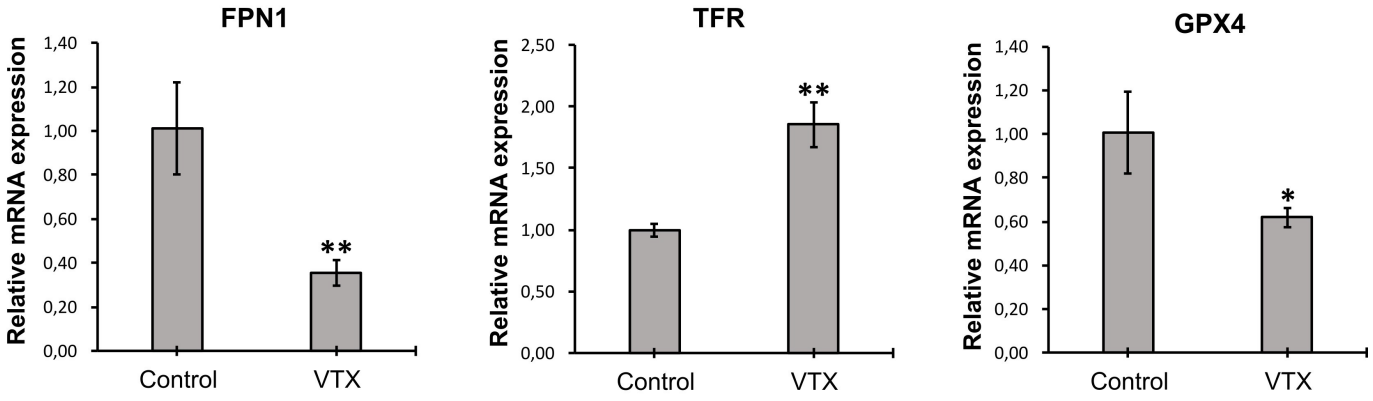

Figure 5. Gene expression analysis using RT-qPCR Cells were treated with VTX (25 μM), and FPN, TFR, and GPX4 mRNA expression was detected after 12 h Data represent the average of at least 3 replicates, *p<0.01, **p<0.001. FPN1: Ferroportin, TFR: Transferrin, GPX4: Glutathione peroxidase-4.

VTX was administered to neuroblastoma cells in the presence of deferoxamine and antioxidants. The findings indicated that deferoxamine suppresses the formation of MDA more than the antioxidants, leading to the conclusion that iron mediates VTX-induced lipid peroxidation (Figure 4b).

Iron is a critical player in ferroptotic cell death [27]. Hence, iron metabolism and associated elements in the cellular environment must be explored to confirm the activation of this pathway. In this regard, transferrin (TFR) and ferroportin1 (FPN1) are among the major regulators of cellular iron metabolism. TFR allows iron entry into the cell, while FPN1 mediates iron export. In ferroptosis, TFR expression is upregulated and FPN1 is downregulated to enrich the intracellular iron content [28]. TFR and FPN1 gene expressions were analyzed in VTX-exposed neuroblastoma cells. After 12 h of treatment, TFR gene expression increased by approximately 2-fold, whereas FPN1 expression was downregulated by 5-fold (Figure 5). These findings support the hypothesis that VTX activates ferroptotic pathways in neuroblastoma cells.

Despite the promising data obtained in this study, some limitations should be addressed in future studies. The potential of VTX as an add-on therapy, such as whether VTX would exhibit ferroptotic activity when combined with chemotherapeutics, should be explored.

https://doi.org/10.5455/annalsmedres.2025.07.192

Furthermore, the long-term effects of VTX use, especially on healthy tissues, should be investigated.

Conclusion

Neuroblastoma is a common neoplasm in children with insufficient treatment options. VTX is a selective Bcl-2 inhibitor that may be a promising treatment candidate. In this study, the ferroptotic behavior of VTX was investigated in neuroblastoma cells for the first time. The data obtained indicated that VTX exposure increased oxidative stress and iron-dependent lipid peroxidation, which are hallmarks of ferroptosis. In addition, iron metabolism was altered with upregulated transferrin and downregulated ferroportin gene expression following VTX administration. Taken together, the findings of this study shed light on the alternative mechanisms of VTX, demonstrating its potential contribution to the treatment of neuroblastoma.

Ethics Committee Approval: It is a cell study that does not require ethics committee approval.

Informed Consent: Not necessary for this manuscript.

Peer-review: Externally peer-reviewed.

Conflict of Interest: The authors declare that they have no known competing interests or personal relationships that could have influenced the work reported in this paper.

Author Contributions: Concept: ZE, EO; Design: ZE, EO; Supervision: ZE, EO; Materials: ZE; Data Collection and/or Processing: ZE, EO; Literature Review: EO; Writing: ZE, EO; Critical Review: ZE, EO.

Financial Disclosure: This research did not receive any specific grant from public, commercial, or not-for-profit funding agencies.

REFERENCES

1. Zahnreich S, Schmidberger H. Childhood cancer: Occurrence, treatment and risk of second primary malignancies. *Cancers (Basel).* 2021;13(11):2607. doi: 10.3390/cancers13112607.
2. Katta SS, Nagati V, Paturi ASV, Murakonda SP, Murakonda AB, Pandey MK, et al. Neuroblastoma: Emerging trends in pathogenesis, diagnosis, and therapeutic targets. *J Control Release.* 2023;357:444–59. doi: 10.1016/j.jconrel.2023.04.001.
3. Kawakatsu R, Tadagaki K, Yamasaki K, Yoshida T. Venetoclax efficacy on acute myeloid leukemia is enhanced by the combination with butyrate. *Sci Rep.* 2024;14(1):4975. doi: 10.1038/s41598-024-55286-0.
4. Gardner EE, Connis N, Poirier JT, Cope L, Dobromilskaya I, Gallia GL, et al. Rapamycin rescues ABT-737 efficacy in small cell lung cancer. *Cancer Res.* 2014;74(10):2846–56. doi: 10.1158/0008-5472.CAN-13-3460.
5. Perini GF, Ribeiro GN, Pinto Neto JV, Campos LT, Hamerschlak N. BCL-2 as therapeutic target for hematological malignancies. *J Hematol Oncol.* 2018;11(1):65. doi: 10.1186/s13045-018-0608-2.
6. Bierbrauer A, Jacob M, Vogler M, Fulda S. A direct comparison of selective BH3-mimetics reveals BCL-XL, BCL-2 and MCL-1 as promising therapeutic targets in neuroblastoma. *Br J Cancer.* 2020;122(10):1544–51. doi: 10.1038/s41416-020-0795-9.
7. de Vos S, Leonard JP, Friedberg JW, Zain J, Dunleavy K, Humerickhouse R, et al. Safety and efficacy of navitoclax, a BCL-2 and BCL-XL inhibitor, in patients with relapsed or refractory lymphoid malignancies: results from a phase 2a study. *Leuk Lymphoma.* 2021;62(4):810–8. doi: 10.1080/10428194.2020.1845332.
8. De Ioris MA, Fabozzi F, Del Bufalo F, Del Baldo G, Villani MF, Cefalo MG, et al. Venetoclax plus cyclophosphamide and topotecan in heavily pre-treated relapsed metastatic neuroblastoma: a single center case series. *Sci Rep.* 2023;13(1):19295. doi: 10.1038/s41598-023-44993-9.
9. Tanos R, Karmali D, Nalluri S, Goldsmith KC. Select Bcl-2 antagonism restores chemotherapy sensitivity in high-risk neuroblastoma. *BMC Cancer.* 2016;16:97. doi: 10.1186/s12885-016-2129-0.
10. Vernooij L, Kamili A, Ober K, van Arkel J, Lankhorst L, Vermeulen E, et al. Preclinical assessment of combined BCL-2 and MCL-1 inhibition in high-risk neuroblastoma. *EJC Paediatr Oncol.* 2024;3(8):100168. doi: 10.1016/j.ejcped.2024.100168.
11. Dixon SJ, Lemberg KM, Lamprecht MR, Skouta R, Zaitsev EM, Gleason CE, et al. Ferroptosis: An Iron-Dependent Form of Non-Apoptotic Cell Death. *Cell.* 2012;149(5):1060–72. doi: 10.1016/j.cell.2012.03.042.
12. Stockwell BR, Friedmann Angeli JP, Bayir H, Bush AI, Conrad M, Dixon SJ, et al. Ferroptosis: A Regulated Cell Death Nexus Linking Metabolism, Redox Biology, and Disease. *Cell.* 2017;171(2):273–85. doi: 10.1016/j.cell.2017.09.021.
13. Zhang, C, Liu X, Jin S, Chen Y, Guo R. Ferroptosis in cancer therapy: a novel approach to reversing drug resistance. *Mol Cancer.* 2022;21(1):47. doi: 10.1186/s12943-022-01530-y.
14. Yu X, Wang Y, Tan J, Li Y, Yang P, Liu X, et al. Inhibition of NRF2 enhances the acute myeloid leukemia cell death induced by venetoclax via the ferroptosis pathway. *Cell Death Discov.* 2024;10(1):35. doi: 10.1038/s41420-024-01800-2.
15. Badawi M, Menon R, Place AE, Palenski T, Sunkersett G, Arrendale R, et al. Venetoclax Penetrates the Blood Brain Barrier: A Pharmacokinetic Analysis in Pediatric Leukemia Patients. *J Cancer.* 2023;14(7):1151–6. doi: 10.7150/jca.81795.
16. Almammadov T, Elmazoglu Z, Atakan G, Kepil D, Aykent G, Kolemen S, et al. Locked and Loaded: β-Galactosidase Activated Photodynamic Therapy Agent Enables Selective Imaging and Targeted Treatment of Glioblastoma Multiforme Cancer Cells. *ACS Appl Bio Mater.* 2022;5(9):4284–93. doi: 10.1021/acsabm.2c00484.
17. Ye LF, Chaudhary KR, Zandkarimi F, Harken AD, Kinslow CJ, Upadhyayula PS, et al. Radiation-Induced Lipid Peroxidation Triggers Ferroptosis and Synergizes with Ferroptosis Inducers. *ACS Chem Biol.* 2020;15(2):469–84. doi: 10.1021/acschembio.9b00939.
18. Abbasi U, Abbina S, Gill A, Bhagat V, Kizhakkedathu JN. A facile colorimetric method for the quantification of labile iron pool and total iron in cells and tissue specimens. *Sci Rep.* 2021;11(1):6008. doi: 10.1038/s41598-021-85387-z.
19. Polychronopoulos PA, Bedoya-Reina OC, Johnsen JI. The Neuroblastoma Microenvironment, Heterogeneity and Immunotherapeutic Approaches. *Cancers (Basel).* 2024;16(10):1863. doi: 10.3390/cancers16101863.
20. Madhavan K, Balakrishnan I, Lakshmanachetty S, Pierce A, Sanford B, Fosmire S, et al. Venetoclax Cooperates with Ionizing Radiation to Attenuate Diffuse Midline Glioma Tumor Growth. *Clin Cancer Res.* 2022;28(11):2409–24. doi: 10.1158/1078-0432.CCR-21-4002.
21. Lochmann TL, Floros K V., Naseri M, Powell KM, Cook W, March RJ, et al. Venetoclax Is Effective in Small-Cell Lung Cancers with High BCL-2 Expression. *Clin Cancer Res.* 2018;24(2):360–9. doi: 10.1158/1078-0432.CCR-17-1606.
22. Lok SW, Whittle JR, Vaillant F, Teh CE, Lo LL, Policheni AN, et al. A Phase Ib Dose-Escalation and Expansion Study of the BCL2 Inhibitor Venetoclax Combined with Tamoxifen in ER and BCL2–Positive Metastatic Breast Cancer. *Cancer Discov.* 2019;9(3):354–69. doi: 10.1158/2159-8290.CD-18-1151.
23. Feng J, Wang ZX, Bin JL, Chen YX, Ma J, Deng JH, et al. Pharmacological approaches for targeting lysosomes to induce ferroptotic cell death in cancer. *Cancer Lett.* 2024;587:216728. doi: 10.1016/j.canlet.2024.216728.

https://doi.org/10.5455/annalsmedres.2025.07.192

24. Lee J, Roh JL. Targeting GPX4 in human cancer: Implications of ferroptosis induction for tackling cancer resilience. *Cancer Lett.* 2023;559:216119. doi: 10.1016/j.canlet.2023.216119.
25. Zhang X, Ma Y, Ma J, Yang L, Song Q, Wang H, et al. Glutathione Peroxidase 4 as a Therapeutic Target for Anti-Colorectal Cancer Drug-Tolerant Persister Cells. *Front Oncol.* 2022;12:913669. doi: 10.3389/fonc.2022.913669.
26. Mortensen MS, Ruiz J, Watts JL. Polyunsaturated Fatty Acids Drive Lipid Peroxidation during Ferroptosis. *Cells.* 2023;12(5):804. doi: 10.3390/cells12050804.
27. Battaglia AM, Chirillo R, Aversa I, Sacco A, Costanzo F, Biamonte F. Ferroptosis and Cancer: Mitochondria Meet the "Iron Maiden" Cell Death. *Cells*. 2020;9(6):1505. doi: 10.3390/cells9061505.
28. Liang W, Ferrara N. Iron Metabolism in the Tumor Microenvironment: Contributions of Innate Immune Cells. *Front Immunol.* 2021;11:626812. doi: 10.3389/fimmu.2020.626812.

https://doi.org/10.5455/annalsmedres.2025.07.192

Ann Med Res

Current issue list available at Ann Med Res

Annals of Medical Research

journal page: annalsmedres.org

Evaluation of postoperative complications and mortality predictors in adult patients undergoing ventriculoperitoneal shunt surgery: A retrospective single-center study

Tamer Tamdogan [a], Ilke Tamdogan [b,*], Sevim Ondul [a]

[a] Giresun University, Faculty of Medicine, Department of Neurosurgery, Giresun, Türkiye
[b] Giresun University, Faculty of Medicine, Department of Anesthesiology and Reanimation, Giresun, Türkiye
*Corresponding author: drilkeipek@gmail.com (Ilke Tamdogan)

MAIN POINTS

- Programmable valve systems were associated with significantly lower mortality rates compared to standard valves in adult VPS patients.
- Hydrocephalus due to intracranial hemorrhage demonstrated a near-significant association with increased mortality, highlighting the need for targeted follow-up.
- Both early and late complication rates were 13.6%, with overdrainage and shunt infection being the most common, respectively.
- The study supports programmable shunt use and individualized patient monitoring to improve outcomes in high-risk hydrocephalus cases.

Cite this article as: Tamdogan T, Tamdogan I, Ondul S. Evaluation of postoperative complications and mortality predictors in adult patients undergoing ventriculoperitoneal shunt surgery: A retrospective single-center study. *Ann Med Res*. 2025;32(12):560--565. doi: 10.5455/annalsmedres.2025.06.145.

ABSTRACT

Aim: The aim of our study is to retrospectively analyze the incidence of postoperative complications in adult patients who underwent ventriculoperitoneal shunt (VPS) surgery for hydrocephalus and to identify clinical, demographic, and surgical predictors of mortality.

Materials and Methods: This is a single-center retrospective analysis including 44 patients aged 18 years and older who underwent primary or revision VPS surgery between September 2021 and January 2025. Data including demographic characteristics, comorbidities, hydrocephalus etiology, type of shunt (programmable vs. standard), clinical presentation, early and late complications, and mortality were collected and analyzed. Statistical analysis involved independent t-tests and chi-square or Fisher's exact tests as appropriate.

Results: The mean patient age was 68.8 ± 10.8 years, with a mortality rate of 29.5% observed during follow-up. Early and late complication rates were each 13.6%. Over-drainage (9.1%) was the most common early complication, while shunt infection (6.8%) predominated among late complications. Mortality was significantly higher in patients with standard valves (61.5%) compared to those with programmable valves (38.5%, p<0.001). Hydrocephalus secondary to intracranial hemorrhage was associated the highest rate and it was slightly above the significance level (30.8%, p=0.053).

Conclusion: The type of shunt system and hydrocephalus etiology, particularly intracranial hemorrhage, were identified as the most significant predictors of mortality. The use of programmable valve systems and close monitoring of high-risk patients may improve outcomes.

Keywords: Ventriculoperitoneal shunt, Hydrocephalus, Postoperative complications, Neurosurgery

Received: Jun 10, 2025 **Accepted:** Sep 29, 2025 **Available Online:** Dec 25, 2025

INTRODUCTION

Hydrocephalus is a significant neurological disorder originating from the central nervous system. It may result from any pathology that affects the production, circulation, or absorption of cerebrospinal fluid (CSF). This condition may be linked to various etiologies, including intraventricular hemorrhage, congenital anomalies, brain tumors, infections such as meningitis, and head trauma. The main characteristics of hydrocephalus are pathological dilation of the ventricular system and subarachnoid space, potentially leading to substantial neurological sequelae due to increased intracranial pressure [1,2].

Currently, surgical interventions are the mainstay of the management of hydrocephalus, with ventriculoperitoneal shunt (VPS) placement being the most frequently employed technique. This procedure is designed to redirect cerebrospinal fluid (CSF) from the intraventricular space to the peritoneal cavity, thereby alleviating intracranial pressure. VPS is regarded as a life-saving intervention, particularly for patients who do not respond to conventional treatments or those ex-

periencing acute elevations in intracranial pressure. The literature indicates that shunt placement significantly reduces postoperative mortality rates [3,4]. However, despite the success of this surgical technique, the relatively high incidence of postoperative complications necessitates shunt revisions, resulting in considerable morbidity and increased hospital costs. Due to their invasive nature and external components, shunt systems are susceptible to various complications, including infections, mechanical obstructions, over-drainage, shunt migration, and peritoneal complications [5-7]. Various studies have reported complication rates of up to 30–40% associated with shunt systems [8].

These complications not only contribute to surgical failure but also adversely affect clinical prognosis by increasing hospital readmission rates, prolonging ICU stays, and elevating healthcare costs [9]. Repeated shunt revisions, in addition to imposing a financial burden on the healthcare system, significantly impact the psychosocial well-being of patients [10]. The primary objective of this study is to retrospectively ascertain the incidence of postoperative complications in adult patients undergoing VPS surgery and to analyze the potential effects of demographic, clinical, and surgical variables on mortality. The findings aim to contribute to the guide the strategies that may mitigate the risk of shunt-related complications and to provide guidance for clinical practices aimed at improving patient outcomes.

MATERIALS AND METHODS

This investigation constitutes a single-center retrospective analysis of patients who underwent ventriculoperitoneal shunt (VPS) surgery at our clinic. The study protocol was approved by the Ethics Committee of Giresun Training and Research Hospital (Ethics Committee Date/Approval Number: 28.05.2025/15) and was conducted in accordance with the ethical principles delineated in the Declaration of Helsinki. Given the retrospective nature of the study, informed consent was not obtained from the patients.

Study population

The study included patients who underwent VPS surgery at our clinic between September 2021 and January 2025. Inclusion criteria encompassed individuals aged ≥18 years, those who had undergone primary or revision VPS surgery, and those with complete medical records. Patients who received non-VPS hydrocephalus treatment or had incomplete clinical data were excluded from the study.

Data collection and evaluation

All data were retrospectively obtained using the hospital automation system and patient medical records. Recorded variables included demographic characteristics (age, sex), comorbid conditions, etiology of hydrocephalus (congenital, acquired, normal pressure, etc.), clinical presentation at admission, nature of the surgery (primary or revision), and type of shunt used (programmable or standard valve). Additionally, early (<30 days) and late (>30 days) shunt dysfunctions, mechanical complications (such as obstruction, fracture, or migration of the shunt system), infectious complications (such as meningitis or peritonitis), and over-drainage-related pathologies (such as subdural hematoma or slit ventricle syndrome) were evaluated along with mortality rates. All data were recorded in a standardized data collection form for analysis.

Statistical analysis

Descriptive statistics were reported as mean, standard deviation, median, minimum, and maximum values for continuous variables, and as frequency and percentage for categorical variables. The distribution of variables was evaluated using the Kolmogorov-Smirnov and Shapiro-Wilk tests. For normally distributed quantitative variables, mean values were compared using the independent samples t-test. For categorical independent variables, the chi-square test was employed. In cases where the assumptions of the chi-square test were not met, Fisher's exact test was applied. Statistical significance was set at $p < 0.05$. All statistical analyses were conducted using IBM SPSS Statistics version 28.0 (Armonk, NY: IBM Corp.). A post hoc power analysis for the mortality–shunt type association (χ^2 test, df = 1; $\alpha = 0.05$; N = 44; group proportions 20.5% vs. 79.5%; assumed effect size w = 0.50) using G*Power 3.1.9.4 yielded an achieved power of 0.91.

RESULTS

A total of 44 patients participated in the study. The mean age was 68.8 ± 10.8 years, with a median age of 69.5 years. In terms of gender distribution, 54.5% (n=24) of the patients were male, while 45.5% (n=20) were female. Comorbidities were present in the 95.5%of cases. The most prevalent comorbidities included hypertension (84.1%), coronary artery disease (27.3%), diabetes mellitus (20.5%), Alzheimer's disease (15.9%), and other systemic disorders (50.0%) (Table 1). Regarding the type of hydrocephalus, 81.8% of the cases were diagnosed with communicating hydrocephalus, and 18.2% with obstructive hydrocephalus. Hemorrhage was identified as the most common etiology (13.6%), followed by trauma (9.1%), tumors (6.8%), and infections (2.3%). The most frequently reported presenting symptoms were gait disturbances (81.8%), altered mental status (79.5%), and urinary incontinence (79.5%). Headache (34.1%) and nausea/vomiting (9.1%) were less commonly observed (Table 1). Programmable valves were utilized in 79.5% of patients, whereas standard valves were employed in 20.5%. Shunt revision was unnecessary in 90.9% of the patients; only four patients (9.1%) required a single revision. Additionally, five patients (11.4%) underwent external ventricular drainage (EVD) prior to shunt surgery (Table 1).

In the early postoperative period, the overall complication rate was observed to be 13.6%. The most prevalent com-

https://doi.org/10.5455/annalsmedres.2025.06.145

Table 1. Demographic data and clinical descriptors.

		Min-Max	Median	Mean ± SD	n	-	%
Age		44.0-93.0	69.5	68.8±10.8			
Gender	Female				20	-	45.5%
	Meal				24	-	54.5%
Comorbidities	No				2	-	4.5%
	Yes				42	-	95.5%
Hypertension (HT)					37	-	84.1%
Coronary artery disease					12	-	27.3%
Diabetes mellitus (DM)					9	-	20.5%
Alzheimer's disease					7	-	15.9%
Others					22	-	50.0%
Type of Hydrocephalus							
Communicative					36	-	81.8%
Obstructive					8	-	18.2%
	Post-traumatic				4	-	9.1%
	Infectious				1	-	2.3%
	Hemorrhagic				6	-	13.6%
	Tumor-related				3	-	6.8%
Presenting Symptoms	Gait disturbance				36	-	81.8%
	Altered mental status				35	-	79.5%
	Urinary incontinence				35	-	79.5%
	Headache				15	-	34.1%
	Nausea/Vomiting				4	-	9.1%
Shunt Type	Standard				9	-	20.5%
	Programmable				35	-	79.5%
Shunt Revision Performed					4	-	9.1%
External Ventricular Drain (EVD)					5	-	11.4%

Table 2. Complication and mortality rates.

		n	%
Early Complications	No	38	86.4%
	Yes	6	13.6%
	- Shunt Obstruction	1	2.3%
	- Overdrainage	4	9.1%
	- Shunt Infection	1	2.3%
Late Complications	No	38	86.4%
	Yes	6	13.6%
	- Shunt Obstruction	1	2.3%
	- Migration	1	2.3%
	- Overdrainage	1	2.3%
	- Shunt Infection	3	6.8%
Mortality Rate		13	29.5%

plication was over-drainage (9.1%), followed by shunt obstruction (2.3%) and shunt infection (2.3%) as other early complications. Late complications occurred at an equivalent rate (13.6%), with shunt infection being the most frequently observed (6.8%), followed by shunt migration (2.3%), overdrainage (2.3%), and shunt obstruction (2.3%). During the follow-up period, the mortality rate was determined to be 29.5% (13 patients) (Table 2). Mortality rates were significantly higher ($p < 0.05$) in patients with standard valves (Table 3).

Upon analyzing variables associated with mortality, a statistically significant difference was observed exclusively concerning the type of ventriculoperitoneal shunt (VPS) utilized. The mortality rate was notably lower among patients who received programmable shunts (38.5%), in contrast to those who received standard valve shunts, which exhibited a mortality rate of 61.5% ($p<0.001$) (Table 3). In the analysis based on the etiology of hydrocephalus, the mortality rate for patients with hemorrhagic hydrocephalus was 30.8%, approaching statistical significance ($p = 0.053$). Although the mortality rates for

https://doi.org/10.5455/annalsmedres.2025.06.145

Table 3. Variables associated with mortality.

		Mortality (-) (n:31)		Mortality (+) (n:13)		p
Age (Mean±SD)		67.4±10.4		72.2±11.2		0.179[t]
		n	%	n	%	
Gender	Female	16	51.6%	4	30.8%	0.205[χ²]
	Male	15	48.4%	9	69.2%	
Comorbidities	No	1	3.2%	1	7.7%	0.508[χ²]
	Yes	30	96.8%	12	92.3%	
Type of Hydrocephalus						
Communicative		27	87.1%	9	69.2%	0.161[χ²]
Obstructive		4	12.9%	4	30.8%	
-Post-traumatic		1	3.2%	3	23.1%	0.071[χ²]
-Infectious		0	0.0%	1	7.7%	0.295[χ²]
-Hemorrhagic		2	6.5%	4	30.8%	0.053[χ²]
-Tumor-related		1	3.2%	2	15.4%	0.204[χ²]
Shunt Type	Standard	1	3.2%	8	61.5%	**<0.001**[χ²]
	Programmable	30	96.8%	5	38.5%	
Early Complications	No	28	90.3%	10	76.9%	0.339[χ²]
	Yes	3	9.7%	3	23.1%	
- Shunt Obstruction		0	0.0%	1	7.7%	0.295[χ²]
- Migration		3	9.7%	1	7.7%	1.000[χ²]
- Overdrainage		0	0.0%	1	7.7%	0.295[χ²]
Late Complications	No	27	87.1%	11	84.6%	1.000[χ²]
	Yes	4	12.9%	2	15.4%	
- Shunt Obstruction		1	3.2%	0	0.0%	1.000[χ²]
- Migration		0	0.0%	1	7.7%	0.295[χ²]
- Overdrainage		1	3.2%	0	0.0%	1.000[χ²]
- Shunt Infection		2	6.5%	1	7.7%	1.000[χ²]

[t] Independent samples t-test/ χ^2 Chi-square test (Fisher's exact test).

patients with trauma-related (23.1%) and tumor-related hydrocephalus (15.4%) were higher compared to other etiological causes, these differences did not achieve statistical significance (p = 0.071 and p = 0.204, respectively) (Table 3).

DISCUSSION

In this retrospective study, clinical findings, postoperative complications, and mortality rates were analyzed in adult patients who underwent VPS surgery for the treatment of hydrocephalus. While our findings are generally consistent with those reported in the literature, some results offer unique contributions.

The most frequently symptoms in our study were gait disturbances (81.8%), cognitive changes (79.5%), and urinary incontinence (79.5%), which are characteristic symptoms of normal pressure hydrocephalus (NPH). This supports the clinical presentation typically observed in elderly individuals with NPH [11]. Headache (34.1%) and nausea/vomiting (9.1%), which are signs of elevated intracranial pressure, were observed at lower rates. The lower frequency of these findings aligns with the predominance of communicating hydrocephalus (81.8%) in our cohort. In cases where the clinical condition deteriorated rapidly and hydrocephalus presented acutely, 11.4% of patients required external ventricular drainage (EVD). Given that NPH generally has an insidious onset and progresses slowly, delays in diagnosis are common and may contribute to increased neurological damage. Therefore, early recognition of these characteristic symptoms is crucial, especially in individuals at risk [12].

Complications associated with shunt surgery continue to pose significant challenges in the management of hydrocephalus. In our study, the overall incidence of both early and late complications was determined to be 13.6%, aligning with the 10–30% range documented in existing literature. The presence of complications during both early and late stages underscores the importance of long-term follow-up. In a systematic review of 28 studies published between 2006 and 2010, Toma et al. [13] reported a surgical complication rate of 8.2%. Moreover, multicenter prospective cohort studies have documented serious complication rates ranging from 15% to 22% [14,15]. Standardization of surgical techniques, appropriate selection of shunt materials, and improvement of postoperative monitoring protocols are critical to reducing complication rates.

Shunt infection remains a prevalent and serious complication associated with shunt surgery. Infection rates in the pediatric population are typically reported to range from 5% to 15%, whereas in adult patients, this rate varies between 3%

https://doi.org/10.5455/annalsmedres.2025.06.145

and 10% [4,7,16]. Although the rates are technically lower in adults, they are influenced by factors such as immune status, the materials used, antibiotic prophylaxis, and revision surgery [13,17]. In our study, the early shunt infection rate was 2.3%, while the late infection rate was 6.8%. This finding suggests that infections are not confined to the perioperative period and pose a significant risk even during long-term follow-up. The disparity between early and late infection rates indicates that the etiology of infections may evolve over time, necessitating the optimization of late follow-up protocols.

The most prevalent early complication identified was over-drainage (9.1%), commonly attributed to the siphon effect, inappropriate selection of valve systems, or inadequate personalization of valve pressure settings. The literature indicates that over-drainage is more frequently observed in the early postoperative period [13,18]. In standard valve systems, the inability to adjust pressure heightens the risk of complications. Conversely, programmable valve systems are specifically engineered to mitigate over-drainage. Despite the extensive use of programmable shunts in our study, early over-drainage (9.1%) was still more prevalent than in the later period (2.3%). This may be attributed to the challenges in determining the optimal valve pressure for the patient during the initial stages. Factors such as the patient's age, cerebrospinal fluid (CSF) production rate, body position, and type of hydrocephalus can influence the ideal valve pressure. This suggests that, notwithstanding the theoretical advantages of programmable shunts, identifying the most appropriate valve pressure for the patient may necessitate time. The literature suggests that the effectiveness of programmable systems in reducing complications becomes more apparent once optimal pressure settings are achieved [19,20].

In our study, the overall mortality rate was 29.5%, and a statistically significant association was observed between shunt type and mortality ($p = .000$). Specifically, the mortality rate was 38.5% among patients with programmable shunts, compared to 61.5% in those with standard valve systems. This finding indicates that programmable systems may be more effective in regulating intracranial pressure, thereby preventing complications and enhancing overall survival. The literature contains a limited number of studies that directly compare mortality rates between programmable and standard shunt systems. In a retrospective cohort study by Chen et al. [21] programmable and standard valves were compared in adult patients with various etiologies of hydrocephalus, revealing that programmable valve systems reduced the need for revision and mortality. Similarly, a study by McGirt et al. [22] conducted in pediatric hydrocephalus patients demonstrated that programmable valve systems reduced the risk of proximal shunt obstruction and revision rates compared to standard systems, although mortality rates were not directly assessed.

Consequently, it can be inferred that programmable valve systems may reduce mortality indirectly by decreasing complication rates and the need for revision. Thus, the implementation of programmable valve systems in high-risk patient groups may represent a significant treatment strategy for improving clinical outcomes.

On the other hand, although the mortality rate was lower in the programmable shunt group in our study, the majority of deaths were found to be unrelated to direct shunt-related complications. Among the 13 patients who died, 3 cases were due to sepsis, 2 to multiple trauma, 1 to massive intracranial hemorrhage, and 1 to malignant brain tumor. In the remaining 6 patients, death occurred due to deterioration in general condition following shunt surgery, primarily attributed to advanced age and pre-existing cardiovascular/metabolic comorbidities. This finding suggests that mortality is not solely influenced by surgical complications but is also significantly affected by the patients' systemic health status and coexisting medical conditions.

In the assessment of etiological factors, mortality approached statistical significance in instances of hydrocephalus secondary to intracranial hemorrhage (30.8%, $p = 0.053$). This finding indicates that hemorrhage-related hydrocephalus is associated with a poorer prognosis, necessitating closer monitoring and individualized treatment strategies for these patients. Corroborating this, a comprehensive database analysis by Nadel et al. [23] also identified significantly elevated mortality rates in cases of hydrocephalus following hemorrhage. Although early and late complications did not exhibit a statistically significant association with mortality, the early complication rate was notably higher among patients who succumbed (23.1% vs. 9.7%), which is clinically significant. The literature suggests that early postoperative complications, particularly infections and drainage-related issues, may adversely affect long-term prognosis [4,16].

Limitations

The limitations of this study include its single-center, retrospective design and relatively small sample size. Additionally, variations in surgical techniques, practitioner experience, and details regarding antibiotic prophylaxis, which may contribute to shunt failure, were not uniformly documented across all patients. Nevertheless, our findings offer original contributions that may inform future large-scale, prospective studies.

CONCLUSION

In conclusion, our study identified shunt type and the etiology of hydrocephalus, particularly intracranial hemorrhage, as the variables exerting the most significant impact on mortality. The adoption of programmable valve systems and the implementation of a multidisciplinary approach for closer monitoring of patients with bleeding etiology emerge as crucial strategies to mitigate mortality rates.

This study underscores that complication rates following VPS surgery remain a significant clinical concern and that certain

https://doi.org/10.5455/annalsmedres.2025.06.145

modifiable factors, particularly shunt type, influence mortality. Based on the data obtained, it is posited that the use of a programmable valve system may be advantageous in reducing complication rates, especially in adult patients with advanced age and comorbidities. In cases of hydrocephalus secondary to intracranial hemorrhage, structured follow-up protocols should be developed to facilitate closer clinical monitoring and early intervention. Multicenter, prospective studies with larger sample sizes in this domain will enhance the generalizability of the data obtained and provide more robust evidence for clinical practice.

Ethics Committee Approval: The study protocol was approved by the Ethics Committee of Giresun Training and Research Hospital (Ethics Committee Date/Approval Number: 28.05.2025/15).

Informed Consent: Informed consent was not obtained due to the retrospective design of the study.

Peer-review: Externally peer-reviewed.

Conflict of Interest: The authors declare no competing interests.

Author Contributions: Conception: TT, İT, SO; Design: TT, İT, SO; Supervision: TT, İT, SO; Materials: TT, İT, SO; Data Collection and/or Processing: TT, İT, SO; Analysis and/or Interpretatio: TT, İT, SO; Literature Review: TT, İT, SO; Writing: TT, İT, SO; Critical Review: TT, İT, SO.

Financial Disclosure: The authors received no financial assistance for this paper's research, authorship, or publishing.

REFERENCES

1. Smith M. Refractory Intracranial Hypertension: The Role of Decompressive Craniectomy. *Anesth Analg*. 2017;125(6):1999-2008. doi: 10.1213/ANE.0000000000002399.
2. Wang QP, Ma JP, Zhou ZM, et al. Hydrocephalus after decompressive craniectomy for malignant hemispheric cerebral infarction. *Int J Neurosci*. 2016;126(8):707-712. doi: 10.3109/00207454.2015.1055357.
3. Hanna RS, Essa AA, Makhlouf GA, et al. Comparative Study Between Laparoscopic and Open Techniques for Insertion of Ventriculperitoneal Shunt for Treatment of Congenital Hydrocephalus. *J Laparoendosc Adv Surg Tech A*. 2019;29(1):109-113. doi: 10.1089/lap.2017.0594.
4. Erps A, Roth J, Constantini S, et al. Risk factors and epidemiology of pediatric ventriculoperitoneal shunt infection. *Pediatr Int*. 2018;60(12):1056-1061. doi: 10.1111/ped.13709.
5. Kutty RK, Sreemathyamma SB, Korde P, et al. Outcome of Ventriculosubgaleal Shunt in the Management of Infectious and Non-infectious Hydrocephalus in Pre-term Infants. *J Pediatr Neurosci*. 2018;13(3):322-328. doi: 10.4103/JPN.JPN_41_18.
6. Kestle J, Drake J, Milner R, et al. Long-term follow-up data from the Shunt Design Trial. *Pediatr Neurosurg*. 2000;33(5):230-236. doi: 10.1159/000055960.
7. Simon TD, Hall M, Riva-Cambrin J, et al. Infection rates following initial cerebrospinal fluid shunt placement across pediatric hospitals in the United States. Clinical article. *J Neurosurg Pediatr*. 2009;4(2):156-165. doi: 10.3171/2009.3.PEDS08215.
8. Drake JM, Kestle JR, Milner R, et al. Randomized trial of cerebrospinal fluid shunt valve design in pediatric hydrocephalus. *Neurosurgery*. 1998;43(2):294-305. doi: 10.1097/00006123-199808000-00068.
9. Tuli S, Drake J, Lawless J, et al. Risk factors for repeated cerebrospinal shunt failures in pediatric patients with hydrocephalus. *J Neurosurg*. 2000;92(1):31-38. doi: 10.3171/jns.2000.92.1.0031.10.3171/jns.2000.92.1.0031
10. Isaacs AM, Riva-Cambrin J, Yavin D, et al. Age-specific global epidemiology of hydrocephalus: Systematic review, metanalysis and global birth surveillance [published correction appears in *PLoS One*. 2019 Jan 10;14(1):e0210851. doi: 10.1371/journal.pone.0210851.]. *PLoS One*. 2018;13(10):e0204926. doi: 10.1371/journal.pone.0204926.
11. Relkin N, Marmarou A, Klinge P, et al. Diagnosing idiopathic normal-pressure hydrocephalus. *Neurosurgery*. 2005;57(3Suppl):S4-16. doi: 10.1227/01.neu.0000168185.29659.c5.
12. Petersen J, Hellström P, Wikkelsø C, et al. Improvement in social function and health-related quality of life after shunt surgery for idiopathic normal-pressure hydrocephalus. *J Neurosurg*. 2014;121(4):776-784. doi: 10.3171/2014.6.JNS132003.
13. Toma AK, Papadopoulos MC, Stapleton S, et al. Systematic review of the outcome of shunt surgery in idiopathic normal-pressure hydrocephalus. *Acta Neurochir (Wien)*. 2013;155(10):1977-1980. doi: 10.1007/s00701-013-1835-5.
14. Saehle T, Farahmand D, Eide PK, et al. A randomized controlled dual-center trial on shunt complications in idiopathic normal-pressure hydrocephalus treated with gradually reduced or "fixed" pressure valve settings. *J Neurosurg*. 2014;121:1257–63. doi: 10.3171/2014.7.JNS14283.
15. Miyajima M, Kazui H, Mori E, et al. One-year outcome in patients with idiopathic normal-pressure hydrocephalus: comparison of lumboperitoneal shunt to ventriculoperitoneal shunt. *J Neurosurg*. (2016) 125:1483–92. doi: 10.3171/2015.10.JNS151894.
16. Riva-Cambrin J, Kestle JR, Holubkov R, et al. Risk factors for shunt malfunction in pediatric hydrocephalus: a multicenter prospective cohort study. *J Neurosurg Pediatr*. 2016;17(4):382-390. doi: 10.3171/2015.6.PEDS14670.
17. Kim M, Choi JH, Park JC, et al. Ventriculoperitoneal shunt infection and malfunction in adult patients: incidence, risk factors, and long-term follow-up of single institution experience. *Neurosurg Rev*. 2024;47(1):269. doi: 10.1007/s10143-024-02505-x.
18. Bozhkov Y, Roessler K, Hore N, et al. Neurological outcome and frequency of overdrainage in normal pressure hydrocephalus directly correlates with implanted ventriculo-peritoneal shunt valve type. *Neurol Res*. 2017;39(7):601-605. doi: 10.1080/01616412.2017.1321300.
19. Ros B, Iglesias S, Linares J, et al Shunt Overdrainage: Reappraisal of the Syndrome and Proposal for an Integrative Model. *J Clin Med*. 2021;10(16):3620. doi: 10.3390/jcm10163620.
20. Yamada S, Ishikawa M, Nakajima M, et al. Reconsidering Ventriculoperitoneal Shunt Surgery and Postoperative Shunt Valve Pressure Adjustment: Our Approaches Learned From Past Challenges and Failures. *Front Neurol*. 2022;12:798488. doi: 10.3389/fneur.2021.798488.
21. Chen KH, Hsu PW, Wu BC, et al. Long-term follow-up and comparison of programmable and non-programmable ventricular cerebrospinal fluid shunts among adult patients with different hydrocephalus etiologies: a retrospective cohort study. *Acta Neurochir (Wien)*. 2023;165(9):2551-2560. doi: 10.1007/s00701-023-05734-z.
22. McGirt MJ, Buck DW, Sciubba D, et al. Adjustable vs set-pressure valves decrease the risk of proximal shunt obstruction in the treatment of pediatric hydrocephalus. *Childs Nerv Syst*. 2007;23(3):289-295. doi: 10.1007/s00381-006-0226-0.
23. Nadel JL, Wilkinson DA, Linzey JR, et al. Thirty-Day Hospital Readmission and Surgical Complication Rates for Shunting in Normal Pressure Hydrocephalus: A Large National Database Analysis. *Neurosurgery*. 2020;86(6):843-850. doi: 10.1093/neuros/nyz299.

https://doi.org/10.5455/annalsmedres.2025.06.145

Ann Med Res

Current issue list available at Ann Med Res

Annals of Medical Research

journal page: annalsmedres.org

Pan-immune inflammation value in systemic lupus erythematosus: Is it associated with organ involvement?

Elif İnanç [a,*], Servet Yolbaş [a], Fuat Albayram [a], Sezgin Zontul [b], Zeynep Kaya [c], Mesude Seda Aydoğdu [d], İpek Balıkçı Çiçek [e]

[a] Inonu University, Faculty of Medicine, Department of Internal Medicine, Division of Rheumatology, Malatya, Türkiye
[b] Inonu University, Faculty of Medicine, Department of Physical Medicine and Rehabilitation, Division of Rheumatology, Malatya, Türkiye
[c] Istanbul Training and Research Hospital, Department of Internal Medicine, Division of Rheumatology, Istanbul, Türkiye
[d] Malatya Training and Research Hospital, Department of Internal Medicine, Division of Rheumatology, Malatya, Türkiye
[e] Inonu University, Faculty of Medicine, Department of Biostatics and Medical Informatics, Malatya, Türkiye
*Corresponding author: eliftemelliinanc@gmail.com (Elif Inanç)

MAIN POINTS

- PIIV were found to be markedly elevated in SLE patients compared with healthy individuals
- Cardiac involvement was associated with elevated PIIV.
- PIIV may reflect both disease activity and organ involvement, indicating its biomarker potential.
- Applying PIIV in clinical practice could assist with risk stratification and guide therapeutic decisions.
- Hydroxychloroquine treatment correlated with lower PIIV, supporting its anti-inflammatory effects in SLE.

Cite this article as: Inanç E, Yolbaş S, Albayram F, Zontul S, Kaya Z, Aydoğdu MS, Balıkçı Çiçek İ. Pan-immune inflammation value in systemic lupus erythematosus: Is it associated with organ involvement?. *Ann Med Res*. 2025;32(12):566--573. doi: 10.5455/annalsmedres.2025.08.247.

ABSTRACT

Aim: This study aimed to investigate the association between pan-immune inflammation value (PIIV) and both disease activity and organ involvement in patients with systemic lupus erythematosus (SLE).

Materials and Methods: A total of 50 adult SLE patients, meeting the 2019 EULAR/ACR classification criteria, and 35 healthy volunteers were included in the study. PIIV was determined using the formula: [neutrophil × platelet × monocyte] / lymphocyte. Disease activity was evaluated with the SLEDAI-2K index. The relationship between PIIV and clinical findings, organ involvement, laboratory results, and disease activity was assessed.

Results: PIIV levels were markedly higher in SLE patients compared to the control group ($p<0.001$). Patients with cardiac involvement had elevated PIIV values compared to those without heart involvement ($p<0.05$). On the other hand, individuals receiving hydroxychloroquine therapy showed lower PIIV than those not using the drug ($p=0.019$). No clear correlation was observed between PIIV and SLEDAI-2K scores ($p=0.532$).

Conclusion: The findings indicate that PIIV levels are increased in SLE patients compared with healthy controls, suggesting its potential role as a supportive diagnostic marker. Additionally, higher PIIV in patients with cardiovascular involvement and lower values in those treated with hydroxychloroquine imply that PIIV could be considered a useful biomarker for evaluating and tracking cardiovascular risk in SLE.

Keywords: Systemic lupus erythematosus, Pan-immune inflammation value, Disease activity, Cardiac involvement

Received: Sep 01, 2025 **Accepted:** Sep 29, 2025 **Available Online:** Dec 25, 2025

INTRODUCTION

Systemic lupus erythematosus (SLE) is a chronic autoimmune disorder marked by alternating periods of exacerbations and remissions. It can involve multiple organs and systems [1]. Proper evaluation of disease activity is crucial for differentiating flare-ups, preventing irreversible organ damage, and guiding therapeutic decisions. Despite the widespread use of current clinical activity indices, these tools may not fully capture the heterogeneous nature of SLE or accurately indicate specific organ involvement [2, 3].

Alterations in hematologic parameters, including anemia, leukopenia, lymphopenia, and thrombocytopenia, are frequently observed in SLE [4]. Collectively, these cellular alterations provide a strong foundation for the development of novel biomarkers for inflammation. While many investigations have focused on simple binary cell ratios, indices incorporating multiple cell types have only recently begun to be explored [5].

Within this framework, the pan-immune-inflammation value (PIIV) is a straightforward and cost-effective index calcu-

lated from neutrophil, monocyte, platelet, and lymphocyte counts [6, 7]. Originally proposed in oncology settings [8], PIIV has since been studied as a prognostic marker in various chronic inflammatory conditions, including cardiovascular disease [9], obesity, rheumatoid arthritis [5, 10], and Behçet's disease [11]. In recent years, compelling evidence has emerged linking PIIV with cardiovascular risk [7, 9].

There is limited research evaluating the association between PIIV and both disease activity and organ involvement in SLE. Gambichler et al. [12] reported no significant correlation between PIIV and SLE Disease Activity Index (SLEDAI) in adult patients; on the other hand, Alasmari et al. [13] observed a positive association between elevated PIIV and SLEDAI in pediatric lupus cases. In a study by Ulutaş and Çobankara on biopsy-proven lupus nephritis patients, PIIV was examined, but its connection to disease activity was not analyzed [14].

Cardiac involvement in SLE can lead to severe complications, such as pericarditis, valvular disorders, atherosclerotic cardiovascular disease, and heart failure, and represents a major determinant of mortality [15]. Population-based studies have demonstrated strong links between PIIV and cardiovascular outcomes [9, 16]. However, the role of PIIV in predicting cardiac involvement among adult SLE patients has not yet been clearly defined.

Considering the central role of cellular components in SLE immunopathogenesis, PIIV may serve as a useful biomarker for disease monitoring. This study aims to investigate the relationship between PIIV, disease activity, and organ involvement in adult SLE patients.

MATERIALS AND METHODS

This research was conducted as a single-center, cross-sectional, observational study. Fifty adult patients diagnosed with SLE according to the 2019 classification criteria of the European Alliance of Associations for Rheumatology (EULAR) and the American College of Rheumatology (ACR) and 35 healthy controls attending the rheumatology outpatient clinic at Malatya İnönü University between January 2024 and January 2025 were included. The control group comprised healthy volunteers without any signs of rheumatic disease who fulfilled the study's exclusion criteria. This study was approved by the İnönü University Clinical Research Ethics Committee on 11 December 2024 (decision no. 2024/167). All procedures were conducted in accordance with the principles of the Helsinki Declaration.

Individuals younger than 18 or older than 65, as well as those with infections, malignancies, or other rheumatologic conditions, were excluded. Demographic information, clinical features, laboratory parameters, disease activity scores, and treatments of SLE patients were documented. Similarly, demographic and laboratory data were collected for the control group. All participants underwent evaluation of complete blood count, renal function, proteinuria, ANA, ds-DNA, complement levels, CRP, and erythrocyte sedimentation rate. Proteinuria was considered positive when spot urine protein exceeded 300 mg. Disease activity in SLE patients was assessed using SLEDAI-2K (Systemic Lupus Erythematosus Disease Activity Index-2000), with a score >6 indicating active disease [17,18]. PIIV was calculated using the formula: [neutrophil count × platelet count × monocyte count] / lymphocyte count.

Statistical analysis

Categorical variables were expressed as percentages, summarizing their distribution within the study population. The Shapiro–Wilk test was employed to assess the normality of continuous data. Variables with a non-normal distribution were presented as median (minimum–maximum), whereas normally distributed variables were reported as mean ± standard deviation. For comparisons of categorical variables, the Pearson chi-square test, Yates-corrected chi-square test, or Fisher's exact test was applied as appropriate. Continuous variables were compared between two independent groups using the Mann–Whitney U test and among more than two groups using the Kruskal–Wallis test, where applicable. Associations between continuous variables were evaluated using the Spearman's rank correlation coefficient. A two-tailed p-value <0.05 was considered statistically significant for all analyses. Statistical computations were performed using IBM SPSS Statistics version 26.0 for Windows (IBM Corp., New York, USA).

The minimum required sample size for the study was calculated using the G*Power 3.1 software. Assuming an alpha error of 0.05, a test power (1-β) of 0.80, a moderate effect size of 0.70, and a two-tailed hypothesis for an independent two-sample t-test, at least 34 participants per group (total 68) were required. Therefore, the study included 50 SLE patients and 35 healthy controls, fulfilling the minimum sample size requirement.

RESULTS

Overall, 85 participants were enrolled in the study, including 50 patients (58.8%) and 35 healthy controls (41.2%). The study population consisted predominantly of women (77 individuals; 90.6%), whereas 8 participants (9.4%) were men. Coexisting medical conditions were identified in 39 participants (45.9%), while 46 individuals (54.1%) had no additional health problems. Regarding smoking habits, 13 participants (15.3%) reported active smoking, whereas 72 individuals (84.7%) did not smoke.

The mean age of the study population was 42.73 ± 10.14 years, with a median of 44 years (range, 22–65). The mean body mass index (BMI) was 25.79 ± 4.61, with a median value of 25.59 (range, 15.24–37.97). Among inflammatory markers, the mean erythrocyte sedimentation rate (ESR) was 12.02 ± 16.05 mm/h, with a median of 7 (range, 0.4–116), and the

https://doi.org/10.5455/annalsmedres.2025.08.247

Table 1. Demographic, clinical and laboratory characteristics of patient and control groups.

Variables	Patient (n=50)	Control (n=35)	P
Age	42.72±11.27	42.74±8.42	0.992[1]
BMI	25.18±5.24	26.66±3.41	0.120[1]
Sex , M / F, [n (%)]	4 (8.00)/ 46 (92.00)	4 (11.43) /31 (88.57)	0.712[2]
Comorbidity, [n (%)]	35 (70.00)	4 (11.43)	<0.001[3]
Smoking [n (%)]	6 (12.00)	7 (20.00)	0.482[3]
ESR, (mm/hour)	8(2-116)	5(0.4-19)	<0.001[4]
CRP, (mg/dL)	0(0-3.18)	0(0-30)	0.940[4]
WBC, (10^3/uL)	7000(3.24-19440)	6.68(0-6790)	<0.001[4]
Neutrophils,(10^3/uL)	4.7(1.92-15.88)	4.05(2.38-6.97)	0.021[4]
Monocytes (10^3/uL)	0.64(0.32-1.76)	0.5(0.3-1.04)	<0.001[4]
Platelets, (10^3/uL)	285(119-449)	271(176-333)	0.054[4]
Lymphocytes, (10^3/uL)	1.68(0.67-5.1)	2.23(1.54-3.67)	0.001[4]
HB, (g/dL)	12.3(9-17.7)	13.5(10.2-17.1)	<0.001[4]
RDW, [n (%)]	45.1(39-68.9)	41.3(0-47.6)	<0.001[4]
PIIV	498.9(213.2-6512)	235.6(38.5-687)	<0.001[4]

(1): Independent samples t-test , (2): Fisher's exact chi-square test, (3): Chi-square test with Yates correction; (4): Mann Whitney U test [median (max-min)]. BMI: Body Mass Index; ESR: Erythrocyte Sedimentation Rate; CRP: C-Reactive Protein; WBC: White Blood Cells; Hb: Hemoglobin; RDW: Red Cell Distribution Width; PIIV: Pan-Immune-Inflammation Value.

Table 2. Distribution of PIIV in SLE patients according to demographic, clinical, and laboratory variables.

Variables		PIIV	p
Sex (Male/Female)	M F	778.85(216-1279) 498.9(213.2-6512)	0.497*
BMI	Under 30 Over 30	509.5(213.2-6512) 470.9(285.5-1086)	0.926*
aPL AC	Yes No	612.7(220.8-6512) 441.9(213.2-1279)	0.401*
Comorbidity	Yes No	530.8(213.2-6512) 423.7(216-1232)	0.505*
Smoking	Yes No	418.15(213.2-1279) 509.5(216-6512)	0.676*
SLEDAI>6 and above	Yes No	470.85(220.8-1232) 523.65(213.2-6512)	0.532*
SLEDAI>10 and above	Yes No	506.75(303.9-902.7) 498.9(213.2-6512)	0.979
SLEDAI>20	Yes No	838.4(774.1-902.7) 488.5(213.2-6512)	0.125
Anti Ds DNA	High Low	573.3(216-6512) 461.8(213.2-1086)	0.663*
Low C3	Yes No	423.7(216-902.7) 502.5(213.2-6512)	0.685*
Low C4	Yes No	612.7(313.8-902.7) 488.5(213.2-6512)	0.428*
RF Positivity	Yes No	465.2(410.7-1232) 523.65(216-6512)	0.815*
Presence of proteinuria	Yes No	557.6(285.5-1279) 477.65(213.2-6512)	0.290*

*: Mann Whitney U test; BMI: body mass index; aPL AC: Antifosfolipid anticoagulant; SLEDAI: The Systemic Lupus Erythematosus Disease Activity Index; anti-dsDNA: Anti-double stranded DNA antibody; C3: Complement 3; C4: Complement 4; RF: rheumatoid factor; Pan-immune inflammation value

mean C-reactive protein (CRP) was 0.71 ± 3.29 mg/L, with a median of 0 (range, 0–30).

Regarding haematological parameters, the mean white blood cell (WBC) count was 4,150.49 ± 4,408.36/mm^3, with a median of 4,960 (range, 0–19,440); the mean neutrophil count was 4.64 ± 1.86, with a median of 4.39 (range, 1.92–15.88); and the mean monocyte count was 0.63 ± 0.26, with a median of 0. The mean platelet count was 279 ± 69.59, with a median of 280 (range, 119–449); the mean lymphocyte count was 2.02 ± 0.81, with a median of 1.88 (range, 0.67–5.1); the mean hemoglobin (Hb) was 12.82 ± 1.75 g/dL, with a median of 12.7 (range, 9–17.7); and the mean red cell distribution width (RDW) was 42.82 ± 9.87, with a median of 43.8 (range, 0–68.9).The mean PIIV value was 498.26 ± 713.61, with a median of 318.4 (range, 38.5–6512) (Table 1).

When comparing the patient and control groups, the mean ages were 42.72 ± 11.27 years and 42.74 ± 8.42 years, respectively, with no significant difference observed (p = 0.992). The mean body mass index (BMI) was 25.18 ± 5.24 in the patient group and 26.66 ± 3.41 in the control group, and this difference was not statistically significant (p = 0.120). Regarding gender distribution, the patient group included 4 males (8.0%) and 46 females (92.0%), while the control group comprised 4 males (11.43%) and 31 females (88.57%), with no significant difference detected (p = 0.712). Comorbidities were present in 35 participants (70%) in the patient group and 4 participants (11.43%) in the control group, representing a statistically significant difference (p<0.001). No significant difference was found between the groups with respect to smoking status, as 6 individuals (12%) in the patient group and 7 individuals (20%) in the control group were smokers (p = 0.482) (Table 1).

When comparing laboratory parameters of the patient and control groups, ESR, WBC, neutrophil, monocyte, RDW, and PIIV were considerably increased in the patient group (p<0.001, p<0.001, p = 0.021, p<0.001, p<0.001, p<0.001). In contrast, lymphocyte and hemoglobin levels were reduced

https://doi.org/10.5455/annalsmedres.2025.08.247

Table 3. Comparison of PIIV (×10³/μL) according to organ ınvolvement and medication use.

Variables		PIIV Median (Min-Max)	p*
Single and Multiple Organ Involvement	Single organ involvement Multiple organ involvement	481.7(219-1279) 516.5(213.2-6512)	0.806
Lung involvement	Yes No	3643.05(774.1-6512) 488.5(213.2-1279)	0.067
Cardiac involvement	Yes No	786.15(603-6512) 470.85(213.2-1279)	0.042
Gastrointestinal involvement	Yes No	324.35(219-530.8) 509.5(213.2-6512)	0.116
Vasculitis involvement	Yes No	695.4(347-902.7) 488.5(213.2-6512)	0.352
Renal involvement	Yes No	516.5(285.5-6512) 427.9(213.2-1086)	0.186
Neurological involvement	Yes No	318.4(244.7-832.2) 516.5(213.2-6512)	0.166
Hematologic involvement	Yes No	558.6(285.5-1086) 495.3(213.2-6512)	0.967
Joint involvement	Yes No	477.65(213.2-1232) 523.65(219-6512)	0.404
Skin involvement	Yes No	470.1(213.2-1076) 498.9(219-6512)	0.430
Azathioprine use	Yes No	699.5(219-1076) 495.3(213.2-6512)	0.606
Mycophenolate use	Yes No	481.7(218.2-6512) 658.8(213.2-1076)	0.884
Hydroxychloroquine use	Yes No	418.15(213.2-1279) 580.8(216-6512)	0.019
Steroid use	Yes No	481.7(218.2-6512) 699.5(213.2-1086)	0.575
Biologics history	Yes No	774.1(285.5-6512) 427.9(213.2-1232)	0.028*

*:Mann Whitney U test, PIIV: Pan-immune inflammation value.

Table 4. Correlations between PIIV and clinical/laboratory parameters in SLE patients.

Variables		ESR	CRP	WBC	Neutrophils	Monocytes	Platelets	Lymphocytes	Hb	RDW	anti-dsDna	C3	C4	Creatinine
PIIV	r	0.152	0.270	0.265	0.561**	0.447**	0.534**	-0.146	0.021	.320*	0.051	0.116	0.089	-0.077
	p	0.298	0.060	0.063	<0.001	0.001	<0.001	0.311	0.886	0.024	0.726	0.421	0.540	0.596

*p<0.05, **p<0.01; r: Spearman's rho correlation coefficient. PIIV: Pan-Immune-Inflammation Value; ESR: Erythrocyte Sedimentation Rate; CRP: C-Reactive Protein; WBC: White Blood Cells; Hb: Hemoglobin; RDW: Red Cell Distribution Width; anti-dsDNA: Anti-double stranded DNA antibody; C3: Complement 3; C4: Complement 4.

among patients compared with controls (p = 0.001 and p<0.001, in that order). Platelet counts showed a modest elevation in the patient group, yet this variation did not demonstrate a meaningful statistical difference (p = 0.054). CRP concentrations remained comparable across the two groups, with no detectable variation (p = 0.940) (Table 1).

Among SLE patients, the most frequently observed organ involvements were joints (52%, n = 26), kidneys (30%, n = 15), and skin (28%, n = 14). Less common involvements included vascular (8%, n = 4), haematological (14%, n = 7), neurological (14%, n = 7), gastrointestinal (8%, n = 4), pulmonary (4%, n = 2), and cardiac (8%, n = 4) systems. Antiphospholipid antibodies (aPL) were detected in 36.1% of patients (n = 13). Regarding non-biological therapies, 56.0% (n = 28) of patients received combination therapy, while 38.0% (n = 19) were on monotherapy with agents such as steroids, mycophenolate,

https://doi.org/10.5455/annalsmedres.2025.08.247

azathioprine, or methotrexate. A small proportion (4%, n = 2) were not receiving any treatment. Specifically, hydroxychloroquine (HCQ) was used by 56% of patients, steroids by 88%, mycophenolate mofetil by 50%, and azathioprine by 22%.

Among SLE patients, the estimated disease duration averaged 9.12 ± 7.41 years, while the median duration was 7.5 years (range 0.1–30). Patient-reported disease activity (Patient-DA) averaged 4.4 ± 2.29, with a median of 5 (range 0–10), while physician-assessed disease activity (Dr-DA) had a mean of 3.74 ± 1.17 and a median of 4 (range 1–6). The average SLEDAI-2K score was 5.32 ± 4.51, with a median of 4 (range 0–20). Serological markers showed a mean anti-dsDNA level of 94.4 ± 145.63, with a median of 30.05 (range 1.1–800). Complement levels were 114.56 ± 30.03 for C3 (median 112.5, range 44–176) and 24.1 ± 13.1 for C4 (median 21.5, range 2–57). The mean creatinine level was 0.87 ± 0.24, with a median of 0.8 (range 0.6–1.9).

The evaluation of PIIV with respect to population profiles and clinical parameters among SLE patients revealed that male participants presented a median PIIV of 778.85 (range: 216–1279), whereas female participants demonstrated a median value of 498.9 (range: 213.2–6512). This variation did not indicate any meaningful statistical difference (p = 0.497). Patients with a BMI below 30 had a median PIIV of 509.5 (range 213.2–6512), compared to 470.9 (range 285.5–1086) in those with a BMI above 30, with no significant difference observed (p = 0.926). Similarly, patients with positive antiphospholipid antibodies (aPL ac) had a median PIIV of 612.7 (range 220.8–6512) versus 441.9 (range 213.2–1279) in those with negative antibodies, showing no significant difference (p = 0.401). When evaluating the presence of comorbidities, patients with additional diseases had a median PIIV of 530.8 (range 213.2–6512), compared to 423.7 (range 216–1232) in those without comorbidities; this difference was also not statistically significant (p = 0.505) (Table 2).

When considering smoking status, the median PIIV among SLE patients who smoked was 418.15 (range 213.2–1279), compared to 509.5 (range 216–6512) in non-smokers, with no statistically significant difference observed (p = 0.676). Among patients with an SLEDAI score of six or higher, the median PIIV was 470.85 (range 220.8–1232), while those with lower scores had a median of 523.65 (range 213.2–6512), showing no significant difference (p = 0.532). Similarly, median PIIV for patients with SLEDAI scores ≥10 and ≥20 were 506.75 (range 303.9–902.7) and 838.4 (range 774.1–902.7), respectively, with neither comparison reaching statistical significance (Table 2)

The analysis revealed no statistically significant associations between PIIV and anti-dsDNA levels, decreased C3, decreased C4, RF positivity, or the presence of proteinuria in patients with SLE (Table 2).

When organ involvement was analyzed, SLE patients with cardiac involvement had a significantly higher median PIIV compared to those without cardiac involvement (p = 0.042). No statistically significant differences were observed for involvement of other organs or systems (p>0.05 for all; Table 3). Median PIIV were 481.7 (range 218.2–6512) for patients using steroids, 481.7 (range 218.2–6512) for those on mycophenolate, and 699.5 (range 219–1076) for patients using azathioprine; none of these differences reached statistical significance. Conversely, patients receiving HCQ had a significantly lower median PIIV of 418.15 (range 213.2–1279) compared to those not using HCQ (p = 0.019). Among patients on combination therapy, the median PIIV was 432.8 (range 218.2–1279), whereas those not taking any non-biological medication had a median of 562.25 (range 216–908.5). Additionally, SLE patients with a history of biological therapy exhibited a significantly higher median PIIV of 774.1 (range 285.5–6512) compared to patients without such therapy, whose median was 427.9 (range 213.2–1232; p = 0.028) (Table 3).

In SLE patients, PIIV demonstrated significant positive correlations with neutrophil (r = 0.561, p<0.001), monocyte (r = 0.447, p = 0.001), platelet counts (r = 0.534, p<0.001) and RDW (r = 0.320, p = 0.024) values. In contrast, no significant correlations were observed between PIIV and hemoglobin (r = 0.021, p = 0.886), C3 (r = 0.116, p = 0.421), C4 (r = 0.089, p = 0.540), or creatinine levels (r = −0.077, p = 0.596). Similarly, PIIV did not show statistically significant associations with CRP (r = 0.270, p = 0.060), WBC (r = 0.265, p = 0.063), or anti-dsDNA levels (r = 0.051, p = 0.726) (Table 4).

DISCUSSION

The present research was conducted to examine the association of PIIV levels with disease activity, organ involvement, and treatment modalities among adult patients with SLE. Our analysis demonstrated that PIIV were significantly elevated in the patient group compared with healthy controls and were particularly higher in those with cardiac involvement. These findings indicate that PIIV may represent a promising biomarker for both diagnostic and prognostic purposes.

SLE is an autoimmune condition that can lead to alterations in hematopoietic stem cells within the bone marrow as well as increased destruction of blood cells in the spleen [19]. Consequently, patients may exhibit variations in circulating blood cell counts, either directly related to the disease itself or associated with disease activation [20]. The alterations in these cells' counts are clinically important, as they contribute both to the diagnosis of SLE and to the evaluation of disease activity. Moreover, the magnitude of change in each cell type varies depending on the degree of disease activation and the specific organ or system involved.

Beyond assessing individual cell counts, previous studies have suggested that simple and cost-effective hematological indices—calculated by comparing these parameters—hold potential as biomarkers [21, 22]. Within this framework, the

https://doi.org/10.5455/annalsmedres.2025.08.247

PIIV index, which reflects proportional shifts across multiple immune cell lines, has emerged as a candidate biomarker for systemic inflammatory disorders such as SLE, where nearly all circulating immune cells are affected.

The PIIV index was originally proposed as a tool to estimate clinical outcomes and prognosis in oncological disorders. Indeed, several studies have demonstrated its prognostic value in malignancies, including advanced colorectal cancer, hepatocellular carcinoma, and breast cancer [6, 23, 24]. More recently, evidence has emerged supporting its potential role in rheumatic inflammatory diseases, not only for diagnostic purposes but also in evaluating disease activity [5, 10, 11, 13, 14].

In the present study, PIIV levels were found to be higher in adult SLE patients compared with the control group. Nevertheless, no statistically significant correlation was observed between PIIV and SLEDAI scores. Similarly, PIIV did not differ significantly between patients with active disease (SLEDAI > 6) and those without.

To date, three studies have explored the potential utility of PIIV in SLE. Among these, one was performed in paediatric patients and another in individuals with lupus nephritis (LN) [13, 14]. Furthermore, Gambichler et al. evaluated 148 SLE patients, 48 individuals with hidradenitis suppurativa, and 35 control subjects, and found that PIIV were markedly higher in the SLE group relative to the control group [12]. This outcome is consistent with our results and strengthens the concept that PIIV may function as a supportive biomarker in identifying SLE. However, in that study, PIIV showed no significant association with SLEDAI-2K, and only ANA titres >1:640 were identified as predictive for disease flares. Consistently, in our analysis, PIIV was not significantly related to conventional activity parameters, including SLEDAI scores, dsDNA levels, complement (C3 and C4) concentrations, or proteinuria. Taken together, these data suggest that although PIIV levels may rise in SLE, they may have limited capacity to directly mirror disease activity.

Similarly, in a study by Alasmari et al. involving 125 pediatric patients with SLE, those with baseline PIIV exceeding 250 were reported to have higher SLEDAI scores [13]. An important limitation of that study, however, was its restriction to a pediatric population and the absence of a healthy control group.

In another case–control study, Ulutaş et al. evaluated 45 patients with biopsy-proven lupus nephritis (LN) [14]. PIIV was calculated before the initiation of any immunomodulatory or immunosuppressive treatment, and higher baseline PIIV was found to be associated with reduced glomerular filtration rate (GFR) in LN patients. Nevertheless, this study focused exclusively on renal involvement and did not account for other organ manifestations of SLE. In addition, the relationship between PIIV and disease activity indices was not explored, as the analysis was limited to its association with GFR [14].

In our study, PIIV were significantly higher in SLE patients with cardiac involvement compared with those without, whereas no association was observed between PIIV and other organ involvements. By contrast, Alasmari et al. reported elevated PIIV in pediatric SLE patients with renal, hematological, musculoskeletal, and mucocutaneous manifestations, but no significant difference between those with and without cardiac involvement [13]. Taken together, these findings highlight a discrepancy between the two studies regarding the relationship between PIIV and organ involvement. We propose that this inconsistency may stem from differences in disease course between pediatric and adult SLE, as well as developmental variations in bone marrow cell production and peripheral cell destruction processes during childhood compared with adulthood [25, 26].

Conversely, accumulating evidence has demonstrated strong associations between PIIV and adverse cardiovascular outcomes, including cardiovascular mortality, heart failure, and coronary artery disease [9, 27]. In SLE, programmed cell death pathways—particularly NETosis and pyroptosis have been shown to contribute to cardiac involvement by amplifying systemic inflammation and promoting myocardial injury [16].

Plasmacytoid dendritic cell (pDC) activation in SLE patients further exacerbates this process through excessive secretion of type I interferons (IFNs) [28, 29]. These cytokines not only impair the balance between endothelial damage and vascular repair but also stimulate the production of multiple pro-inflammatory interleukins and cytokines, enhance plaque instability, and facilitate prothrombotic events via platelet activation. Sustained IFN signaling has therefore been recognized as a central mechanism driving accelerated atherosclerosis in SLE [30]. In light of these findings, the significantly higher PIIV levels observed in our patients with cardiac involvement suggest that PIIV may serve as a potential biomarker reflecting cardiovascular risk in SLE.

HCQ represents a cornerstone therapy for autoimmune conditions such as systemic lupus erythematosus, with established cardioprotective effects. HCQ modulates both the number and function of peripheral blood cells by influencing multiple signaling pathways and suppressing antigen presentation. Specifically, HCQ inhibits type I interferon (IFN) signaling from plasmacytoid dendritic cells (pDCs) and prevents endosomal activation of Toll-like receptors 7 and 9, thereby reducing cytokine production [31]. This inhibition attenuates the IFN signaling pathway, a critical component in SLE pathogenesis, and decreases expression of IFN-regulatory genes, ultimately limiting both innate and adaptive immune activation. At the lymphocyte level, HCQ interferes with Ca^{2+} release from the endoplasmic reticulum, resulting in multi-level suppression of T and B cell activation and dampening the overall immune response [32, 33].

In our cohort, analysis of non-biological treatment subgroups revealed that only patients receiving HCQ exhibited signif-

https://doi.org/10.5455/annalsmedres.2025.08.247

icantly lower PIIV. This observation can be explained by HCQ's dual effect of increasing lymphocyte counts (denominator of the PIIV formula) while simultaneously suppressing neutrophils, monocytes, and platelets (numerator). The concurrent presence of elevated PIIV in patients with cardiovascular involvement and reduced PIIV in those on HCQ highlights the potential utility of the PIIV index as a biomarker for assessing and monitoring cardiovascular risk in SLE.

Key aspects of our study include the inclusion of both SLE patients and healthy controls, the calculation of PIIV using detailed hematological data, and the comprehensive comparison of clinical and laboratory parameters. Special attention was given to cardiac involvement, which has been assessed in only a limited number of previous studies.

Limitations

However, several limitations should be noted. The study was single-center, and the sample sizes for some subgroups, particularly those with cardiac involvement (including tamponade, pericarditis, and myocardial infarction), were very small, limiting the ability to perform separate analyses for each cardiac subtype; therefore, prospective studies evaluating each cardiac subtype separately are warranted. Future prospective studies with larger SLE populations, detailed assessment of cardiovascular risk factors, and regular PIIV evaluations using cardiovascular imaging are needed to better understand the clinical relevance of PIIV.

CONCLUSION

Our findings indicate that elevated PIIV in SLE patients compared to healthy controls may support its role as a diagnostic biomarker. Furthermore, the observation that PIIV is higher in patients with cardiovascular involvement and lower in those receiving HCQ suggests that PIIV could be a useful marker for predicting and monitoring cardiovascular risk, a significant contributor to morbidity and mortality in SLE.

Ethics Committee Approval: The study was approved by the İnönü University Clinical Research Ethics Committee on 11 December 2024 (decision no. 2024/167).

Informed Consent: Informed consent was obtained from all participants.

Peer-review: Externally peer-reviewed.

Conflict of Interest: The authors have no conflict of interest to declare.

Author Contributions: Concept: Eİ, SY, FA, SZ, ZK, MSA, İBÇ.; Design: Eİ, SY, FA, SZ, ZK, MSA, İBÇ.; Supervision: Eİ, SY, FA, SZ, ZK, MSA, İBÇ; Fundings: Eİ, SY; Materials: Eİ, FA, MSA.; Data Collection and/or Processing: Eİ, FA, ,İBÇ ; Analysis and/or Interpretation: Eİ, SY, SZ, ZK, MSA, İBÇ.; Literature Review: Eİ, SZ, ZK; Writing: Eİ, FA,; Critical Review: Eİ, SY, SZ.

Financial Disclosure: The authors declared that this study has received no financial support.

REFERENCES

1. Su X, Yu H, Lei Q, et al. Systemic lupus erythematosus: pathogenesis and targeted therapy. *Mol Biomed.* 2024;5(1):54. doi: 10.1186/s43556-024-00217-8.
2. Thanou A, Jupe E, Purushothaman M, Niewold TB, Munroe ME. Clinical disease activity and flare in SLE: current concepts and novel biomarkers. *J Autoimmun.* 2021;119:102615. doi: 10.1016/j.jaut.2021.102615.
3. Sabin Göktaş Aydın, Bahar Artım Esen. Assessment of disease activity in systemic lupus erythematosus and activity indices. *RAED J.* 2018;10(1):6–13. doi: 10.2399/raed.18.727.
4. Fozya Bashal. Hematological disorders in patients with systemic lupus erythematosus. *Open Rheumatol J.* 2013;7:87–95. doi: 10.2174/1874312901307010087.
5. Okutan İ, Aci R, Keskin Â, Bilgin M, Kızılet H. New inflammatory markers in RA: PIV, SII, SIRI. *Reumatologia.* 2024;62(6):439–446. doi: 10.5114/reum/196066.
6. Yang X-C, Liu H, Liu D-C, Tong C, Liang X-W, Chen R-H. Prognostic value of pan-immune-inflammation value in colorectal cancer patients: a systematic review and meta-analysis. *Front Oncol.* 2022;12:1036890. doi: 10.3389/fonc.2022.1036890.
7. Zhang Y, Yue Y, Sun Z, et al. PIV and its association with all-cause mortality in the general population: a nationwide cohort study. *Front Endocrinol.* 2025;16:1534018. doi: 10.3389/fendo.2025.1534018.
8. Fucà G, Guarini V, Antoniotti C, et al. The Pan-Immune-Inflammation Value is a new prognostic biomarker in metastatic colorectal cancer. *Br J Cancer.* 2020;123(3):403–409. doi: 10.1038/s41416-020-0894-7.
9. Chen F, Mao Y. Association between PIV and heart failure: NHANES 2011–2020. *J Int Med Res.* 2025;53(3):3000605251325176. doi: 10.1177/03000605251325176.
10. Başaran PÖ, Doğan M. The relationship between disease activity with PIV and SII in rheumatoid arthritis. *Medicine (Baltimore).* 2024;103(9):e37230. doi: 10.1097/MD.0000000000037230.
11. Ocak T, Lermi N, Yılmaz Bozkurt Z, et al. PIV as a new marker in vascular Behçet's disease. *Eur Rev Med Pharmacol Sci.* 2024;28(5):1751–1759. doi: 10.26355/eurrev_202403_35588.
12. Gambichler T, Numanovic Z, Apel I, et al. Novel inflammation biomarkers in SLE: PIV and others. *Lupus.* 2024;33(14):1556–1561. doi: 10.1177/09612033241295865.
13. Alasmari A, Aldakhil H, Almutairi A, et al. Utility of PIV in childhood lupus. *Lupus.* 2024;33(12):1365–1372. doi: 10.1177/09612033241275227.
14. Ulutaş F, Çobankara V. PIV in lupus nephritis. *Med Sci Discov.* 2023;10(4). doi: 10.36472/msd.v10i4.918.
15. Alghareeb R, Hussain A, Maheshwari MV, Khalid N, Patel PD. Cardiovascular complications in SLE. *Cureus.* 2022;14(7):e26671. doi: 10.7759/cureus.26671.
16. Wei J, Wang A, Li B, et al. Pathological mechanisms and crosstalk among various cell death pathways in cardiac involvement of systemic lupus erythematosus. *Front Immunol.* 2024;15:1452678. doi: 10.3389/fimmu.2024.1452678.
17. Yee CS, Farewell VT, Isenberg DA, Griffiths B, et al. The use of SLEDAI-2000 to define active disease and minimal clinically meaningful change based on data from a large cohort of SLE patients. *Rheumatology (Oxford).* 2011;50(5):982–988. doi: 10.1093/rheumatology/keq376.
18. Koelmeyer R, Nim HT, Nikpour M, et al. High disease activity status suggests more severe disease and damage accrual in SLE. *Lupus Sci Med.* 2020;7(1):e000372. doi: 10.1136/lupus-2019-000372.
19. Anderson E, Shah B, Davidson A, Furie R. Lessons learned from bone marrow failure in SLE: Case reports and review of the literature. *Semin Arthritis Rheum.* 2018;48(1):90–104. doi: 10.1016/j.semarthrit.2017.12.004.

https://doi.org/10.5455/annalsmedres.2025.08.247

20. Velo García A, Castro SG, Isenberg DA. The diagnosis and management of the haematologic manifestations of lupus. *J Autoimmun.* 2016;74:139–160. doi: 10.1016/j.jaut.2016.07.001.
21. Baodong Qin, Ning Ma, Qingqin Tang, et al. Neutrophil to lymphocyte ratio (NLR) and platelet to lymphocyte ratio (PLR) were useful markers in assessment of inflammatory response and disease activity in SLE patients. *Mod Rheumatol.* 2016;26(3):372–376. doi:10.3109/14397595.2015.1091136.
22. Ermurat S, Tezcan D. Sistemik lupus eritematozus hastalarında inflamasyon belirteci ve yüksek hastalık aktivite göstergesi olarak yeni hematolojik indeksler. *Uludağ Üni Tip Fak Der.* 2022;48(2):189–196. doi: 10.32708/uutfd.1110778.
23. Karadag I, Karakaya S, Yilmaz ME, Öksüzoglu OBC. The potential prognostic novel markers PIV and PILE score to predict survival outcomes in hepatocellular cancer. *Eur Rev Med Pharmacol Sci.* 2022;26(20):7679–7686. doi: 10.26355/eurrev_202210_30044.
24. Lin F, Zhang LP, Xie SY, et al. Pan-immune-inflammation value: a new prognostic index in operative breast cancer. *Front Oncol.* 2022;12:830138. doi: 10.3389/fonc.2022.830138.
25. Tarr T, Dérfalvi B, Győri N, et al. Similarities and differences between pediatric and adult patients with SLE. *Lupus.* 2015;24(8):796–803. doi: 10.1177/0961203314563817.
26. Esan AJ. Hematological differences in newborn and aging: a review study. *Hematol Transfus Int J.* 2016;3(3):178–190. doi: 10.15406/htij.2016.03.00067.
27. Ma R, Ren J, Chen X, Li X, Zhao Y, Ding Y. Association between pan-immune-inflammation value and coronary heart disease in elderly population: a cross-sectional study. *Front Cardiovasc Med.* 2025;12:1538643. doi: 10.3389/fcvm.2025.1538643.
28. Song X, Zhang H, Zhao et al. HMGB1 activates myeloid dendritic cells by up-regulating mTOR pathway in SLE. *Front Med (Lausanne).* 2021;8:636188. doi: 10.3389/fmed.2021.636188.
29. Salvi V, Gianello V, Busatto S, et al. Exosome-delivered microRNAs promote IFN-α secretion by human plasmacytoid DCs via TLR7. *JCI Insight.* 2018;3(10):e98204. doi: 10.1172/jci.insight.98204.
30. Lewandowski LB, Kaplan MJ. Update on cardiovascular disease in lupus. *Curr Opin Rheumatol.* 2016;28(5):468–476. doi: 10.1097/BOR.0000000000000307.
31. Sacre K, Criswell LA, McCune JM. Hydroxychloroquine is associated with impaired interferon-alpha and TNF-alpha production by plasmacytoid dendritic cells in SLE. *Arthritis Res Ther.* 2012;14(3):R155. doi: 10.1186/ar3895.
32. Goldman FD, Gilman AL, Hollenback C, Kato RM, Premack BA, Rawlings DJ. Hydroxychloroquine inhibits calcium signals in T cells: a new mechanism to explain its immunomodulatory properties. *Blood.* 2000;95(11):3460–3466. PMID: 10828029.
33. Schmidt RLJ, Jutz S, Goldhahn K, et al. Chloroquine inhibits human CD4+ T-cell activation by AP-1 signaling modulation. *Sci Rep.* 2017;7:42191. doi: 10.1038/srep42191.

https://doi.org/10.5455/annalsmedres.2025.08.247

Ann Med Res

Current issue list available at Ann Med Res

Annals of Medical Research

journal page: annalsmedres.org

Low dose cytarabine-induced posterior reversible encepalopathy syndrome with atypical features

Mehmet Fatih Erbay [a,*], Ilhami Berber [b]

[a] Inonu University, Faculty of Medicine, Department of Radiology, Malatya, Türkiye
[b] Inonu University, Faculty of Medicine, Department of Internal Medicine, Division of Hematology, Malatya, Türkiye
*Corresponding author: drfatiherbay@hotmail.com (Mehmet Fatih Erbay)

Cite this article as: Erbay MF, Berber I. Low dose cytarabine-induced posterior reversible encepalopathy syndrome with atypical features. *Ann Med Res*. 2025;32(12):574–575. doi: 10.5455/annalsmedres.2025.11.370.

Received: Nov 25, 2025 **Accepted:** Dec 02, 2025 **Available Online:** Dec 25, 2025

A 70-year-old man presented with fatigue and weight loss and was diagnosed with AML-M5b after pancytopenia was detected. Low-dose cytarabine treatment (20 mg twice daily, subcutaneously) was initiated. Five days after completing therapy, he developed blurred vision. Apart from bilateral visual impairment on ophthalmologic evaluation, his vital signs, physical examination, serum metabolic parameters, ECG, and echocardiography were normal.

Contrast-enhanced brain MRI revealed bilateral, symmetrical T2-FLAIR hyperintensities in the parieto-occipital watershed regions with gyral and leptomeningeal enhancement. These areas showed both restricted diffusion and T2 shine through on DWI/ADC, indicating mixed cytotoxic and vasogenic edema, along with small hemorrhagic foci (Figure 1). Non-contrast MRA demonstrated non-visualization of the distal P2 segments of both posterior cerebral arteries, likely secondary to vasospasm. After excluding other etiologies, cytarabine-associated posterior reversible encephalopathy syndrome (PRES) was diagnosed.

PRES results from impaired cerebrovascular autoregulation and is commonly triggered by acute hypertension, cytotoxic agents, or renal dysfunction, typically presenting with symmetric vasogenic edema in the parieto-occipital regions of brain [1]. In this case, the mixed diffusion pattern, presence of hemorrhagic products, and contrast enhancement were atypical for classical PRES and are also not expected in the hyperacute phase of arterial ischemia [2]. While PRES associated with intermediate- and high-dose cytarabine (2 × 3 g/m^2/day) has been reported, no cases linked to low-dose cytarabine have been described to date. Even low-dose cytarabine may lead to PRES; therefore, both classical and atypical imaging features should be recognized.

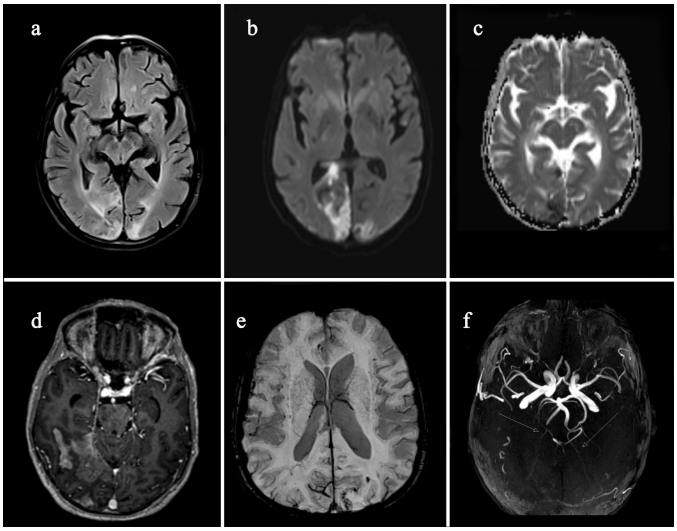

Figure 1. (a) Bilateral parieto-occipital cortical and subcortical hyperintensities on FLAIR; (b, c) DWI and corresponding ADC map show restricted diffusion together with areas of T2 shine-through in these regions; (d) Contrast-enhanced T1-weighted image demonstrates a gyral enhancement pattern in the right temporo-occipital region; (e) SWI reveals a few punctate blooming artifacts representing small hemorrhagic foci in the left parietal cortex; (f) Non-contrast MRA demonstrates absence of the distal P2 segments of both posterior cerebral arteries.

Informed Consent: Written informed consent for publication and accompanying images was obtained from the patient.

Conflict of Interest: The authors declare that they have no con-

flict of interest.

Author Contributions: Conception: M.F.E; Design: M.F.E; Supervision: İ.B; Materials: İ.B; Analysis and/or Interpretation: M.F.E; Literature Review: M.F.E; Writing: M.F.E; Critical Review: İ.B.

Financial Disclosure: No financial support was received for this work.

REFERENCES

1. Anderson R-C, Patel V, Sheikh-Bahaei N, Liu CSJ, Rajamohan AG, Shiroishi MS, et al. Posterior Reversible Encephalopathy Syndrome (PRES): Pathophysiology and Neuro-Imaging. *Front Neurol.* 2020;11:463. doi: 10.3389/fneur.2020.00463.
2. Adam G, Ferrier M, Patsoura S, Gramada R, Meluchova Z, Cazzola V, et al. Magnetic resonance imaging of arterial stroke mimics: a pictorial review. *Insights Imaging.* 2018;9(5):815-831. doi: 10.1007/s13244-018-0637-y.

https://doi.org/10.5455/annalsmedres.2025.11.370